



THE  
2  
2008

**LIBRARY**  
**Michigan State**  
**University**

This is to certify that the  
dissertation entitled

DEVELOPMENT OF A WIRELESS INSTRUMENTED  
PROJECTILE FOR IMPACT TESTING BASED ON  
ELASTIC WAVE REDUCTION

presented by

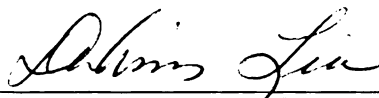
Guojing Li

has been accepted towards fulfillment  
of the requirements for the

Doctoral

degree in

Engineering Mechanics



Major Professor's Signature

7/30/08

Date

**PLACE IN RETURN BOX** to remove this checkout from your record.  
**TO AVOID FINES** return on or before date due.  
**MAY BE RECALLED** with earlier due date if requested.

DATE DUE	DATE DUE	DATE DUE

DEVELOPMENT OF A WIRELESS INSTRUMENTED  
PROJECTILE FOR IMPACT TESTING BASED ON  
ELASTIC WAVE REDUCTION

By

Guojing Li

A DISSERTATION

Submitted to  
Michigan State University  
In partial fulfillment of the requirements  
for the degree of

DOCTOR OF PHILOSOPHY

Department of Mechanical Engineering

2008



## ABSTRACT

### DEVELOPMENT OF A WIRELESS INSTRUMENTED PROJECTILE FOR IMPACT TESTING BASED ON ELASTIC WAVE REDUCTION

By

Guojing Li

Dynamic loadings, such as impact, crash and blast loadings, are commonly encountered in the real world. Multiple dynamic testing techniques and devices, instrumented as well as non-instrumented, have been developed for material characterizations and laboratory simulations. The objective of this thesis research is to develop a wireless instrumented projectile for low-velocity impact. The research is divided into three sections. The first section addressed the fundamental difference between horizontal impact and vertical impact. Sensors based on strain gages and accelerometers were also compared. It was found that a horizontal impactor equipped with strain gages could be used for investigations on impact loading if the wave propagation associated with the dynamic loading could be reduced or eliminated. In the second section, wave reflection and wave superposition induced by impact loading in short projectiles were studied. Both mechanical and numerical methods were proposed for reducing the effect due to wave reflection so the initial wave associated with the impact could be identified. Parabola-like surfaces at the free end of projectiles were found to be able to reduce the effect of wave reflection and were incorporated into the design of the projectile. Issues concerning the damage of lead wires during impact testing were important to the success of the

instrumented projectile. The third section presented the detailed construction of a wireless instrumented projectile, including the selection of the geometry, the manufacturing procedures, the circuit design of the microprocessor, and the assembly of the projectile. Calibrations on projectile body and electronic components were carefully performed. Testing results seemed to validate the feasibility of using the wireless instrumented projectile for impact events with a velocity up to 20m/s and bandwidth of 170 kHz. Both the impact velocity and the bandwidth are much higher than what are available commercially.

## **ACKNOWLEDGEMENTS**

I would like to thank my professor, mentor, and good friend Dr. Dahsin Liu for his insight and directions; he directed my thesis research step by step from the very beginning and helped me to review the thesis. I am very grateful to Dr. Gary Cloud, Dr. Brian Feeny, Dr. Andre Y. Lee and Dr. Alfred Loos for serving on my committee. I would like to thank Dr. Hanqing Zhao and Mr. Brian Wright for their help and directions on the circuit designs. I would like to thank Dr. Chun-Ying Lee and Mr. Shawn Klann for reviewing my thesis. I would also like to thank my wife Sen Li, and my daughter Xinui Li for all of their love and understanding, though they probably don't know it. Thank you, I appreciate everything you have done for me.

## TABLE OF CONTENTS

LIST OF TABLES.....	ix
---------------------	----

LIST OF FIGURES.....	x
----------------------	---

### CHAPTER ONE INTRODUCTION

1. BACKGROUND.....	1
2. STATEMENT OF PROBLEM.....	4
3. ORGANIZATION OF THE THESIS.....	6
REFERENCES.....	9

### CHAPTER TWO SENSOR EFFECTS AND SIGNAL ANALYSIS IN DYNAMIC MEASUREMENTS

ABSTRACT.....	13
1. INTRODUCTION.....	14
2. EXPERIMENTAL TECHNIQUES.....	17
2.1 Sensors and Data Acquisition.....	17
2.2 Experimental Setup and Procedure.....	18
A. Vertical Impact Systems.....	19
a. Load-cell type.....	19
b. Striker-bar type.....	20
B. Horizontal Impact Tests.....	21
a. Type I.....	21
b. Type II.....	21
c. Type III.....	22
3. EXPERIMENTAL RESULTS.....	23
3.1 Vertical Impact Test Systems.....	23
A. Load Cell Type.....	23
B. Striker-Bar Type.....	27
3.2 Horizontal Impact Systems.....	29
A. Type I.....	29
B. Type II.....	31
C. Type III.....	32
3.3 Structures' spectrum tests and signals' spectral analysis.....	32
4. DISCUSSION.....	33
4.1 Load Cell vs. Stricker Bar.....	33
4.2 Quartz Accelerometers vs. Piezoresistive Accelerometer.....	34
4.3 Strain Gages vs. Accelerometers.....	34

4.4 Vertical Impact vs. Horizontal Impact.....	36
5. ANALYSIS.....	37
5.1 Effects of Masses.....	37
5.2 Effect of Wave Propagation.....	40
A. Basic Wave Equation.....	40
B. Simulation.....	42
6. CONCLUSIONS.....	46
ACKNOWLEDGMENTS.....	46
REFEFENCES.....	47

### **CHAPTER THREE**

#### **WAVE PROPAGATION IN LOAD TRANSDUCERS**

ABSTRACT.....	49
1. INTRODUCTION.....	50
2. FORCE TRANSDUCERS.....	52
3. WAVE PROPAGATION IN RODS.....	54
3.1 Experiments on Effect of Rod Length.....	55
3.2 Experiments on Contact Duration.....	57
3.3 Experiments Based on Three Sets of Gages.....	60
3.4 Experiments on Wave Dissipation.....	62
4. MECHANICAL METHODS FOR WAVE REDUCTION.....	64
4.1 Rod with Cone-Ball End.....	64
4.2 Bar with Double Parabolic-Lines and Double Tails.....	67
5. NUMERICAL METHODS FOR WAVE REDUCTION.....	72
5.1 Technique Based on Assuming an Initial Wave.....	72
5.2 Two-Position Technique.....	75
6. CONCLUSIONS.....	79
REFERENCES.....	81

### **CHAPTER FOUR**

#### **DESIGN AND CALIBRATION OF AN INSTRUMENTED PROJECTILE**

ABSTRACT.....	84
1. INTRODUCTION.....	85
2. SIGNAL TRANSFER.....	87
2.1 Wired Method.....	87
2.2 Wireless Technique.....	90
A. Conductive Technique.....	90
B. Radio Signal Transfer Technique.....	91
C. Wireless Technique.....	91
3. DESIGN OF AN INSTRUMENTED PROJECTILE.....	91
3.1 Cutting Tools.....	93
3.2 Projectile Body.....	95
3.3 Wave Transferring Section.....	95
3.4 Instrumentation and Assembly.....	97

4. TESTING OF SIGNAL MEASUREMENTS.....	99
4.1 Accuracy Test.....	100
4.2 Dynamic Signal Test.....	101
5. TESTING WAVE REDUCTION.....	103
6. CALIBRATION OF THE INSTRUMENTED PROJECTILE.....	106
7. CASE STUDY OF THE INSTRUMENTED PROJECTILE.....	109
8. DISCUSSIONS.....	112
8.1 Longer Gun Barrel.....	112
8.2 Wave Transfer Section.....	112
8.3 The Sampling Rate.....	112
8.4 Trigger Mechanism.....	113
8.5 The Connectors.....	113
8.6 Assembly Issues.....	114
9. CONCLUSIONS.....	114
REFERENCES.....	115

## **CHAPTER FIVE**

### **CONCLUSIONS AND RECOMMENDATIONS**

1. CONCLUSIONS.....	117
2. RECOMMENDATIONS.....	118

## **APPENDIX A**

### **DESIGN A PENNY-SIZE SIGNAL PROCESSING AND DATA ACQUISITION SYSTEM**

1. INTRODUCTION.....	121
2. DESIGN OVERVIEW.....	121
2.1 Strain Gages and Wheatstone Bridge.....	123
2.2 Amplifier.....	124
2.3 Data Acquisition and Saving.....	125
2.4 Trigger.....	126
3. DESIGN AND MANUFACTURING.....	127
3.1 Strain Gages.....	127
3.2 Trigger.....	127
3.3 Signal Processing, Data Acquisition and Saving Unit.....	128
3.4 Microprocessor.....	130
3.5 Amplifiers.....	131
3.6 Resistors for the Wheatstone Bridge.....	132
3.7 Print Board and Soldering.....	132
3.8 Battery.....	134
3.9 Wiring.....	135
3.10 Connectors.....	136
3.11 Protection of the Battery and SP&DAQ unit.....	136
4. SUPPORTING SYSTEMS.....	137

4.1 The Control Programs.....	137
4.2 Data Transferring Circuit and Software.....	138
4.3 Program for Data Processing.....	141
4.4 Velocity Measurement.....	142
REFERENCES.....	144

<b>APPENDIX B</b>	
<b>THE MICROPROCESSOR'S CONTROL PROGRAM FOR DATA</b>	
<b>SAMPLING AND SAVING – IN ASSEMBLY LANGUAGE.....</b>	<b>145</b>

<b>APPENDIX C</b>	
<b>THE MATLAB PROGRAM FOR CHANGING DATA FORMAT</b>	
<b>FROM HEXADECIMAL TO DECIMAL.....</b>	<b>152</b>

<b>APPENDIX D</b>	
<b>MATLAB PROGRAM FOR THE NUMERICAL METHOD</b>	
<b>-- INITIAL WAVE ASSUMPTION.....</b>	<b>154</b>

<b>APPENDIX E</b>	
<b>LABVIEW PROGRAM FOR THE NUMERICAL METHOD</b>	
<b>– TWO POSITION.....</b>	<b>161</b>

## **LIST OF TABLES**

Table 2.1 Parameters of sensors and their data acquisition system.....	18
Table 2.2 Spectrum testing results.....	33
Table 2.3 Spectrum analysis of the signals in figure 2.3(b), 2.4(b), 2.5(b) and 2.7.....	33
Table A1 Electrical current consumption of each component.....	135



## LIST OF FIGURES

Figure 2.1(a) Vertical impact tests: the load-cell type.....	19
Figure 2.1(b) Vertical impact tests: the striker-bar type.....	20
Figure 2.2 Horizontal impact systems (a) type I, (b) type II, and (c) type III.....	23
Figure 2.3(a) Aluminum with thick vinyl under vertical impact, load cell type....	25
Figure 2.3(b) Aluminum with thin vinyl under vertical impact, load cell type.....	26
Figure 2.4(a) Aluminum with thick vinyl under vertical impact, striker-bar type.....	28
Figure 2.4(b) Aluminum with thin vinyl under vertical impact, striker-bar type....	28
Figure 2.5(a) Steel with rubber under horizontal impact, type I.....	30
Figure 2.5(b) Glass/epoxy under horizontal impact, type I.....	30
Figure 2.6 Striker bar and load cell under horizontal impact, type II.....	31
Figure 2.7 Force histories from type III horizontal impact.....	32
Figure 2.8 Schematic diagrams of (a) impactor and (b) individual components .....	38
Figure 2.9 Wave patterns based on measurement and simulations.....	44
Figure 2.10 Simulation of apparent dent in force history due to blunt impact....	45
Figure 3.1 Testing setup for the impact rod.....	56
Figure 3.2 Strain histories from the impact rods with various lengths.....	56
Figure 3.3 Experimental setup for impact duration and strain history.....	59
Figure 3.4 Impact duration (upper) and the strain history (lower).....	59
Figure 3.5(a) Experimental setup of the three sets of strain gages.....	60
Figure 3.5(b) Experimental results of the three sets of strain gages.....	61
Figure 3.6 The signal in frequency domain obtained from the pair	

of strain gages located 38 mm from the impact end.....	62
Figure 3.7(a) Experimental setup for wave dissipation.....	63
Figure 3.7(b) Experimental result of wave dissipation.....	63
Figure 3.8(a) Schematic of a rod with a cone-ball end.....	65
Figure 3.8(b) Detailed drawings of a rod with a cone-ball end.....	65
Figure 3.8(c) Image of a cylindrical rod and a rod with a cone-ball end.....	66
Figure 3.9 Force histories in the rod with a flat end (top) and a rod with a cone-ball end (bottom).....	67
Figure 3.10(a) Bar with double parabolic-lines and double tails.....	68
Figure 3.10(b) Drawing of the bar with double parabolic-lines and double tails.....	68
Figure 3.10(c) Image of bar with double parabolic-lines and double tails.....	69
Figure 3.11 Impact response of the flat bar with double parabolic-lines and double tails.....	71
Figure 3.12 Impact response of the bar with double-lines and double tails.....	71
Figure 3.13 The assumed input wave, superimposed wave and experimental curve .....	74
Figure 3.14 Experimental setup of the two-position technique.....	77
Figure 3.15(a) Experimental curves from two-position of a short bar and from a long bar.....	78
Figure 3.15(b) Results based on the two-position technique.....	78
Figure 4.1 Assembly of the wired projectile.....	89
Figure 4.2 Result measured by an instrumented rod with the protected wound-lead wire .....	90
Figure 4.3 Layout of the instrumented projectile.....	93
Figure 4.4 Images of endmill (left) and round-corner cutting tool (right).....	94

Figure 4.5(a) Overall geometry and dimensions of the projectile body.....	96
Figure 4.5(b) Schematic of the wave transfer mechanism.....	96
Figure 4.6(a) Schematic layout of the instrumented projectile.....	98
Figure 4.6(b) Parts of the instrumented projectile.....	99
Figure 4.6(c) Assembled instrumented projectile.....	99
Figure 4.7 Input and output of a constant voltage test.....	101
Figure 4.8 Square wave testing result.....	103
Figure 4.9 Setup of the wave reduction test experiment.....	104
Figure 4.10 Comparison between the results from the long bar and the projectile body.....	106
Figure 4.11 Setup for the calibration of the instrumented projectile.....	107
Figure 4.12 Impact result measured by the instrumented projectile.....	108
Figure 4.13 Comparison between the result from the long bar and that from the instrumented projectile when they impact with each other.....	109
Figure 4.14(a) Setup for impact test based on instrumented projectile.....	110
Figure 4.14(b) Force history measured by instrumented projectile.....	111
Figure 4.14(c) Force history measured by a low-velocity drop-weight impact tester.....	111
Figure A1 Schematic layout of the measurement system of the instrumented projectile.....	122
Figure A2 Schematic of the Wheatstone bridge.....	123
Figure A3 Schematic of the amplifier circuit.....	125
Figure A4 The schematic triggering circuits.....	127
Figure A5 The circuit drawing of the signal processing, data acquisition and saving.....	129

Figure A6 Both sides of the print board.....	133
Figure A7 Pictures of the soldered signal processing and data acquisition unit.....	134
Figure A8 Circuit drawings of the data transferring and its power supply.....	140
Figure A9 Picture of the data transferring box.....	141
Figure A10 Schematic of the velocity measurement.....	143

## **CHAPTER ONE**

### **INTRODUCTION**

#### **1. BACKGROUND**

Impact loading is commonly found in the real world. For example, two ground vehicles crash into each other, an air vehicle is struck by a bird, and a marine structure collides with icebergs. The crash, strike, and collision can cause damage to vehicles. Injury to occupants is the primary concern in the study of vehicle survivability and occupant safety. Many impact testing techniques and devices have been developed in laboratories for material characterizations and loading simulations. In characterizing the behavior of materials and structures subjected to impact loading, measurements of stress and strain histories are required for establishing the constitutive models. In simulating the impact loading, measurements of displacement, velocity, acceleration, and force histories during impact events are necessary [1-4]. With the measured histories, impact characteristics such as the maximum deflection and the energy absorption of the materials and structures, and the peak force and the contact duration between them and the impactor can be subsequently identified.

Among the various impact characteristics, energy absorption capability plays the most important role in the study of vehicle survivability and occupant safety. In order to characterize the energy absorption capabilities of materials and structures subjected to impact loading, several experimental techniques have been developed and used by researchers. Among them, the simplest one is

perhaps to measure the velocities of the impactor before and after it contacts the specimen [5, 6]. The energy absorbed by the specimen can be taken as the difference of the kinetic energies of the impactor before and after the impact event. This technique requires a relatively simple setup for velocity measurements and works in both perforation and non-perforation (rebounding from the specimen) cases. However, this technique does not give detailed information during the impact event, such as the deformation of the specimen and the change of impact force.

To better understand the energy absorption capability of a specimen and even its mechanism of energy absorption, it is necessary to identify the interaction between the impactor and the specimen through the entire impact event. Several experimental techniques for measuring the histories of displacement, velocity, acceleration, and force during impact events have been developed and are commercially available.

High-speed cameras can provide detailed images of what exactly happens during an impact event [5-9]. With sufficient photographs, the displacement history, the velocity history, and even the acceleration history can be identified. Since most impact events last only a very short period, such as no more than 1 millisecond, high-speed cameras with a very high frame rate and a capability of recording sufficient frames within the short time period are required for extracting accurate displacement, velocity, and acceleration histories. However, high-speed photography is expected to be high cost.

With the advancement in laser diodes, high-speed photo-detectors and fiber optics, researchers are able to build velocity measurement devices based on integrating these components together to measure the velocity of impactors [10, 11]. The devices are able to sense very small changes in velocity and give the velocity history with high accuracy. However, the complexities of testing environment and impactor geometry should not be underestimated because they can further complicate the testing setup and affect the measurement.

Accelerometers of various designs and data acquisition systems with high-speed capability have been developed for measuring acceleration history in impact tests [12,13,33,34]. They have been found to be useful for investigating relatively soft materials and structures, although their low natural frequencies may hinder their uses in high-speed impact events.

Some force transducers are commercially available for measuring impact force histories [14,15]. They measure the dynamic forces by sensing the motion of piezoelectric elements inside them during impacts although they are usually not calibrated dynamically. The application bandwidth of the force transducers is often only around a few kHz and may limit their uses in high-precision applications.

Strain-gage based load cells are also commonly used in impact tests [16-18]. The load cells measure the force history based on the deformation of specially designed and machined components involved in the construction of the load cells. The force history obtained from the load cells and the acceleration history obtained from the accelerometers are commonly assumed to be interchangeable

with each other based on the corresponding mass of the impactor. However, due to the difference in the nature of the individual sensors, care must be exercised.

## 2. STATEMENT OF PROBLEM

Multiple dynamic testing techniques have been developed for laboratory uses ranging from material characterization to loading simulation. Examples are the split Hopkinson's pressure bar (SHPB) for characterizing dynamic stress-strain relations [19-24], Taylor's impact test [25] for finding dynamic yielding stress, instrumented weight-drop impact test for obtaining material response under low-velocity impacts, and gas gun for simulating ballistic impacts. Among the four techniques mentioned, the SHPB and weight-drop impact test are instrumented tests while Taylor's impact and gas gun tests are non-instrumented.

Non-instrumented tests are much simpler than instrumented tests in construction. They are usually built for simulating loading conditions that occur in the real world. Instrumented tests, however, are equipped with sensors to detect physical quantities and require sophisticated data acquisition and signal processing systems for further understanding the physics of the tests. Since dynamic loadings usually last a very short instant and involve many physical parameters during the events, instrumented tests are preferred over non-instrumented tests in studying dynamic loading events.

There are many candidates for dynamic measurements. Optical methods, such as fiber Fabry-Perot interferometer (EFPI) strain sensors and fiber Bragg grating (FBG) strain sensors [26], are suitable for sensing dynamic strain



histories [27]. Magnetic methods, such as linear variable differential transformers (LVDT) [28,29], are normally used for measuring dynamic displacements [30]. Electrical methods are more commonly used in dynamic measurements. Capacitances based device can be used for sensing minimal distances [31]. Resistances based gages can be attached to an elastic element for sensing strains. Piezoelectric effect based sensors [32] are used for sensing forces and accelerations. The dynamic signals measured by these methods can be converted into dynamic force histories under certain conditions.

Strain gages have been commonly used for measuring strain history [35-37]. Owing to their technology maturity, low sensitivity to environmental impact, accessibility, and low cost, strain gages may be the most commonly used techniques for measuring parameters involved in impact events [16-24,38]. The measured strain history can then be converted into stress history and even force history.

For characterizing materials and structures under impact loading, the instrumented projectiles will be accelerated to certain speeds before impacting on the specimens. Fumes and fragments can occur in most cases. Therefore, the methods concern delicate sensors, such as optical methods and the magnetic methods, are not very suitable for use in the impact environment.

A major issue in measuring the signals in impact events is the understanding of wave propagation [39-41]. When a rod is impacted on a specimen, the compressive strain wave generated at the impact-contact surface would propagate to the opposite end of the rod. The wave is then reflected back from

the free end of the rod as a tensile strain wave. This process could repeat many times until the strain wave was completely attenuated. If the rod was long, the strain wave would propagate in the rod back and forth without superposition. A good example could be found in a split Hopkinson's pressure bar. On the contrary, if the rod was relatively short and the length of the strain wave was relatively long, superposition of the transmitted portion and the reflected portion of the strain wave would take place. The superposed wave pattern could become very complex and be recorded in the measurements.

This thesis research is aimed at developing an instrumented free projectile for simulating and characterizing impact events. Selecting a suitable sensor for detecting the wave propagation in the projectile, converting the signal into loading history, and solving the manufacturing issues are the primary goals of the research.

### 3. ORGANIZATION OF THE THESIS

This thesis contains five chapters. Chapter 1 gives a general introduction. Chapter 2 discusses the impact techniques and the effects of the types of sensor on dynamic measurements. Chapter 3 addresses the elastic wave reduction techniques and their applications in instrumented cylinders. Chapter 4 presents the detailed procedures for designing and constructing a wireless instrumented projectile for low-velocity impact tests. Chapter 5 summarizes the conclusions and suggests recommendations for future studies.

Chapters 2, 3 and 4 are the core contents of this thesis research. They are essentially arranged following the order of research progress but presented as three independent documents with the latter ones closely referencing to the former ones for clarity, continuity and completeness. For example, some materials presented in Chapter 2 are repeated in Chapters 3 and 4. Similarly, some materials given in Chapter 3 are also duplicated in Chapter 4. Hence, the thesis may be considered as a collection of research works grouped into three main subjects.

Chapter 2 is entitled “Sensor Effects and Signal Analysis in Impact Measurements.” It compares the differences between vertical impact and horizontal impact and evaluates the advantages and disadvantages of strain-gage based load cells and piezoelectric/ piezoresistive accelerometers in measuring low-velocity impact events. Horizontal impact with strain-gage based load cell is found to be a better choice for studying the wave propagation involved in dynamic impacts.

Chapter 3 is entitled “Wave Propagation in Force Transducers.” Although strain wave reflection and superposition have been identified in Chapter 2, this chapter presents two techniques for isolating the primary strain wave in cylinders subject to impact loading, namely mechanical method and numerical method. The former is based on geometrical effect to remove unnecessary wave components reflecting from boundaries while the latter is essentially based on a numerical process. Both methods are found to be efficient for identifying the primary strain waves.

Chapter 4 is entitled “Design and Calibration of an Instrumented Projectile.” It is also the ultimate goal of this thesis research. Many details involving the manufacturing of the projectile body, the instrumentation of the sensor and the calibration of the projectile are included in the study.

The design of a microprocessor is also the critical part to achieve a wireless, high-bandwidth free projectile, which is presented in Appendix A.

## REFERENCES

- [1] Jan Hjelmgren, "Dynamic Measurement of Force-A literature Survey", SP Swedish National Testing and Research Institute, SP Measurement Technology, SP REPORT 2002:27
- [2] S. P. Virostek, J. Dual and W. Goldsmith, "Direct Force Measurement in Normal and Oblique Impact of Plates by Projectiles", Int. J. Impact Engng. Vol. 6, No. 4, p247-269, 1987
- [3] Ralph Burton, "Vibration and Impact", Dover Publications, Inc. New York 10014, 1968
- [4] Jonas A. Zukas, Theodore Nicholas and Hallock. F. Swift, "Impact Dynamics", John Wiley & sons Inc. 287-308, 1982.
- [5] Guoqi Zhu, Werner Goldsmith and C. K. H. Dharan, "Penetration of Laminated Kevlar by Projectiles—I. Experimental Investigation", Int. J. Solids Structures, Vol. 29, No 4, pp.399-420, 1992
- [6] Werner Goldsmith, Eric Tam, David Tomer, "Yawing Impact on Thin Plates by Blunt Projectiles", Int. J. Impact Engng, Vol. 16, No. 3, pp.479-498, 1995
- [7] S. J. Bless, D. R. Hartman, "Ballistic Penetration of S-2 Glass Laminates", 21<sup>st</sup> International SAMPE Technical Conference, Sept. 25-28, 1989
- [8] Stephan J. Bless, Moshe Benyami, David Hartman, "Penetration Through Glass-Reinforced Phenolic", 22<sup>nd</sup> International SAMPE Technical Conference, Nov. 6-8, 1990. pp.293-303
- [9] J.H. Choi, C. H. Lee, S.N. Chang and S.K. Moon, "Long-Rod Impact Phenomena: Role of Wave Interaction on Crack Propagation", Int. J. Impact Engng. Vol. 17, pp.195-204, 1995
- [10] Jun Lu, Subra Suresh, Guruswami Ravichandran, "Dynamic indentation for determining the strain rate sensitivity of metals", Journal of the Mechanics and Physics of Solids, 51(2003), pp.1923 – 1938
- [11] Jun Lu, "Mechanical Behavior of a Bulk Metallic Glass and its Composite over a Wide Range of Strain Rates and Temperatures", Thesis for the Degree of Doctor of Philosophy, California Institute of Technology, California, March, 2002

- [12] Eirik Svinsas, Cathy O'Carroll, Cyril M. Wentzel, and Anders Carlberg, "Benchmark Trial Designed to Provide Validation Data for Modelling"
- [13] Michael A. Christopher, Tim S. Edwards, "Instrumented Projectile", NDIA 48<sup>th</sup> Annual Fuze Conference, NSWC / Dahlgren Division
- [14] [www.omega.com](http://www.omega.com)
- [15] [www.instron.com](http://www.instron.com)
- [16] Michael J. Dixon, "Development of a Load-cell compensation System", *Experimental Mechanics* (31), p21-24, 1991
- [17] Michael J. Dixon, "A Traceable Dynamic Force Transducer", *Experimental Mechanics* (30), p152-157, 1990
- [18] D. R. Ambur, C. B. Prasad and W. A. Waters, Jr., "A Dropped-weight Apparatus for Low-speed Impact Testing of Composite Structures", *Experimental Mechanics* 35(1), p77-82, 1995
- [19] C. Bacon, "Numerical prediction of the propagation of elastic waves in longitudinally impacted rods: application to Hopkinson testing", *International Journal of Impact Engineering*, 13 (4), 527-539, 1993.
- [20] Jonas A. Zukas, Theodore Nicholas and Hallock. F. Swift, "Impact Dynamics", John Wiley & sons Inc. 287-308, 1982.
- [21] D. J. Frew, M. J. Forrestal and W. Chen. "Pulse shaping techniques for testing brittle materials with a split Hopkinson pressure bar", *Experimental Mechanics*, 42 (1), 93-106, 2002.
- [22] Michael Adam Kaiser, "Advancements in the split Hopkinson bar test", Master's thesis, Blacksburg, Virginia, 1998.
- [23] Frank E. Hauser, "Techniques for measuring stress-strain relations at high strain rates", *Experimental Mechanics*, 395-402, 1966.
- [24] J. F. Bell, "An experimental diffraction grating study of the quasi-static hypothesis of the split Hopkinson bar experiment", *J. Mech. Phys. Solids*, 14, 309-327, 1966.
- [25] Gong, Song, "The Analysis of dynamic stress and plastic wave propagation in the Taylor impact test", PhD thesis, Michigan State University, Dept. of Mechanical Engineering, 2006
- [26] Liu, J-G., Schmidt—Hattenberger, C. and Borm, G., "Dynamic strain Measurement with a fiber Bragg Gating Sensor System", *Measurement*,

Vol. 32, 2002, pp. 151-161

- [27] Jin, W. L., Venuvinod, P.K. and Wang, X., "An Optical Fiber Sensor based Cutting Force Measuring Device", International Journal of Machining and Tools Manufacturing, Vol. 35, No. 6, 1995, pp. 877-883
- [28] [www.rdpe.com](http://www.rdpe.com)
- [29] [www.sensotec.com](http://www.sensotec.com)
- [30] L. E. Malvern, "The Propagation of Longitudinal Waves of Plastic Deformation in a Bar of Material Exhibiting a Strain-rate Effect", Journal of applied mechanics, Trans. ASME, 18, p203-208, 1951
- [31] [www.synaptics.com](http://www.synaptics.com)
- [32] [www.pcb.com](http://www.pcb.com)
- [33] Robert W. Lally, PCB Piezotronics, Inc. Buffalo, N. Y. "Testing the Behavior of structures", Reprinted from TEST, Aug./September 1978
- [34] William G. Halvorsen, David L. Brown, "Impulse Technique for Structural Frequency Response Testing, Sound and Vibration", November 1977, p8-21, 1977
- [35] Sia Nemat-nasser; Jon B. Isaacs; John E. Starrett, "Hopkinson Techniques for Dynamic Recovery Experiments", Proc. Roy. Soc. London 435 (A), p371-391, 1991
- [36] M. Vural and D. Rittel, "An Educational Visualization Technique for Kolsky (split Hopkinson) Bar", Experimental Techniques, Nov-Dec 2003, p35-39. 2003
- [37] Daniel J. Inman, "Engineering Vibration", Prentice Hall, Englewood Cliffs, New Jersey 07632, 1994
- [38] S. Venzi, A. H. Priest, and M. J. May, "Influence of Inertial Load in Instrumented Impact Tests", Impact Testing of Metals, ASTM STP 466, American Society for Testing and Materials, 1970, pp.165-180
- [39] J Reed, "Energy losses due to elastic wave propagation during an elastic impact", J. Phys. D: Appl, Phys. 18(1985) pp. 2329-2337, Printed in Great Britain
- [40] Karl F. Graff, "Wave Motion in Elastic Solids", Unabridged Dover (1991)

- [41] M. T. Martin and J. F. Doyle, "Impact force identification from wave propagation responses", *International Journal of Impact Engineering* Vol. 18, Issue 1, January 1996, pp. 65-77



**CHAPTER TWO**  
**SENSOR EFFECTS AND SIGNAL ANALYSIS**  
**IN IMPACT MEASUREMENTS**

**ABSTRACT**

Comparison between vertical impact and horizontal impact was of primary interest in this study. Both accelerometers and strain gages were used in the impact measurements. These two types of sensors gave comparable measurements of acceleration/force histories for relatively soft materials subjected to relatively low-velocity impacts. However, as impacted materials become harder and impact velocities became higher, the dynamic measurements from these two types of sensors become more significantly different. During impact events, reflected waves and transmitted waves superimposed with one another and resulted in a mountain-shaped strain history. In order to investigate the details of wave propagation in the impact events in a more analytical manner so that experimental results could be compared with the numerical simulation, some instrumented rods were built.

## 1. INTRODUCTION

In studying the behavior of materials subjected to impact loading, the measurement of force or acceleration history during the impact events is necessary [1, 2]. With the measured history, some mechanical characteristics such as the peak force, the maximum deflection, and the energy absorption of the materials [3, 4] can be subsequently identified.

There are many methods suitable for the measurement. Optical [5] and magnetic [6] methods had been used for particle velocity history measurement; strain gages [7-9] were widely used for strain history as well as wave traveling measurement; and accelerometers [10,11] were used for measuring acceleration history. The measured particle velocity history or strain history can then be transferred into force history or acceleration history under certain conditions. Since the impact sensors have to endure a harsh environment due to the impact events, the optical and magnetic methods are not suitable for general purpose impact sensor designs.

Sensors such as load cells and accelerometers are commonly used in the impact tests [12-14]. Load cells measure the force history, while accelerometers measure the acceleration history. The force history and the acceleration history are commonly assumed to be interchangeable with each other if the corresponding mass of the impactor can be taken as a rigid body. However, due to the difference in the nature of the individual sensors, care must be exercised.

A calibration is required before the use of a sensor [15]. Load cells based on electrical resistance strain gages are usually calibrated with static loading, as

they are sensitive to deformation. For example, several deadweights can be added to a load cell to establish the relationship between the loads and the corresponding electronic outputs to identify the calibration factor. The calibration factor obtained from the static loading, however, may pose errors when used in dynamic measurements as static loading involves deformation while dynamic loading comes with wave propagation.

Being different from load cells, accelerometers are sensitive to motions but not deformations. When an accelerometer is subject to a motion, it can cause relative movements in the internal mass blocks and result in a corresponding reading associated with the acceleration it experiences. Accordingly, accelerometers are frequency dependent and require extra care in obtaining constant calibration factors.

The installation of sensors is not a trivial task. To avoid being damaged, the sensors should not be mounted on the impact surfaces. Often times, they are also encapsulated by a cover component for protection [16]. The dislocation and the additional mass in front of the sensors can introduce additional errors to the measurements [17].

The distance between the contact surfaces to the sensor's positions exists for most measurements. The impact forces generate when the impact occurs, but the sensors can not measure the forces immediately because of the time required for the impact force to transfer from the contact end to the sensors' positions. The transferring dynamic force/acceleration shows as the strain wave propagates along the whole sensor structure at the sound speed of its material

[18-20]. The strain waves will rebound and superimpose with each other, making the measured values complex.

Stainless steel 347 is a well-known material for elastic wave propagation from the former research about split Hopkinson pressure bar. If a one-dimensional bar is deformed in elastic stage and just the elastic wave stays in the bar, the strain could be proportional to the stress. Therefore, the stress will be proportional to the impact force. Hence, a stainless steel 347 bar with 19mm diameter was cut into several pieces to work together with a load cell and accelerometers. Strain gages were installed on the surface of the bar along the axis direction to measure the dynamic strain during impacts. The bars are called “strikers” in the following chapters when strain gages have been installed.

The impact devices could be roughly divided into two groups: vertical impact devices and horizontal impact devices. The vertical impact devices usually raise a weight to a certain height and then release it to achieve the impact velocities. Sometimes an extra power source such as pressure gas or a spring is used to achieve a higher-impact velocity. Extra-weight blocks could be added to the weight to increase the impact energy [21]. Horizontal impact devices usually use a gas gun as a power source to push bullets to impact the specimen. Some researchers use a gas gun and a spring together. The bullet could be accelerated to very high velocities to impact the specimens. These two impact methods are both used in this research.

In order to compare the differences among the different measurement methods, several impact tests were designed and carried out. There are two

groups of tests in vertical impact tests: one is the load cell, a striker, and an accelerometer together for several different specimens; another is the load cell and two accelerometers that work together for different specimens. There are three groups of tests in horizontal tests: the first has a striker and an accelerometer working together for different specimens, the second is a striker impacts on the load cell directly, and the third one involves three pairs of gages on the different positions of a striker for different specimens. A simulation for the wave superposition is also presented.

## 2. EXPERIMENTAL TECHNIQUES

### 2.1 Sensors and Data Acquisition

Two accelerometers and one load cell were used in the experiments. One accelerometer was of piezoelectric type and had a mass of 10.5 gm (gram). It had high precision for measurements of acceleration up to 500 g (gravitational acceleration) and frequency up to 10 kHz. The other accelerometer weighed only 1 gram and was of a piezoresistive type. It is useful for applications that require accelerometers with small mass. Its capability was up to 2,000 g for acceleration and up to 7 kHz for frequency. The load cell was based on electrical resistance strain gages and had a maximum capacity of 22.5 kN.

Three cylindrical striker bars with a diameter of 19 mm were also prepared. They were made of stainless steel 347 because of its low-sensitivity to strain rate. Several sets of strain gages were mounted on the striker bars. Each set contained two gages located on two opposite sides of a striker bar. They were

then connected to the opposite arms of a Wheatstone bridge circuit to allow the measurements of axial deformation while eliminating the bending effect. Power supplies and amplifiers were required to enhance the output signals from the accelerometers and the Wheatstone bridge circuits.

Table 2.1 summarized the sensors and their signal amplifying and data acquisition systems.

Table 2.1 Parameters of sensors and data acquisition system

	<b>Piezoelectric accelerometer</b>	<b>Piezoresistive accelerometer</b>	<b>Strain gage based load cell</b>	<b>Strain Gage Based Striker bars</b>
<b>Measurement range</b>	± 500 g	± 2000 g	22.5 kN	58 kN
<b>Frequency range</b>	0.7Hz-10 kHz	0.7Hz-7 kHz	4 kHz	To be determined
<b>Resonance frequency</b>	38 kHz	25 kHz	To be determined	To be determined
<b>Amplifier's bandwidth</b>	100 kHz	150 kHz	4 kHz	150 kHz
<b>Sampling rate</b>	5MS/s	5MS/s	5MS/s	5MS/s

## 2.2 Experimental Setup and Procedure

Both vertical impact and horizontal impact tests were investigated. One objective of the studies was to identify the effects of gravitational acceleration on the dynamic force measurements.

## A. Vertical Impact Systems

In the vertical impact system, a drop-weight impact testing machine was used. Two types of tests were performed.

### a. Load-cell type

In the first type, as shown in Figure 2.1(a), the load cell was located between the drop-weight and the impactor tup. The impactor tup was made of hardened steel and had a diameter of 12.7 mm and length of 55 mm. The piezoelectric accelerometer was attached to the drop-weight, while the piezoresistive accelerometer was mounted between the load cell and the impactor tup. In this type of test, the load cell was the primary impactor, hence, this type of vertical impact system was called the load-cell type.

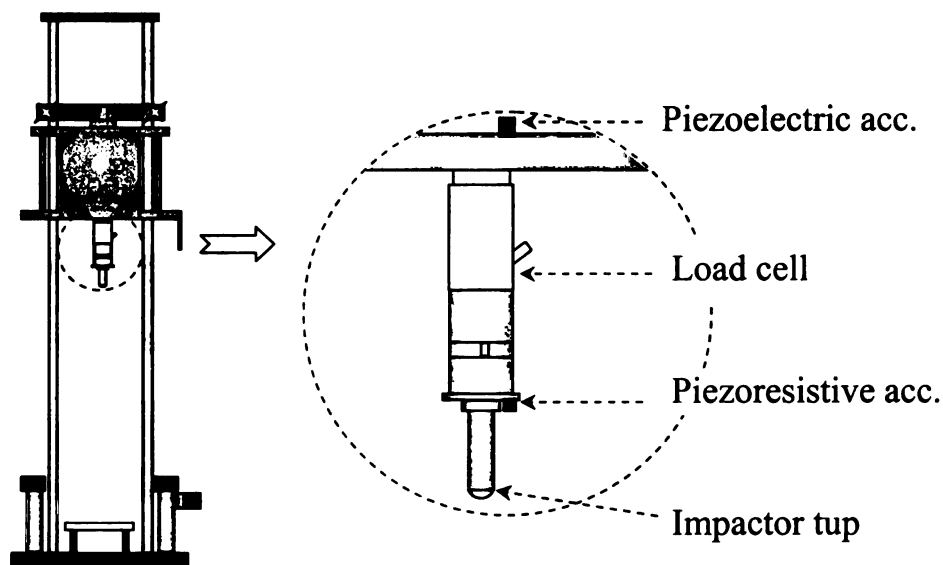


Figure 2.1(a) Vertical impact tests: the load-cell type

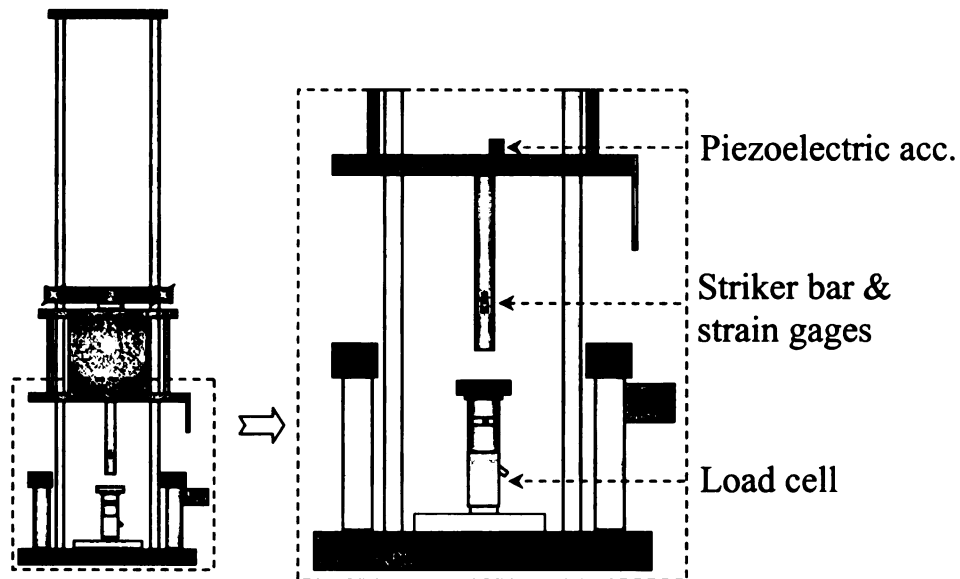


Figure 2.1(b) Vertical impact tests: the striker-bar type

#### b. Striker-bar type

In the second type, as shown in Figure 2.1(b), a 200 mm-long striker bar was added to the impact testing machine. It was attached to the drop-weight and was used as the impactor with a set of strain gages 32 mm from the free end. Hence, this type of vertical impact was called the striker-bar type. Similar to the load-cell type, the piezoelectric accelerometer was attached to the drop-weight. The load cell was located underneath the specimen.

A triggering device based on an infrared photocell was used to start the recording of the outputs from the striker bar, the load cell, and the accelerometers. The recorded data points were stored in a computer for processing. The purpose of performing these two types of test was to compare the measurements from the strain gages and the accelerometers.



## B. Horizontal Impact Systems

In horizontal impact systems, a gas gun was used to accelerate striker bars. A connector was designed as a transition unit between the gun barrel and the striker bars, because the former had an inner diameter of 12.7 mm while the latter had an outer diameter of 19mm. In each impact system, half of the striker bar was inserted into the transition unit and accelerated by a high-pressure nitrogen gas. Three types of setup were carried out in the horizontal impact tests. The comparison of the measurements based on strain gages and accelerometers could be made, as could the effect of sensor location on the measurements.

### a. Type I

The setup of type I included a 200 mm-long striker bar. The bar was instrumented with the piezoresistive accelerometer and a set of strain gages. They were located 15 mm from the impacting end as shown in Figure 2.2(a). Several kinds of material were tested with this type of horizontal impact system.

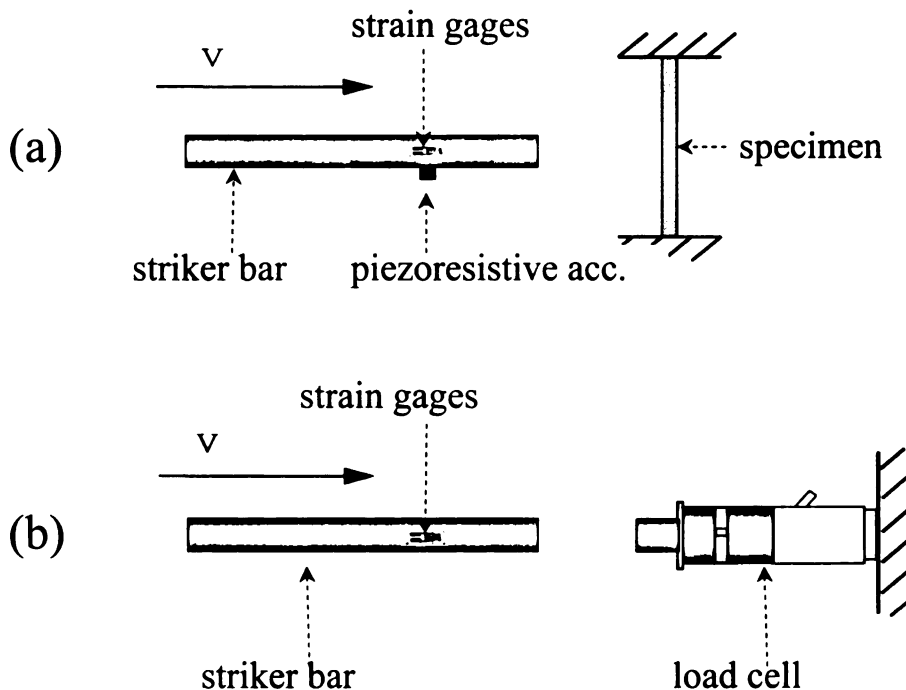
### b. Type II

The setup of type II included a striker bar and the load cell, as shown in Figure 2.2(b). The striker bar was 250 mm long, a set of strain gages were located 37.5 mm from the impacting end. The load cell was held horizontally to a solid wall. The horizontal axes of the load cell and the striker bar were carefully aligned.

The data acquisition system for the striker bars was triggered by the electromagnetic valve of the gas gun. The triggering device for the load cell, as mentioned earlier, was based on an infrared photocell. A triggering device was designed to synchronize the readings of the striker bar and the load cell.

### c. Type III

The setup of type III was similar to that of type I, as shown in Figure 2.2(c). However, it used a 250 mm striker bar and three sets of strain gages. The sets of strain gages were located 37.5 mm, 75 mm, and 112.5 mm from the impact end. Several types of material were tested.



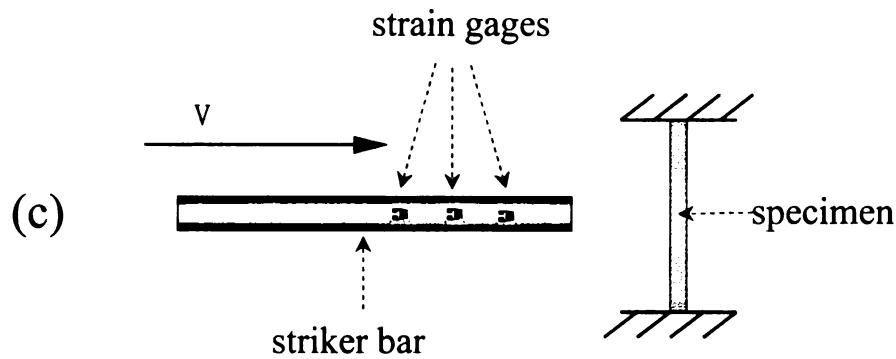


Figure 2.2 Horizontal impact systems (a) type I, (b) type II and (c) type III

### 3. EXPERIMENTAL RESULTS

In impacting tests, the output of a load cell was force history, while that of an accelerometer was acceleration history. In order to compare the different measurements from the different types of sensors, all dynamic measurements were converted into the same unit, either force or acceleration. Based on careful alignment, the striker bars in all these systems were assumed to be under one-dimensional, elastic deformation during impacting. The strain histories recorded by the sets of strain gages could be multiplied by the Young's modulus and cross-sectional areas of the striker bars to determine the correspond impacting forces. The corresponding accelerations were calculated by dividing the impact forces by the mass of the bars.

#### 3.1 Vertical Impact Test Systems

##### A. Load Cell Type

In this type of impacting testing, two kinds of specimen were used in the investigations: one was a 19mm-thick aluminum plate covered by a 13 mm-thick vinyl layer, while the other was covered by a 3 mm-thick vinyl layer.

For the specimen covered with the thicker-vinyl layer, all three sensors had very similar acceleration histories through the entire impact event if the maximum acceleration was around 50 g. If the maximum acceleration was increased to 140 g, the similarity of the acceleration histories maintained very well except at the very end of the impact event, as shown in Figure 2.3(a). It was also noted that the curve obtained from the load cell was quite smooth. The curves obtained from the piezoelectric and piezoresistive accelerometers, however, had very large oscillations. If the maximum acceleration was raised to 250 g, the oscillation in the accelerometers became very significant. In Figure 2.3(a), the oscillation frequency in the curves from the accelerometers, after 8 ms, matches well with one of the natural frequencies of the drop weight (710 Hz), and the oscillation frequency in the curve from the piezoresistive accelerometer, especially from 3 ms to 7 ms, is close to the first bending frequency of the impact tup (~3.2 kHz).

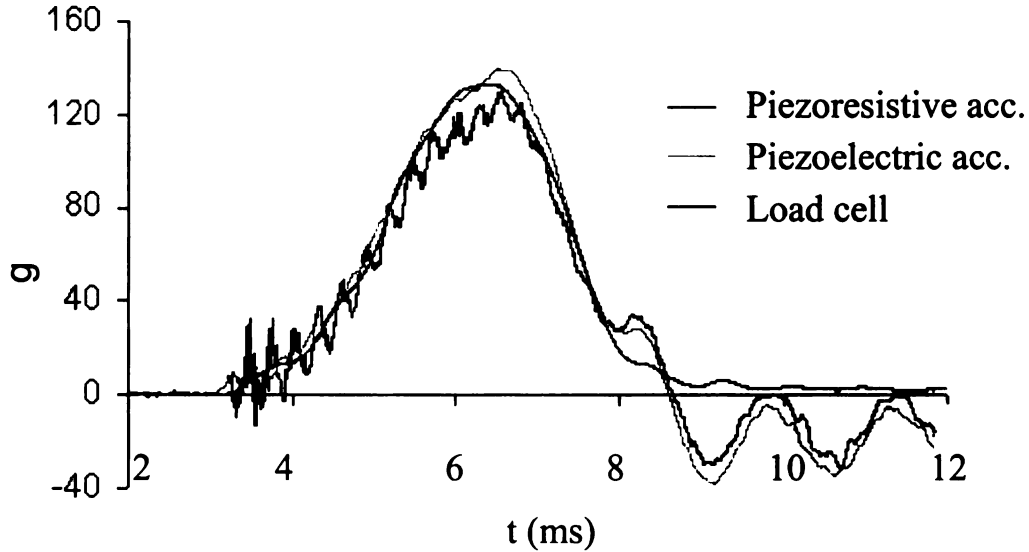


Figure 2.3(a). Aluminum with thick vinyl under vertical impact, load cell type

For the specimen covered with the thinner-vinyl layer, the acceleration curves obtained from the two accelerometers were very similar, though the curve from the piezoelectric accelerometer was slightly higher than that from the piezoresistive accelerometer. However, the result obtained from the load cell was quite different from those obtained from the accelerometers. As shown in Figure 2.3(b), all three curves are very similar up to the peak acceleration. Beyond it, however, huge oscillations are seen in the curves from the accelerometers, while that obtained from the load cell remains to be very smooth. The major oscillation frequency in the curves from the accelerometers matches well with one of the natural frequencies of the drop weight (710 Hz).

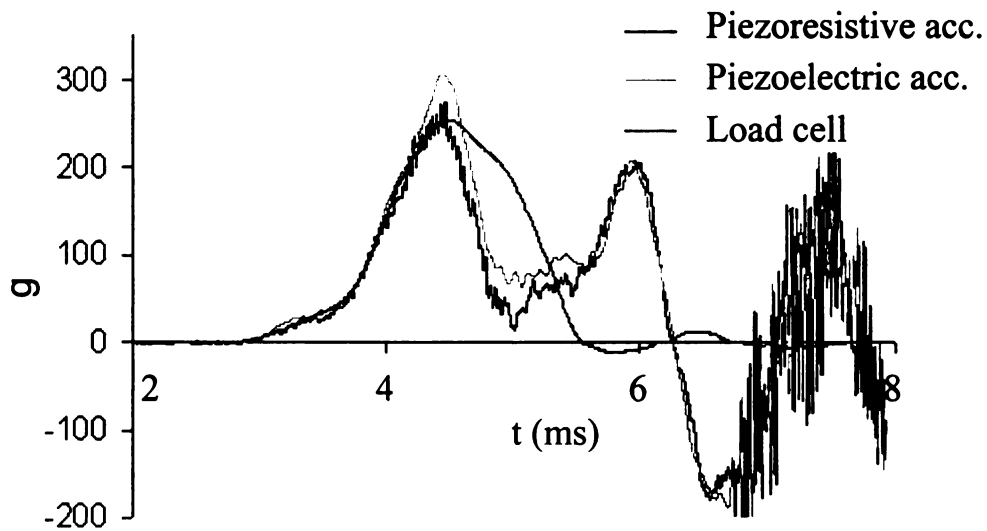


Figure 2.3(b) Aluminum with thin vinyl under vertical impact, load cell type

The results from the foregoing experiments seemed to indicate that the measurements from the two types of accelerometers agreed with each other quite well in all tests. However, the measurements from the load cell and the accelerometers agreed well only when the maximum acceleration was relatively low and the impacted specimen was relatively soft. When the maximum acceleration became higher and the impacted specimens became harder, the results between them deviated greatly.

## B. Striker-Bar Type

In these vertical impact tests, the specimens were identical to those used in the vertical impact tests based on the load-cell type. The specimens were placed on the specimen holder supported by the load cell.

When the maximum acceleration was relatively low and the impact specimen was relatively soft, the acceleration histories from the striker bar, the load cell, and the piezoelectric accelerometer were very similar although minor oscillation was found in the result obtained from the striker bar. Figure 2.4(a) shows the results for the aluminum plate covered with the thick vinyl when the maximum acceleration was up to 70 g.

When the maximum acceleration became higher and the impact specimen became harder, the acceleration histories from the striker bar and the load cell remained to be consistent. However, that obtained from the piezoelectric accelerometer had major oscillation and deviated significantly from those obtained from the strain-gage based sensors. Figure 2.4(b) shows the results for the aluminum plate covered with the thin vinyl when the maximum acceleration was up to 250 g. Once again, the curve from the accelerometer shows the natural frequency of the drop weight – 710 Hz.

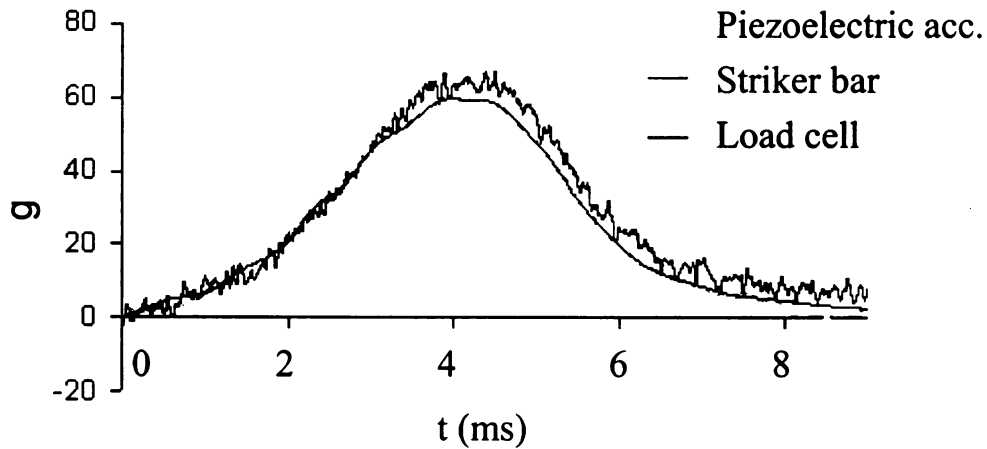


Figure 2.4(a) Aluminum with thick vinyl under vertical impact, striker-bar type

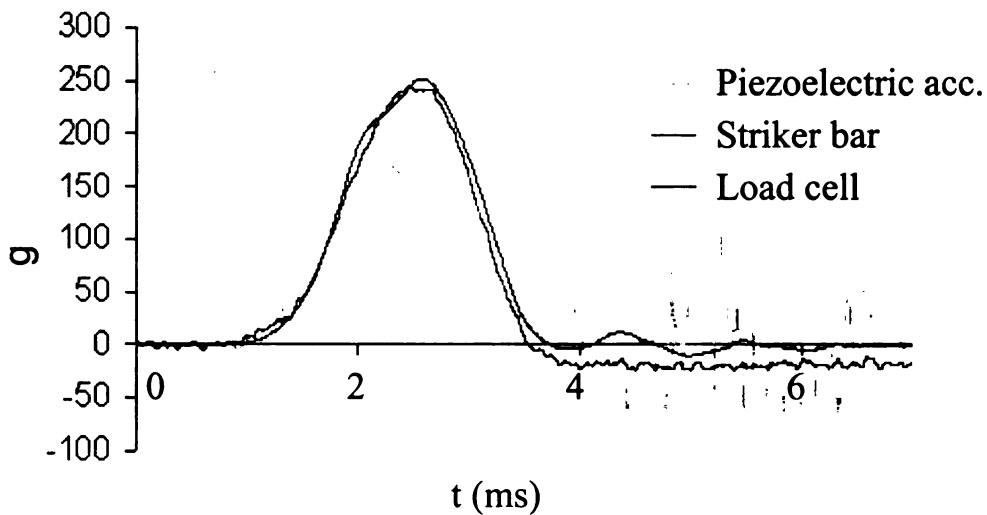


Figure 2.4(b) Aluminum with thin vinyl under vertical impact, striker-bar type

It was also noted that the results from the striker bar and the load cell agreed with each other very well in all cases. These agreements were believed to be attributed to the fact that both the striker bar and the load cell were based on



deformation. The different characteristics between the strain-gage-based sensors, e.g. the striker bar and the load cell, and the accelerometers, either piezoelectric type or piezoresistive type, were once again verified.

### 3.2 Horizontal Impact Systems

#### A. Type I

Two kinds of specimen were investigated. One was a 25.4 mm steel plate covered with a layer of rubber of 12.7 mm and the other was a 3.2 mm thick glass/epoxy plate. The two sensors gave similar acceleration histories for both kinds of specimen. Figure 2.5(a) and 2.5(b) show the results. The striker bar seems to oscillate more than the piezoresistive accelerometer in the impact test for the steel plate covered with rubber. However, the piezoresistive accelerometer seems to oscillate more than the striker bar in the impact test for the glass/epoxy plate. In Figure 2.5(b), the oscillation frequency in the curve from the piezoresistive accelerometer is very close to the striker's first bending frequency – 2020 Hz.

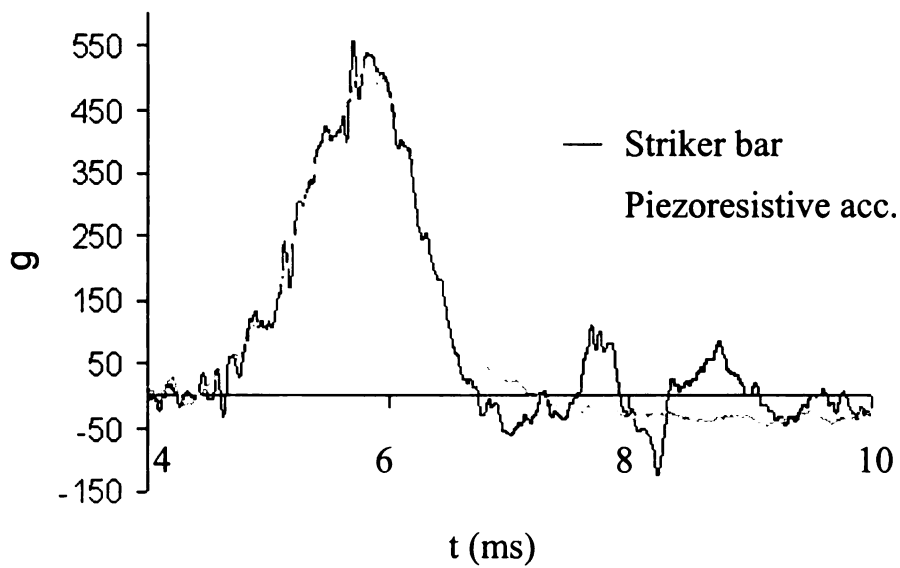


Figure 2.5(a) Steel with rubber under horizontal impact, type I

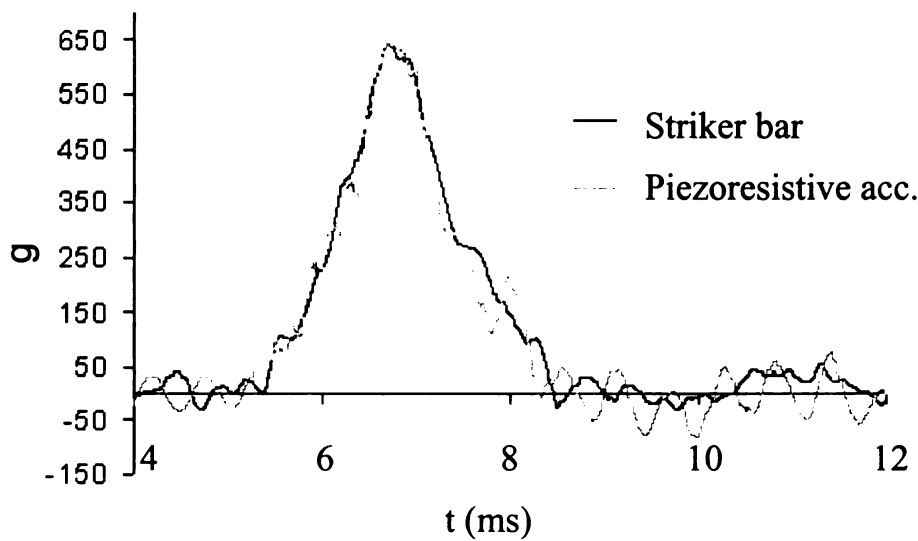


Figure 2.5(b) Glass/epoxy under horizontal impact, type I

## B. Type II

In this test, the load cell was impacted by a striker bar horizontally. The spherical nose of the top of the load cell used in the vertical impact test (the load cell type) was replaced by a flat nose with a diameter slightly smaller than that of the striker bar. The impact duration was very short due to the high rigidities of the top of the load cell and the striker bar. The force histories are shown in Figure 2.6. The force history from the striker bar has double peaks while that from the load cell has only one single peak. The slow increasing / decreasing shapes of the curve from the load cell are probably due to its low frequency range (4 kHz). The oscillation frequency in the curve from the striker bar (~20 kHz) matches well with the inverse of the elastic wave traveling time in the 250 mm striker bar.

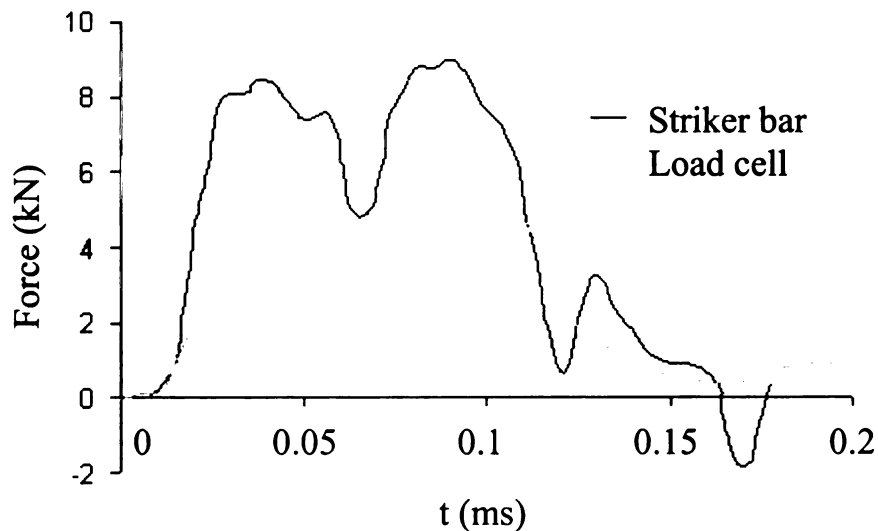


Figure 2.6 Striker bar and load cell under horizontal impact, type II

### C. Type III

In this test, the striker bar impacted perpendicularly on a 25 mm thick steel plate covered with a layer of rubber of 1 mm. There were three sets of strain gages on the striker bar. Their force histories are shown in Figure 2.7. They have similar oscillation patterns. Each major oscillation seems to include three to four minor oscillations. As shown in the diagram, the maximum force decreased as the gages were located farther away from the impact end.

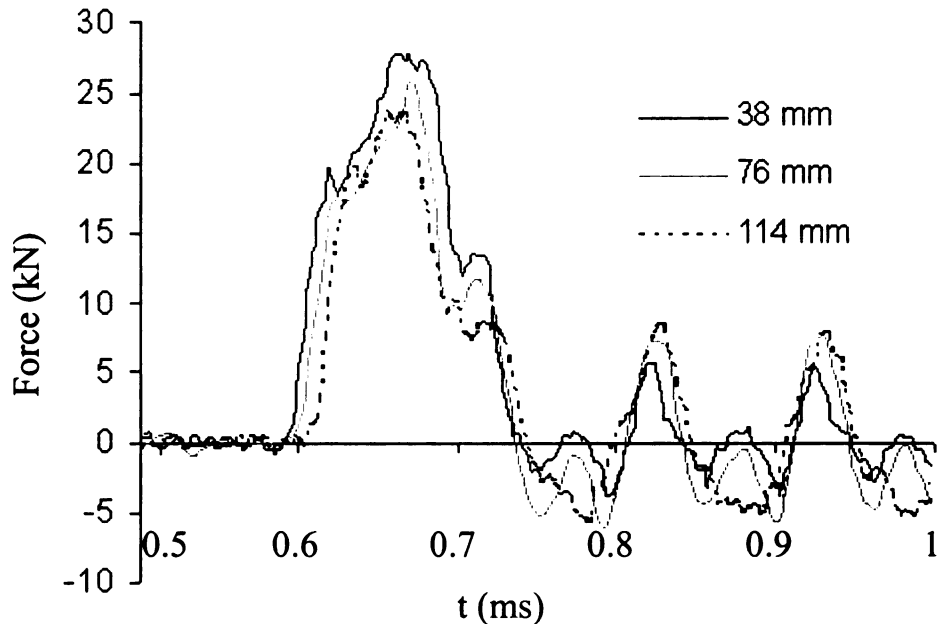


Figure 2.7 Force histories from type III horizontal impact

### 3.3 Structures' spectrum tests and signals' spectral analysis

Spectral testing results for the drop weight system and the striker bar with piezoresistive accelerometers are presented in Table 2.2.

Table 2.2 Spectrum testing results

<b>Drop weight impact device</b>	The whole system	84 Hz
	The cover plate on drop weight	240 Hz
	Drop weight, vibrate horizontally	420 Hz
	Drop weight, knock on top beam	528 Hz
	Drop weight, knock on lower beam	710 Hz
<b>Striker with piezoresistive accelerometer</b>	First bending mode	2020 Hz
	Second bending mode	5360 Hz

The spectral analysis of the signals in Figure 2.3(b), Figure 2.4(b), Figure 2.5(b), and Figure 2.7 are listed in Table 2.3.

Table 2.3 Spectrum analysis of the signals in Figure 2.3(b), 2.4(b), 2.5(b) and 2.7

		<b>Major frequencies of the signals in frequency domain</b>				<b>Comments</b>
		<b>Piezo-electric Acc.</b>	<b>Piezo-resistive Acc.</b>	<b>Load Cell</b>	<b>Striker</b>	
<b>vertical</b>	<b>Figure 2.3(b)</b>	100 Hz, 700 Hz	100 Hz, 700 Hz, 26500 Hz	100 Hz	N/A	Drop weight natural frequency: 710 Hz; Piezoresistive Accelerometer's resonance frequency: 25000 Hz
	<b>Figure 2.4(b)</b>	200 Hz, 710 Hz	N/A	200 Hz	200 Hz	
<b>horizontal</b>	<b>Figure 2.5(b)</b>	N/A	170 Hz, 1920 Hz	N/A	170 Hz	First natural frequency of the striker: 2020 Hz
	<b>Figure 2.7</b>	N/A	N/A	N/A	10 kHz, 20 kHz	They are the longitudinal natural frequencies of the striker

## 4. DISCUSSIONS

### 4.1 Load Cell vs. Striker Bar

The striker bars were built based on strain gages. When the striker bars deformed, they caused the strain gages attached to them to undergo the same deformations. The deformation histories were then converted into force histories with a calibration factor. The load cell was constructed based on the same principle. Experimental results based on Figures 2.4 clearly indicated that the load cell and the striker bars, both based on strain gages, gave similar measurements. Their differences in Figure 2.6 are due to the low frequency range of the load cell and the wave superposition effect in the striker bar. The wave superposition effect will be discussed later.

#### 4.2 Piezoelectric Accelerometer vs. Piezoresistive Accelerometer

The two accelerometers used in this research were quite different in their constructions and measurement principles. When subjected to excitation, the piezoelectric accelerometer produced charges while the piezoresistive accelerometer experienced resistance change. The application ranges of acceleration and frequency were different for the accelerometers, as was the error percentage. However, the results obtained from the experiments, as shown in Figures 2.3, were very similar. The small differences between their results are probably due to the different locations at which they were mounted.

#### 4.3 Strain Gages vs. Accelerometers

The difference between the measurements from the strain gage based sensors and the accelerometers were very significant. The strain gage based

sensors measured the impact forces based on the deformation of the strain gages, which was also the deformation of the impactor. The accelerometer measured the accelerations based on the relative motions between the inside mass of the accelerometer and its base, which is also the impactor on which the accelerometers attached. When an impactor is subjected to contact-impact, it experiences both deformation and rigid body motion. If a strain gage is carefully mounted on the impactor, it should deform with the impactor, and its measurement should be almost the same as the deformation of the impactor. The strain gages, however, can not sense the rigid body motion. On the contrary, accelerometers measure the rigid body motion of its base, and the motion is from both the deformation and the whole impactor's motion. Hence, the sensitivities of the strain gage and the accelerometer are strongly dependent on the rigidity (or flexibility) of the impactor. An impactor with adequate flexibility is required for strain measurements, while high rigidity is desired for high accuracy of acceleration measurements. The strain rate dependency and viscoelastic property of the impactor are also important to the responding time and the measurement accuracy of the sensors. Rigid materials tend to respond instantly, while flexible materials have a time delay. Hence, time lagging and response overshooting can occur. They usually are not significant, except that the impact period is very short.

Experimental results seemed to support the aforementioned statements. In the vertical impacts, as shown in Figures 2.3(a) and 2.4(a), the strain gage based sensors and the accelerometers gave similar acceleration curves when the

specimen was relatively soft and the impact velocity was relatively low. However, as the specimen became harder and the impact velocity became higher, the measurements from the accelerometers showed significant oscillations, as shown in Figure 2.3(b) and 2.4(b). This resulted in much larger discrepancies with those from the strain gage based sensors. The source of the oscillations was believed to be tied to the vibrations of the impactor, the specimen, and the impact test system. The discrepancies between the two types of sensors, however, were not significant, as shown in Figures 2.5.

#### 4.4 Vertical Impact vs. Horizontal Impact

The vertical impact systems used gravitational force to perform low-velocity impacts, up to 4m/s. A pneumatic system could be added to double the impact velocity. The horizontal impact systems, however, were able to achieve higher impact velocities with the use of a high compressed gas. The experimental results of the vertical impacts, shown in Figures 2.3 and 2.4, revealed that the difference of acceleration histories between the two types of sensors became very significant at high acceleration levels. However, the difference of acceleration histories between the two types of sensors from the horizontal impacts, shown in Figures 2.5, was not affected significantly at high acceleration levels. This is because the lower natural frequencies of the vertical impact systems played a key role in the vertical impacts.



## 5. ANALYSIS

### 5.1 Effects of Masses

The impact-contact forces occurred between the impactors and the test specimens were of primary interest in the impact tests. However, both strain gages and accelerometers could not be installed exactly at the contact surfaces. There was always a fore-mass, such as the tup of the impactor, located in front of the sensing component. An aft-mass was also frequently added behind the sensing component for various impact simulations. Both the fore-mass and the aft-mass were usually made of rigid materials and firmly connected to the sensing component. These masses, however, had a significant effect on the measurements.

Figure 2.8(a) shows the organization of an impactor, while Figure 2.8(b) shows the free-body diagrams of individual components. Based on Newton's second law, the following equation of motions for the aft-mass component, sensing component, and fore-mass component can be established.

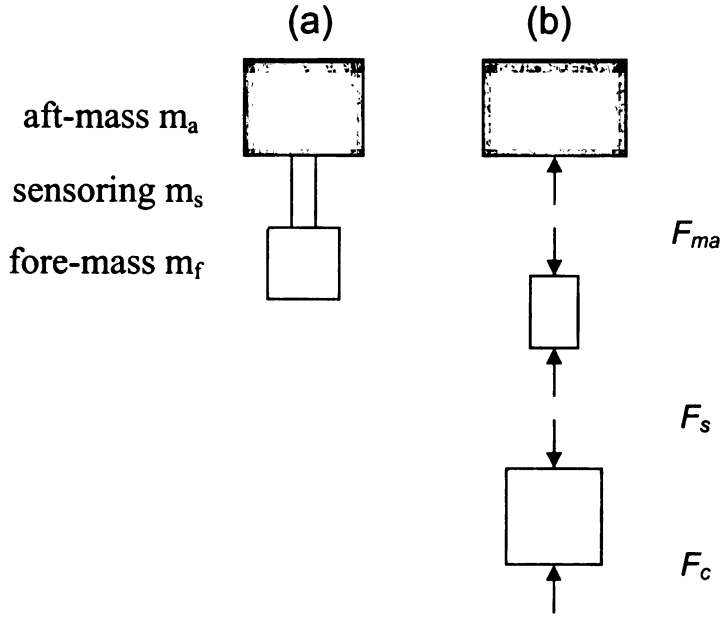


Figure 2.8 Schematic diagrams of (a) impactor and (b) individual components

$$F_{ma} - m_a g = m_a a_{ma} \quad (1a)$$

$$F_s - m_s g - F_{ma} = m_s a_{ms} \quad (1b)$$

$$F_c - m_f g - F_s = m_f a_{mf} \quad (1c)$$

Rewriting the equations, they become

$$F_{ma} = m_a (g + a_{ma}) \quad (2a)$$

$$F_s = F_{ma} + m_s (g + a_{ms}) = m_a (g + a_{ma}) + m_s (g + a_{ms}) \quad (2b)$$

$$F_c = F_s + m_f (g + a_{mf}) = m_a (g + a_{ma}) + m_s (g + a_{ms}) + m_f (g + a_{mf}) \quad (2c)$$

If the mass of the sensor  $m_s$  is negligible, the foregoing equations can be simplified as follows.

$$F_{ma} = m_a (g + a_{ma}) \quad (3a)$$

$$F_s = F_{ma} + m_s (g + a_{ms}) = m_a (g + a_{ma}) \quad (3b)$$

$$F_c = F_s + m_f (g + a_{mf}) = m_a (g + a_{ma}) + m_f (g + a_{mf}) \quad (3c)$$

Apparently, there is always a difference between the force measured by the sensor  $F_s$  and the real contact force  $F_c$ . The difference between them is associated with the inertia force of the fore-mass, i.e.  $m_f (g + a_{mf})$ . Hence, in order to reduce the measurement error, it is necessary to reduce the fore-mass. Similarly, in order to compare the measurements from different sensors, it is imperative that the sensors must be installed in the same locations. Results given in Figure 2.7 seem to support this analysis.

Once the fore-mass becomes negligible, all three force measurements become the same and are equal to the inertia force of the aft-mass, i.e.

$$F_{ma} = F_s = F_c = m_a (g + a_{ma}) \quad (4)$$

Besides, it is interesting to point out that the gravitational acceleration will vanish if the vertical impact system is changed to a horizontal impact system, i.e.

$$F_{ma} = m_a a_{ma} \quad (5a)$$

$$F_s = F_{ma} + m_s a_{ms} = m_a a_{ma} \quad (5b)$$

$$F_c = F_s + m_f a_{mf} = m_a a_{ma} + m_f a_{mf} \quad (5c)$$

Moreover, in static loading, the following equilibrium equations hold.

$$F_{ma} = F_s = F_c \quad (6)$$

## 5.2 Effect of Wave Propagation

When a striker bar was impacted on a specimen, the compressive strain wave generated at the impact-contact surface would propagate to the opposite end of the striker bar. The wave then was reflected back from the free end of the bar as a tensile strain wave. This process could repeat many times until the strain wave was completely attenuated. If the striker bar was long, the strain wave would propagate in the striker bar back and forth without superposition. A good example could be found in a split Hopkinson's pressure bar. On the contrary, if the striker bar was relatively short and the length of the strain wave was relatively long, superposition of the transmitted portion and the reflected portion of the strain wave would take place. The superposed wave pattern could become very complex and be recorded in the measurements.

The striker bars used in the foregoing horizontal impact tests had a cylindrical shape. The wave patterns in them, hence, could be analyzed with ease even if complex superposition were involved. On the contrary, the wave patterns in the load cell could not be simple because of the complex geometry of the load cell.

### A. Basic Wave Equation

Consider a slender bar under uniaxial stress and neglect the Poisson's effect. For a small segment of the bar, the equation of motion can be expressed as, [22]

$$\frac{\partial}{\partial x} \left[ EA \frac{\partial u}{\partial x} \right] = \rho A \frac{\partial^2 u}{\partial t^2} + \eta A \frac{\partial u}{\partial t} - q \quad (7)$$

where  $E$  is Young's modulus,  $\rho$  is density,  $A$  is the cross-sectional area,  $\eta$  is damping coefficient per unit volume,  $q$  is the external force per unit length,  $t$  is time, and  $u$  is displacement along the axial direction  $x$ . Assuming that both the modulus and the cross-sectional area do not vary with position and the solution of Eqn. (7) can be expressed in spectral representation, it yields

$$EA \frac{d^2 \hat{u}}{dx^2} + (\omega^2 \rho A - i\omega \eta A) \hat{u} = 0 \quad (8)$$

where  $\omega$  is the angular frequency. The solution of the foregoing equation is

$$\hat{u}(x) = C_1 e^{-ikx} + C_2 e^{+ikx}$$

$$k \equiv \sqrt{\frac{\omega^2 \rho A - i\omega \eta A}{EA}} \quad (9)$$

where  $C_1$  and  $C_2$  are undetermined amplitudes. With the inclusion of time variation, this solution corresponds to two waves: a forward wave and a backward wave.

$$u(x, t) = \sum C_1 e^{-i(kx - \omega t)} + \sum C_2 e^{+i(kx + \omega t)} \quad (10)$$

If a force history  $P(t)$  is applied to a bar end, then at  $x=0$  (*the bar end*)

$$EA \frac{\partial u(x, t)}{\partial x} = -p(t)$$

Let all functions of time have the spectral representation; the boundary condition becomes, in expanded form

$$EA \frac{d}{dx} \sum_n \hat{u}_n(x) e^{i\omega_n t} = - \sum_n \hat{p}_n e^{i\omega_n t}$$

This has to be true for all time, hence the equality must be true on a term by term basis giving

$$EA \frac{d \hat{u}_n}{dx} = - \hat{p}_n$$

At  $x=0$ , there is only a forward moving wave, so the condition becomes

$$EA \{-ikC_1\} = -\hat{P} \quad \text{or}$$

$$C_1 = \frac{\hat{P}}{ikEA}$$

The displacement of the forward wave becomes

$$u(x, t) = \frac{1}{EA} \sum \frac{\hat{P}}{ik} e^{-i(kx - \omega t)} \quad (11)$$

and the corresponding force is

$$F(x, t) = -ikEAu = - \sum \hat{P} e^{-i(kx - \omega t)} \quad (12)$$

## B. Simulation

As mentioned earlier, a compression wave occurred in a striker bar when it collided with a solid. The wave propagated into the free end and reflected back with a tensile magnitude. It was believed that this tension wave caused the separation effect of the striker bar from the solid when it reached the contact-impact surface. The wave would again rebound from this surface as compression wave and continue to propagate between the two free ends until the strain energy dissipated.

In simulating the wave propagation in the striker bar, a sinusoidal wave was input into the striker bar, as shown in Figure 2.9. The following material properties and wave parameters were used in the simulation:  $E = 192 \text{ GPa}$ ,  $\rho = 7,560 \text{ kg/m}^3$ ,  $\omega = 2\pi f$ ,  $T = 1/f = 2L/C$ ; where the length of the striker bar  $L = 250 \text{ mm}$  and the elastic wave velocity  $C = \sqrt{E/\rho} = 5,040 \text{ m/s}$ . With six rebounds, the overlapped wave pattern is shown in the diagram along with the experimental measurement. They seem to agree with each other reasonably. This result indicated the nature of wave propagation in the cylindrical striker bar and the difference between the input signal and what was experienced in the bar.

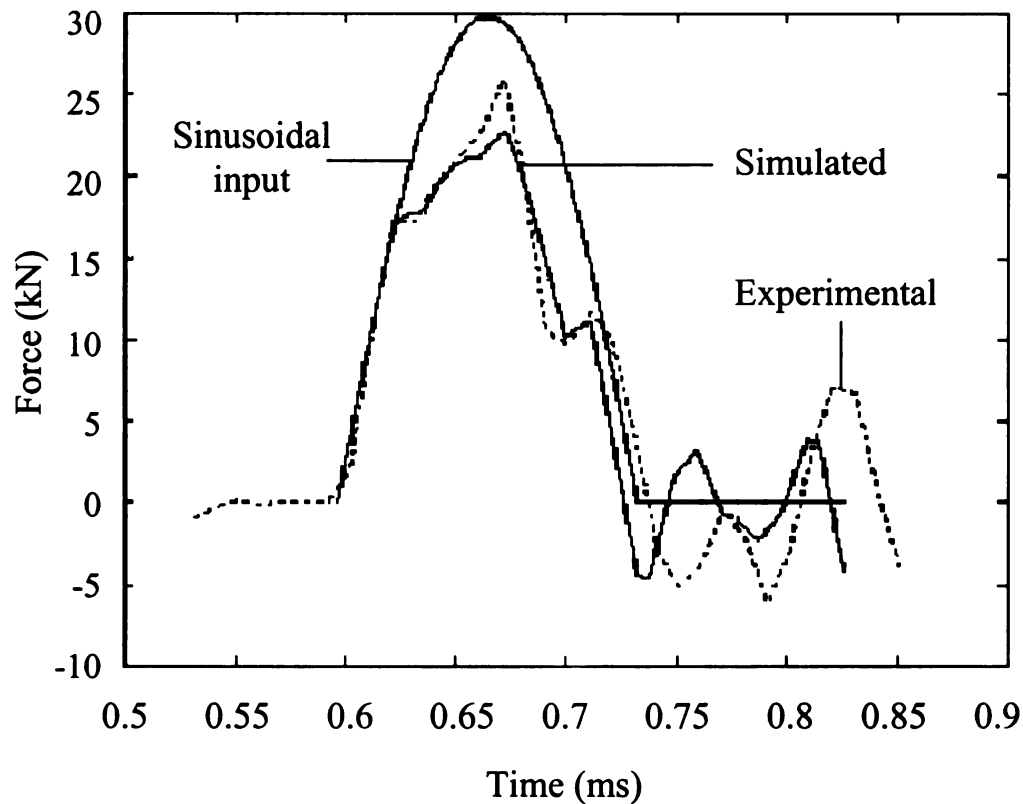


Figure 2.9 Wave patterns based on measurement and simulation.

A similar analysis was also applied to the horizontal impact of type II, as shown in Figure 2.6. Apparently, there was a dent in the force history measured by the striker bar. Figure 2.10 also shows the apparent dent in the simulation. The “square” input was based on a 30-term Fourier series to represent the blunt impact between the striker bar and the load cell. This result further confirmed the nature of wave propagation in the striker bar.



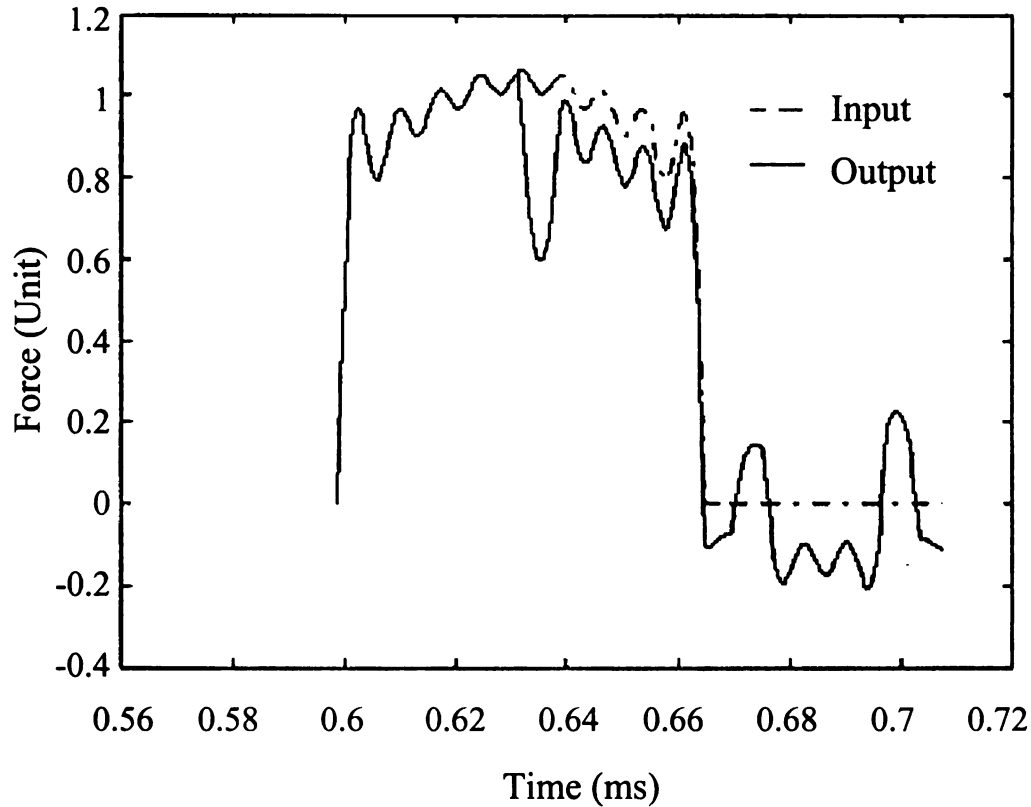


Figure 2.10 Simulation of apparent dent in force history due to blunt impact.

Since the compression wave generated at the impact end of the striker will reflect from the free end as a tension wave, and this tension wave will reflect from the impact end again as compression wave, they may cancel each other at the sensor position if the tension wave does not lose much at the impact end. This explains the phenomena that the striker gave the same results with the load cell in soft impacts, which had relatively longer impact durations and the wave superposition made minor oscillation around the true impact curve. For the hard impacts, such as type II and III of the horizontal impact, the impact duration was close to the wave traveling period, and the wave superposition effect shows up and can not be neglected.

## 6. CONCLUSIONS

The vertical impact systems are simpler and less costly than the horizontal impact systems. However, the latter are free of gravitational effect and can achieve higher impact velocity. In measuring the contact-impact forces, the strain-gage based sensors are not sensitive to oscillation as much as the accelerometers because the former are based on deformation while the latter, the motion. This is especially true in vertical impact tests. Among the strain-gage based sensors, the load cell seems to be more effective for relatively soft specimens, while the striker is more suitable for recording hard impact if the wave superposition effects can be eliminated. Accordingly, a horizontal impact system using a strain-gage-based force transducer seems to be an ideal system for contact-impact testing.

## ACKNOWLEDGMENTS

The author thanks to the U.S. Army TARDEC, Warren, Michigan, for financial support.

## REFERENCES

- [1] S. P. Virostek, J. Dual and W. Goldsmith, Direct Force Measurement in Normal and Oblique Impact of Plates by Projectiles, Int. J. Impact Engng. Vol. 6, No. 4, p247-269, 1987
- [2] Ralph Burton, Vibration and Impact, Dover Publications, Inc. New York 10014, 1968
- [3] Liu, D., Lee, C. Y., and Lu, X., "Reparability of Impact-induced Damage in SML Composites", J. Composite Materials, 27(13), 1257-1271, 1993
- [4] Liu, D., and Dang, X., "Testing and Simulation of Laminated Composites Subjected to Impact Loading", ASTM STP 1330, R. B. Bucinell, Ed. 273-284, 1998
- [5] Jun Lu, Mechanical Behavior of a Bulk Metallic Glass and its Composite over a Wide Range of Strain Rates and Temperatures, Thesis for the Degree of Doctor of Philosophy, California Institute of Technology, Pasadena, California, 2002
- [6] L. E. Malvern, The Propagation of Longitudinal Waves of Plastic Deformation in a Bar of Material Exhibiting a Strain-rate Effect, Journal of applied mechanics, Trans. ASME, 18, p203-208, 1951
- [7] Sia Nemat-nasser; Jon B. Isaacs; John E. Starrett, Hopkinson Techniques for Dynamic Recovery Experiments, Proc. Roy. Soc. London 435 (A), p371-391, 1991
- [8] M. Vural and D. Rittel, An Educational Visualization Technique for Kolsky (split Hopkinson) Bar, Experimental Techniques, Nov-Dec 2003, p35-39. 2003
- [9] Daniel J. Inman, Engineering Vibration, Prentice Hall, Englewood Cliffs, New Jersey 07632, 1994
- [10] Robert W. Lally, PCB Piezotronics, Inc. Buffalo, N. Y. Testing the Behavior of structures, Reprinted from TEST, Aug./September 1978
- [11] William G. Halvorsen, David L. Brown, Impulse Technique for Structural frequency Response Testing, Sound and Vibration, November 1977, p8-21, 1977
- [12] Michael J. Dixon, Development of a Load-cell compensation System,

- Experimental Mechanics (31), p21-24, 1991
- [13] Michael J. Dixon, A Traceable Dynamic Force Transducer, Experimental Mechanics (30), p152-157, 1990
- [14] Jan Hjelmgren, Dynamic Measurement of Force-A literature Survey, SP Swedish National Testing and Research Institute, SP Measurement Technology, SP REPORT 2002:27
- [15] Mark Sheplak, Aravind Padmanabhan, Martin A. Schmidt, and Kenneth S. Breuer, Dynamic Calibration of a Shear-stress Sensor Using Stokers-layer Excitation, Massachusetts Institute of Technology, Cambridge, Massachusetts 02139 AIAA Journal, Vol. 39, No. 5, May 2001
- [16] Jurg Dual, Application of a Transducer Embedded in a Projectile for Penetration Force Measurement, Master's thesis, University of California, Berkeley, 1984
- [17] S. Venzi, A. H. Priest and M. J. May, Influence of Inertial Load in Instrumented Impact Tests. Impact Testing of Metals, ASTM STP 466, American Society for Testing and Materials, p165-180, 1970
- [18] D. J. Frew, M. J. Forrestal, W. Chen, Pulse Shaping Techniques for Testing Brittle Materials with a Split Hopkinson Pressure Bar, Experimental Mechanics (42), No. 1, p93-106, 2002
- [19] W. Chen, F. Lu, D. J. Frew, M. J. Forrestal, Dynamic Compression Testing of Soft Materials, Journal of Applied Mechanics (69), p214-223, 2002
- [20] D. J. Frew, M. J. Forrestal, W. Chen, A Split Hopkinson Pressure Bar Technique to Determine Compressive Stress-strain Data for Rock Materials, Experimental Mechanics (41), No. 1, p40-67, 2001
- [21] D. R. Ambur, C. B. Prasad and W. A. Waters, Jr., A Dropped-weight Apparatus for Low-speed Impact Testing of Composite Structures, Experimental Mechanics 35(1), p77-82, 1995
- [22] James F. Doyle, Waves Propagation in Structures, Spectral Analysis Using Fast Discrete Fourier Transforms, Second Edition, Mechanical Engineering Series, 1997

## **CHAPTER THREE**

### **WAVE PROPAGATION IN FORCE TRANSDUCERS**

#### **ABSTRACT**

Instrumented projectiles for impact testing have great advantages over non-instrumented projectiles. Because of the length restriction on the impact projectiles, wave reflection and wave superposition can take place in the projectiles and result in distorted wave signals. In order to recover the initial impact wave, several techniques based on both mechanical and numerical methods are proposed. Experimental results based on instrumented short rods showed the feasibility of the proposed techniques for reducing the wave reflection and reconstructing the initial impact wave to some extent. The techniques were used for designing an instrumented projectile for ballistic impacts.

## 1. INTRODUCTION

The capability of energy absorption plays an important role in the design of vehicle survivability and occupant safety. In order to characterize the energy absorption capability of a material or a structure subjected to impact loading, several experimental techniques have been developed and used. Among them, the simplest one is perhaps the method to measure the velocities of the impactor before and after it contacts a specimen [1,2]. The energy absorbed by the specimen can be taken as the difference of the kinetic energy of the impactor before and after the impact event. This technique requires a relatively simple setup for velocity measurements and works for both perforation and non-perforation (rebounding from the specimen) cases. However, this technique does not give detailed information during the impact event, such as the deformation of the specimen and the change of the impact force.

To characterize the energy absorption capability of a specimen and even to understand the mechanism of energy absorption of it, it is necessary to identify the interaction between the impactor and the specimen through the entire impact event. Several experimental techniques for measuring the histories of displacement, velocity, acceleration, and force during impact events have been developed and are commercially available. For example, accelerometers of various designs and data acquisition systems with high-speed capability have been developed for measuring acceleration history in crash tests [3,4]. They have been found to be useful for investigating relatively soft materials and

structures. However, their low natural frequencies may hinder their uses in high-speed impact events.

With the advancement in laser diode technology, high-speed photo-detectors, and fiber optics, researchers have been able to build velocity measurement devices of various kinds to measure the velocity of impactors [5,6]. Most of them are able to sense very small changes in velocity and give velocity history with high accuracy. However, the complexity of the testing environment and impactor geometry should not be underestimated because they can complicate the testing setup and affect the measurement.

High-speed photography can provide detailed images of what exactly happens during impact events [1,2,7,8,9]. With sufficient photographs, the displacement history, the velocity history, and even the acceleration history can be identified. Since most impact events last only a very short time period, such as less than 1 millisecond, high-speed cameras with the capability of recording sufficient frames are required for obtaining accurate displacement, velocity, and acceleration histories. It should be noted that high-speed cameras capable of recording 1 million frames per second are very costly.

Strain gages have been commonly used for measuring strain history. Owing to their technology maturity, low sensitivity to environmental impact, accessibility, and low cost, strain gages have been used in device designs more frequently than many modern sensors such as laser and fiber-optic based sensors. In fact, strain-gage techniques are the most common methods used for measuring mechanical parameters involved in impact events [10]. The measured strain

history can then be converted into stress history and force history for further applications.

Based on the advantages of strain gages mentioned above, the objective of this study is to investigate the feasibility of using strain gages for measuring dynamic forces during impact events. High speed, high acceleration, large force, and short duration are expected to be involved in these events. Issues concerning the wave propagation are expected to be the dominant subjects in the study.

## 2. FORCE TRANSDUCERS

Many force transducers are commercially available. Although they have various geometries and use different types of sensors, many of them are based on a common design fundamental – measuring force history from deformation history. Accordingly, each deformation based force transducer has a precisely designed body to sense the deformation during loading while the remaining components of the transducer are considered to be rigid bodies.

The sensors for measuring deformation can be based on electrical, mechanical, acoustical, or optical fundamentals. Once a deformation history is identified, it can be converted into a force history with the use of physical laws. A coefficient called the calibration factor is usually established for direct conversion from a measured signal to an output reading. The procedures required for obtaining a calibration factor are called calibration procedures.



Deformation-based force transducers work adequately for static and dynamic force measurements involving long contact duration and low skew rate (small force ramping). If the force duration is very short or the magnitude of force changes very rapidly (high skew rate), the deformation-based force transducer may not sense the force signals accurately. This is because the deformation signals at different instants may superimpose one another or some components of the transducers may not be taken as rigid bodies.

When a force transducer is loaded, the loaded area of the transducer undergoes an immediate deformation. However, the portion where the sensor is located, usually a short distance away from the loaded area, does not experience the deformation immediately. A short time period is necessary for the deformation to take place at the position where the sensor is located. The traveling of the deformation from one location to another resembles wave propagation, and the wave is called elastic if the deformation is within the elastic range of the transducer body.

The elastic wave travels through the entire force transducer and rebounds from boundaries, such as material interfaces and free ends. The sensor does not only sense the initial deformation signal corresponding to the loading but also the signals reflected from the boundaries subsequently. Besides, because the elastic wave travels quickly along hard materials commonly used for the force transducer, the signals should be of high frequency. The shape of the elastic wave may be very complex if the geometry of the transducer is of highly irregular shape. Many transducer designers choose to eliminate high-frequency signals

during signal processing. However, filtering out high-frequency signals may result in the loss of useful signals, especially for the force history with a high skew rate. In order to design a force transducer for high-speed loading, such as impact loading, the superposition of initial deformation wave and rebounded waves reflected from boundaries must be investigated.

### 3. WAVE PROPAGATION IN RODS

In understanding the fundamentals of wave propagation due to dynamic loading and its effect on signal acquisition and processing, some experiments were performed. To begin with, a cylindrical rod made of stainless steel 347 and having a diameter of 19 mm and a length of 254 mm was prepared as an impacting rod. A pair of strain gages with a gage length of 1.575 mm was mounted on the opposite surfaces, 38 mm from the impacting end. The two gages were then connected to the opposite arms of a Wheatstone bridge circuit for measuring the axial deformation while eliminating any bending effect due to impact loading. The signal from the Wheatstone bridge circuit was then transferred to a differential amplifier with a bandwidth of 10 MHz and then an oscilloscope with a sampling rate up to 100 S/s.

In impact testing, an aluminum plate with dimensions of 150 mm x 150 mm and a thickness of 13 mm was used as a target specimen. The specimen was held by two steel square plates with dimensions of 150 mm x 150 mm, a central opening of 125 mm x 125 mm, and a thickness of 13 mm. The impacting rod was launched from a gas gun with a low speed up to 20 m/s. The resultant strain

signal combining the initial strain wave signal and reflected strain wave signals was recorded by the strain gages.

### 3.1 Experiments on Effect of Rod Length

In understanding the effect of rod length on wave propagation, the 254 mm rod was trimmed by removing a section of 41 mm from the non-impacting end after the impact test, leaving the remaining length of the rod to be 203 mm for a second impact test. Similar removals were repeated. Accordingly, impacting rods with lengths of 254 mm, 203 mm, 152 mm, 127 mm, 102 mm and 76 mm were formed and used for tests.

A strain gage measures the strain at the location where the gage is mounted. If a rod undergoes elastic deformation due to static loading, the multiplication of the strain with the Young's modulus of the rod should equal the stress in the rod. Subsequently, the multiplication of the stress with the cross-sectional area of the rod should equal the force exerted on the rod. When the rod undergoes dynamic loading, the calculation of the stress, however, should be based on a dynamic Young's modulus. The stainless steel 347 mentioned earlier has an almost identical static Young's modulus and dynamic Young's modulus [11]. Hence, it is suitable for use as the body of force transducers.

Figure 3.1 shows the overall setup for the impact testing while Figure 3.2 gives the measured strain histories from the rods with various lengths. The results are significantly different, and it is believed that the differences are attributed to the difference of the length. In comparing the wave propagation in

the rods, the shape of the strain curves bears more important fundamentals than the magnitude, since the former is depended on the length of the rods while the latter is subjected to the individual impact forces.

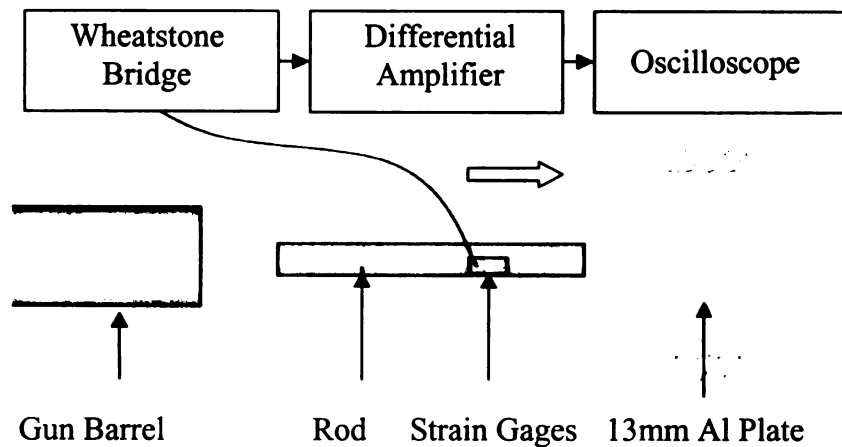


Figure 3.1 Testing setup for impacting rod.

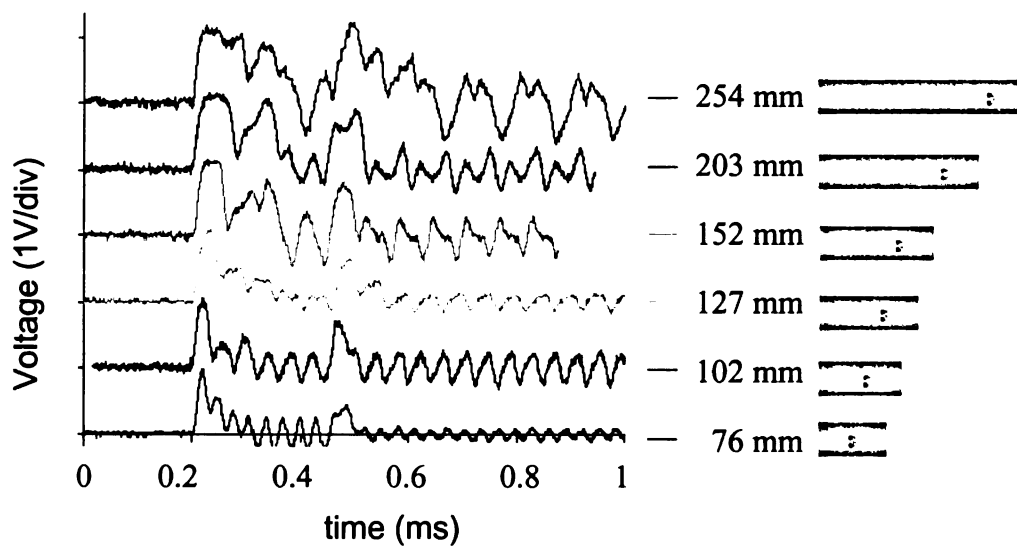


Figure 3.2 Strain histories from the impact rods with various lengths.

Some conclusions can be drawn from comparing the strain curves.

- a. The steady oscillation seems to begin around 0.5 ms for each case.
- b. As the rod becomes shorter, the oscillation frequency becomes higher.

The oscillation frequency is proportional to the inverse of the period of the elastic wave traveling between the ends of a rod.

- c. The longer the rod, the longer the flat portion of the very beginning oscillation. It indicates that a longer rod is less influenced by oscillation.

### 3.2 Experiments on Contact Duration

In order to gain insight into the strain wave propagation in the rods, a second type of experiment was performed on the rod of 76 mm length. The setup is shown in Figure 3.3 and the impact testing procedures were similar to the first type of experiments. The second type of experiment was aimed at measuring the impact duration. The fundamental design concept of the second type of experiment was to take advantage of the contact and separation between the metallic rod and a metallic specimen as a power switch. More specifically, one terminal of a DC power supply was connected to the specimen and the other terminal was connected to the rod through two resistors in series. An oscilloscope was used to measure the voltage of one resistor. Before impact, the circuit was open due to the separation between the rod and the specimen; hence, there was no reading in voltage. During the impact, however, the circuit was closed due to the contact between the rod and the specimen; hence, there was a

reading in voltage. The duration of the voltage measured by the oscilloscope should be the impact duration.

Figure 3.4 shows the measured curves. The upper one is the contact duration history while the lower one is the output of strain signal. When the rod impacts with the specimen, the duration curve shows a jump in reading. About 0.024 ms later, the strain curve shows a significant change in compressive strain. This time delay is attributed to the distance between the impact end and the gage location. During the impact, the contact between the rod and the specimen continues. The voltage remains high while the compressive strain reduces. It should be noted that the strain gages experience oscillation with tensile and compressive strains. Since an impact event should only result in compressive strains, the measured tension-compression signals may indicate an involvement of complicated wave propagation during the impact event and require more careful examination.

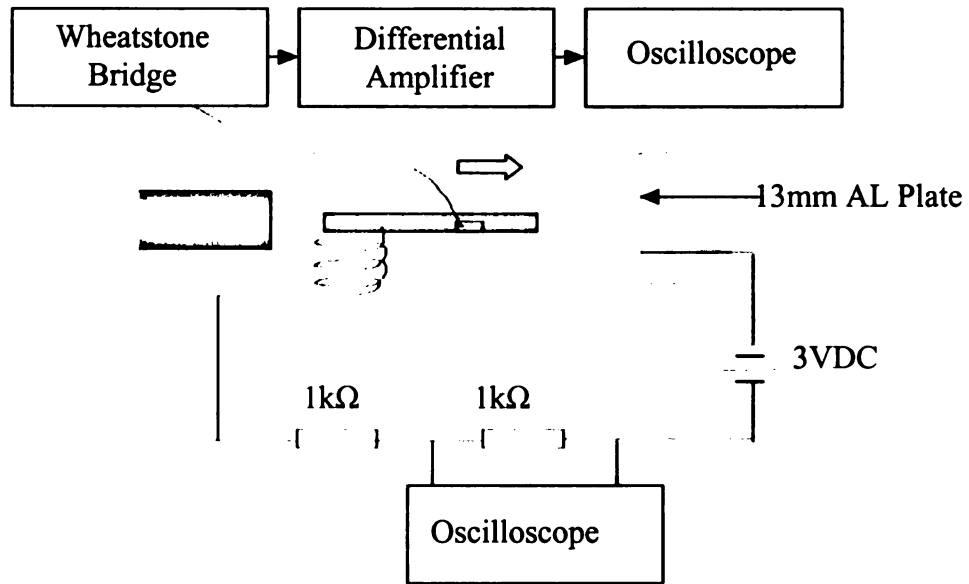


Figure 3.3 Experimental setup for impact duration and strain history.

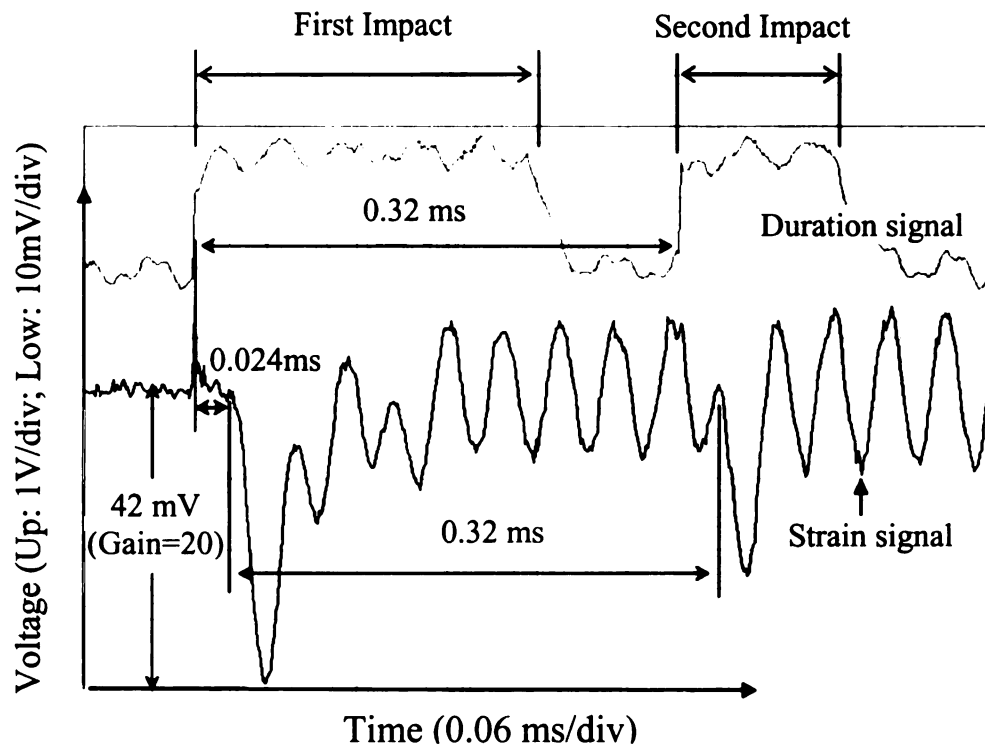


Figure 3.4 Impact duration (upper) and strain history (lower).

### 3.3 Experiments Based on Three Sets of Gages

To further understand the wave propagation and superposition in the rods, another cylindrical rod made of stainless steel 347 and having a diameter of 19 mm and a length of 254 mm was prepared. It was then installed with three sets of strain gages at 38 mm, 76 mm and 114 mm from the impact end as shown in Figure 3.5(a). Each set of strain gages consisted of two gage elements mounted on opposite surfaces of the rod. The experimental setup and the Wheatstone bridge circuit were similar to previous experiments. The rod was then launched from a gas gun and impacted onto a specimen. The three sets of strain gages measured the impact signals individually. Figure 3.5(b) shows experimental results in all three sets of strain gages.

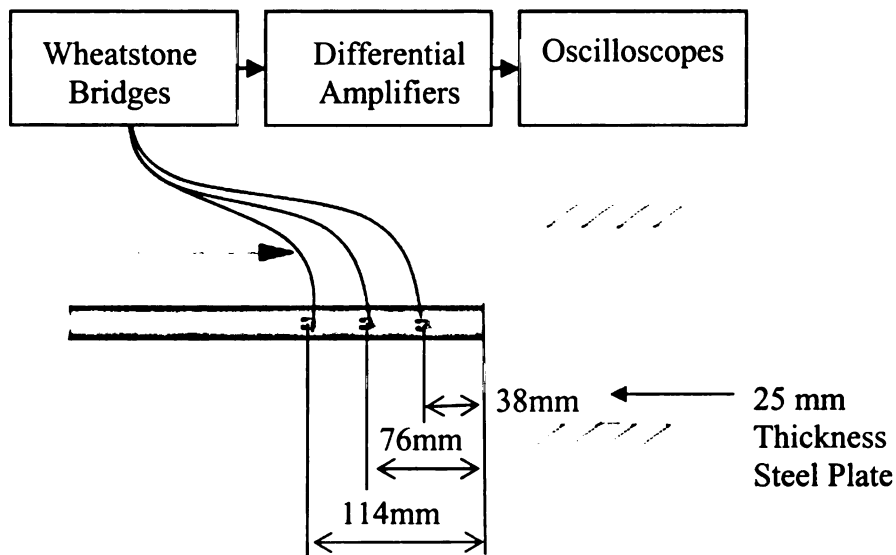


Figure 3.5(a) Experimental setup of the three sets of strain gages.



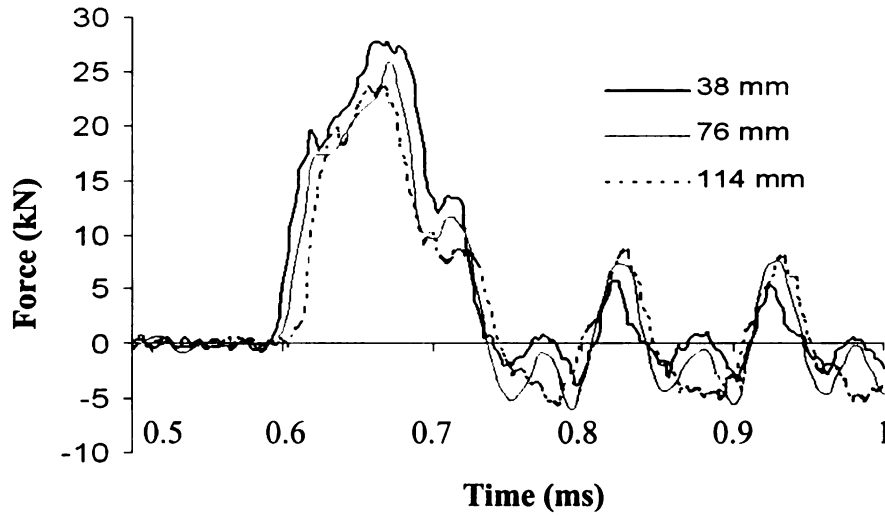


Figure 3.5(b) Experimental results of the three sets of strain gages.

As shown in Figure 3.5(b), the elastic wave was generated at the impact end and traveled along the rod. It reached the first set of strain gages located at 38 mm from the impact end, then the second set located at 76 mm from the impact end, and finally the third set located at 114 mm from the impact end. The reflected wave reached the strain gages in a reverse way, i.e. the third set of strain gages was the first to sense, followed by the second set, and the first set was the last to sense the reflected wave. The study based on comparing the magnitudes of the forces shown in Figure 3.5(b) clearly indicates the order of the wave propagation along the rod.

The wave length of the strains is also of interest. Figure 3.6 shows the signals of the strain gages located 38 mm from the impact end in the frequency domain. Two major peaks appear around 10 kHz and 20 kHz. Since the wave speed in the stainless steel 347 is around 4,934 m/s and the rod has a length of 254 mm, it takes about 0.05 ms for the wave to travel between the impact end and the free

end. Hence, the total traveling time of 0.1 ms back and forth between the two ends seems to match well with the fundamental frequency of 10 kHz and the higher order frequency of 20 kHz. It then can be concluded that superposition of the elastic wave can take place and cause the change of wave shape.

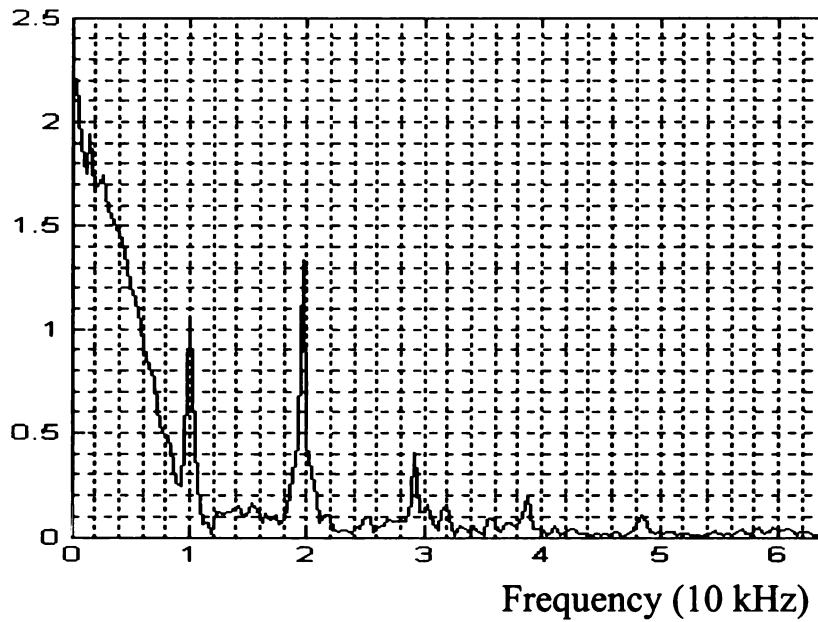


Figure 3.6 The signal in frequency domain obtained from the pair of strain gages located 38mm from the impact end.

### 3.4 Experiments on Wave Dissipation

The wave traveling inside rods will dissipate finally. To understand the dissipative rate, a cylindrical rod made of stainless steel 347 and having a diameter of 19 mm and a length of 840 mm was prepared. A pair of strain gages was installed at the middle as usual. The rod was then hanged up with fishing thread as shown in Figure 3.7(a). A hammer was used to apply the impact force to the rod.

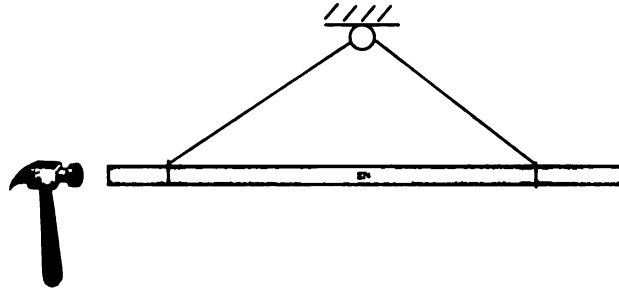


Figure 3.7(a) Experimental setup for wave dissipation.

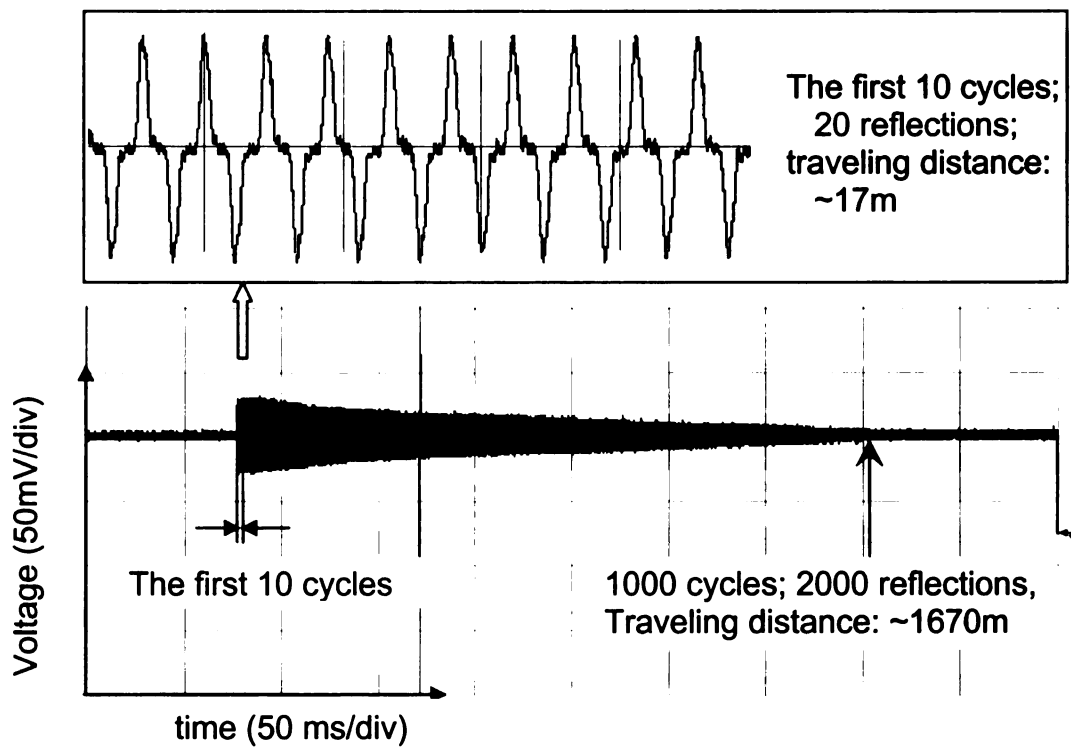


Figure 3.7(b) Experimental result of wave dissipation.

Figure 3.7(b) shows one of the experimental results of the wave dissipation in the stainless steel rod. The wave traveled roughly half second before dissipated totally. There is no obvious difference in the magnitudes of the first ten cycles, in which the wave reflected 20 times from ends, traveled about 17 m totally.

#### 4. MECHANICAL METHOD FOR WAVE REDUCTION

The wave propagation in a cylindrical rod can be considered as one-dimensional phenomenon. However, the wave formed in the rod can be very complex due to the superposition of the impact-induced wave with reflected waves resulting from finite boundary or inhomogeneous material of the rod. The superimposed wave may not be useful, or at least not easy, for applications. The initial impact-induced wave should hold the fundamental information of the impact mechanism and needs to be identified. The identification requires a technique to remove, or even eliminate, the reflected waves. A mechanical method for wave reduction, or even wave elimination, was proposed.

##### 4.1 Rod with Cone-Ball End

A cylindrical rod with a short cone section followed by a ball section is shown in Figure 3.8(a). The design concept of the cone-ball end was aimed at trapping the impact-induced wave inside the ball end without rebounding back to the cylindrical section. When the axial wave reached the cone section, it would be reflected from the conic surface according to the wave reflection law. The cone was carefully machined such that the reflected wave was guided into the ball section. Once the wave got into the ball section, the majority of it would move around continuously and get trapped inside the ball. Figure 3.8(b) and 3.8(c) show the dimensions and image of the rod with a cone-ball end.

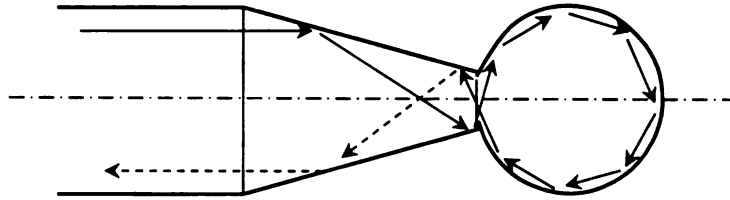


Figure 3.8(a) Schematic of a rod with a cone-ball end.

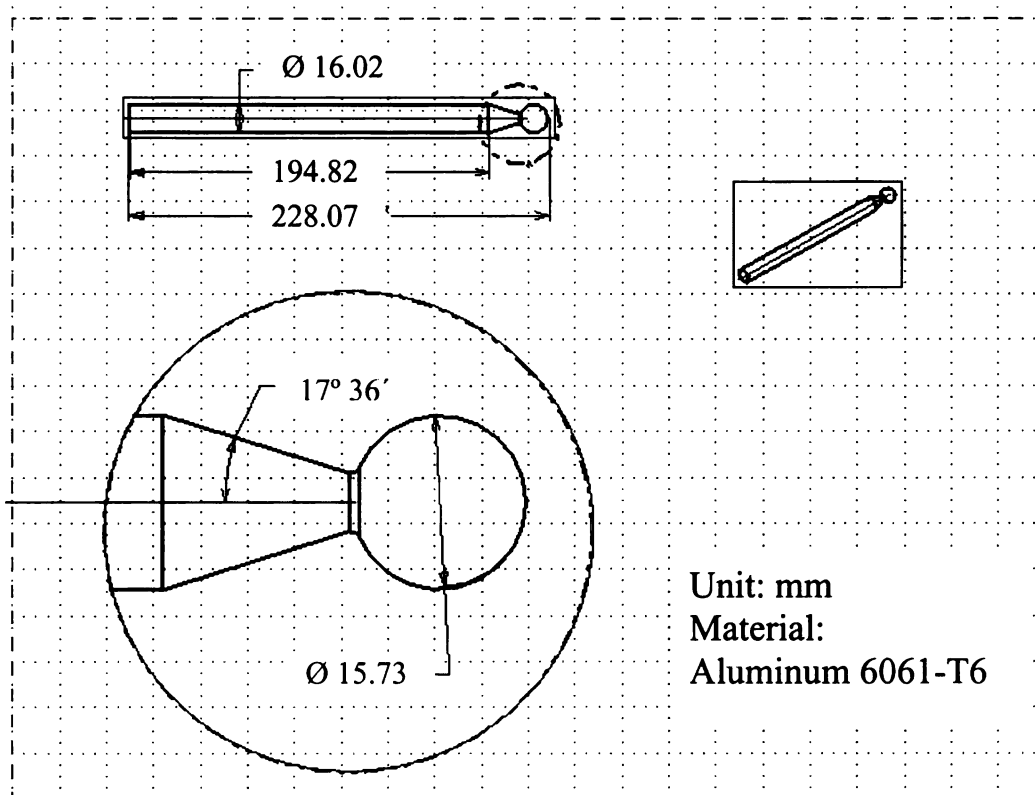


Figure 3.8(b) Detailed drawings of a rod with a cone-ball end.

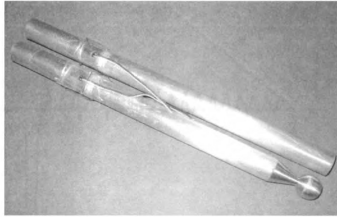


Figure 3.8(c) Image of a cylindrical rod and a rod with a cone-ball end.

The rod was installed with a set of strain gages at a distance of 51 mm from the impact end. The testing setup and the testing procedures were identical to the previous experiments. Figure 3.9 shows the measured force histories for a rod with a flat end and a rod with a cone-ball end. It is obvious that the wave travels and reflects in the rod with a flat end many times. However, the wave travels and reflects in the rod with a cone-ball end fades more quickly. The difference is apparently due to the reduction of the wave in the rod with the cone-ball end.

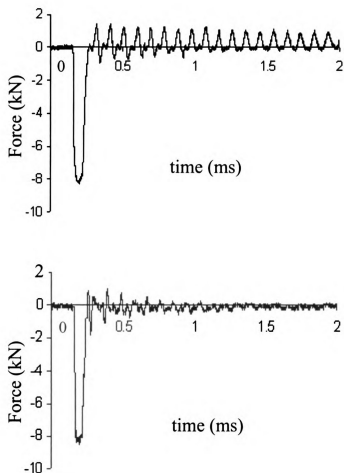


Figure 3.9 Force histories in the rod with a flat end (top) and a rod with a cone-ball end (bottom).

#### 4.2 Bar with Double Parabolic-Lines and Double Tails

A concave mirror with a parabolic surface can converge all incoming rays onto a focal point. This phenomenon can be used to manipulate the wave propagation at the end of a cylindrical rod. However, due to the difficulty involved in machining a three-dimensional cylindrical rod with a parabolic-surface end, a

two-dimensional flat bar with a parabolic-line end was used to demonstrate the fundamental concept. Figure 3.10(a) shows the schematic while Figures 3.10(b) and 3.10(c) are detailed drawings and image of the bar with a double parabolic-line end and double tails.

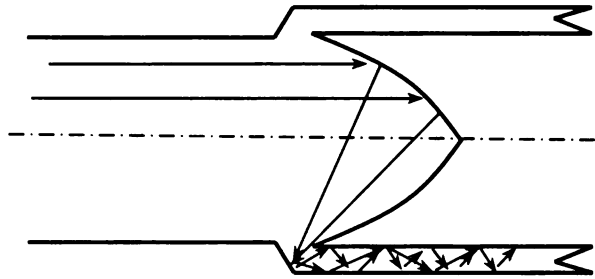


Figure 3.10(a) Bar with double parabolic-lines and double tails.

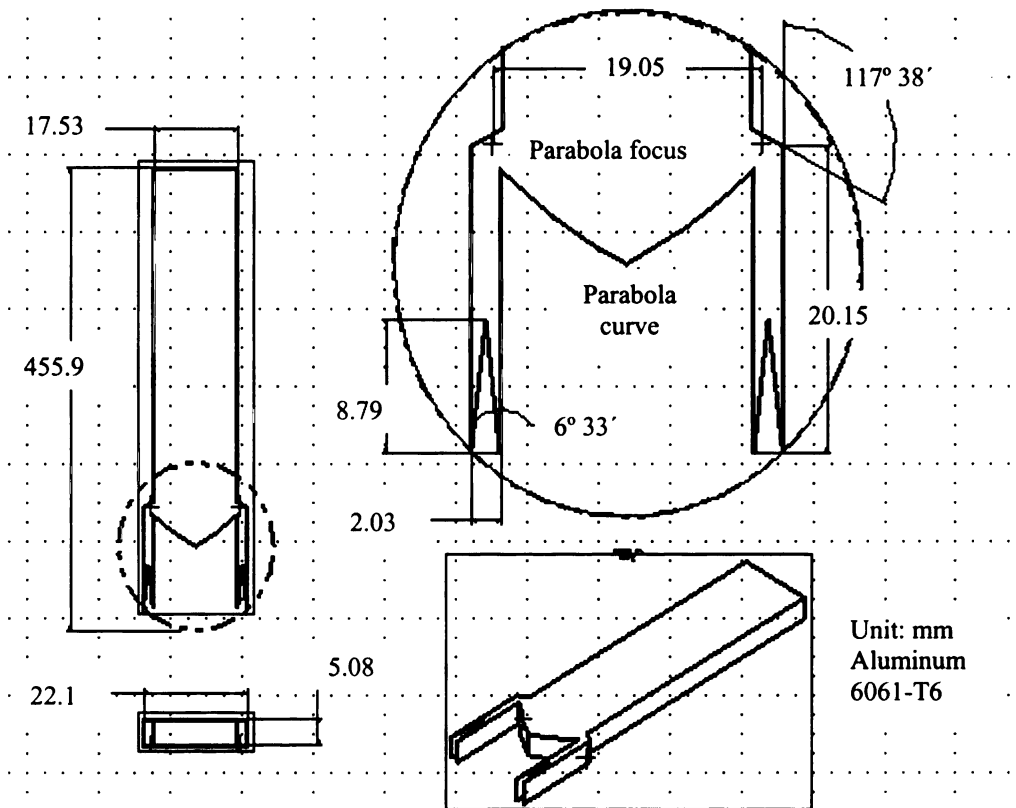


Figure 3.10(b) Drawing of the bar with double parabolic-lines and double tails.



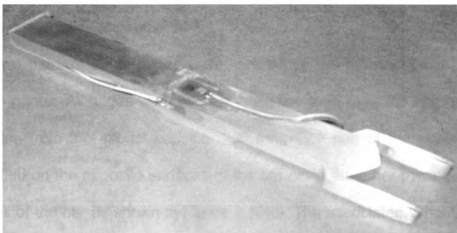


Figure 3.10 (c) Image of bars with double parabolic-lines and double tails.

Because the two-dimensional flat bar could not be launched by the gas gun, it was hung up with wires at two positions close to the bar ends and impacted by a cylindrical rod launched from the gas gun. When impact takes place, the elastic wave generated at the flat bar end can be viewed as a combination of numerous wave fronts traveling together along the axis of the bar. As they reach the parabolic line, they will be redirected to the individual focal points. Shown in Figure 3.10(a) is a flat bar with double parabolic-lines and double tails. The wave fronts on the upper half will be converged to a focal point located at the lower half while those on the lower half will be converged to a focal point located at the upper half. The two focused waves at the two focal points will then be redirected to the two tails and propagate along the tails until they fade out at the very ends of the tails. In order to realize this design, an aluminum plate with a thickness of 5 mm was machined according to the drawing in Figure 3.10(b). The flat bar was chosen over a cylindrical rod because it was much simpler to machine a two-

dimensional flat bar than a three-dimensional circular rod while retaining similar wave propagation phenomena.

Two pairs of strain gages were installed in the flat bar. Each pair had two strain gages. All gages were aligned along the axial direction and had the same location from the impact end, i.e. 200 mm. One pair of the strain gages was installed on the opposite surfaces of the bar while the other pair on the opposite edges of the bar as shown in Figure 3.10(c). The associated Wheatstone bridge circuits were identical to those used in previous experiments; so were the amplifiers and oscilloscope.

Since the flat bar was very light, a low-speed impact was performed, resulting in low magnitude of strain signals. In order to distinguish the difference, Wheatstone bridge circuits for the two pairs of strain gages were set to have opposite outputs, as shown in Figure 3.11. The upper curve was obtained from the gages on the edges while the lower one was obtained from the gages on the surfaces. The oscillations in both curves are very smaller, implying a good reduction of the reflected wave back to the bar section by the double parabolic-lines and the double tails.

Figure 3.12 shows the strain signal and contact duration from the gages on the edges. The contact duration is longer than the strain signal. The contact duration before the strain signal is due to the distance between the impact end and the position of the gages while the contact duration after the strain signal is likely due to the simultaneous travel of the flat bar and the cylindrical rod with no contact between them.

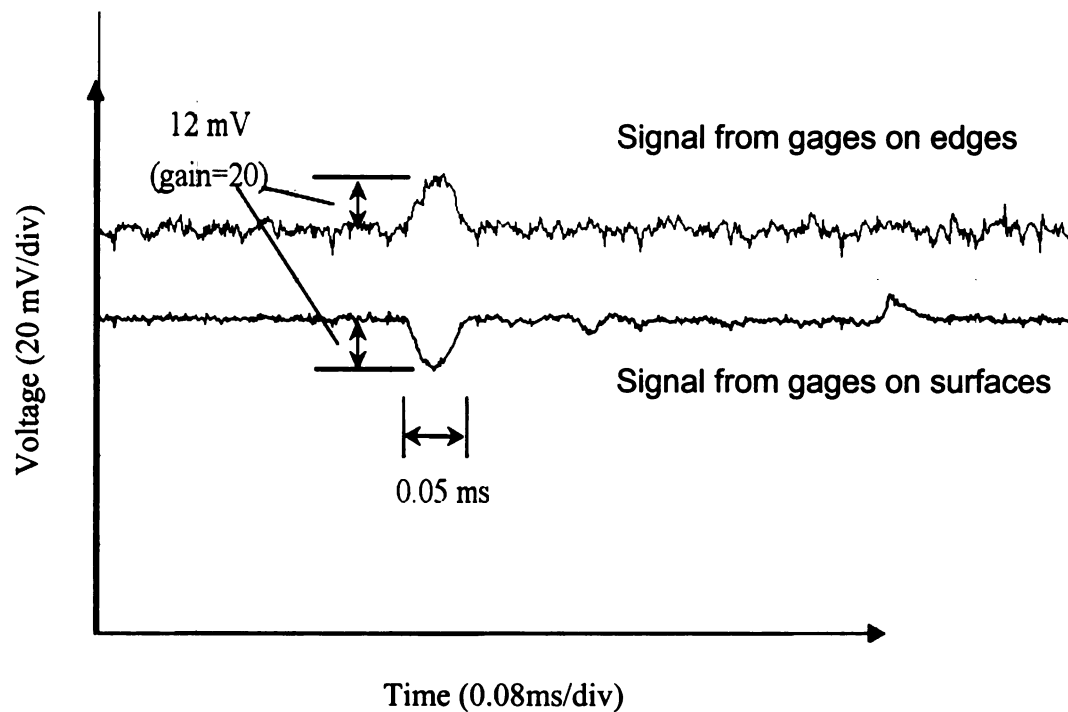


Figure 3.11 Impact response of the flat bar with double parabolic-lines and double tails.

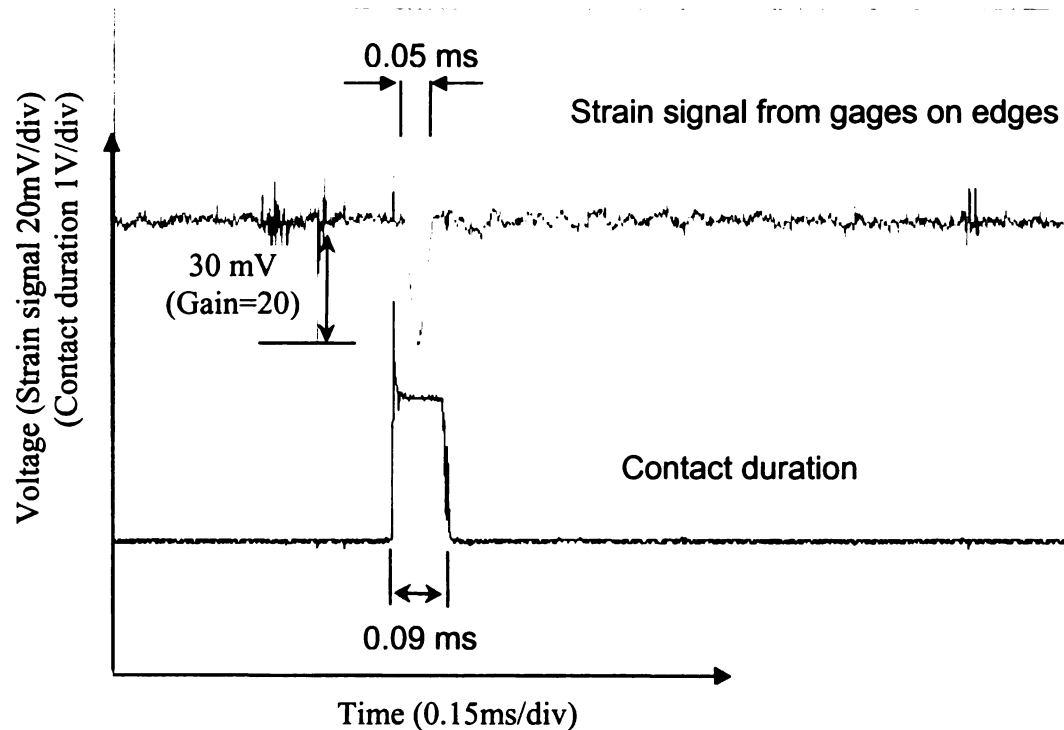


Figure 3.12 Impact response of the bar with double parabolic-lines and double tails.

## 5. NUMERICAL METHODS FOR WAVE REDUCTION

Besides the mechanical method for reducing wave reflection, numerical methods can also be used to achieve the goal. Details of wave propagation equations and the physical fundamentals can be found in the references [12-16]. The primary concept to be used in this thesis research is that a compressive wave reflects as a compressive wave after hitting a rigid boundary while a tensile wave reflects as a tensile wave after hitting a rigid boundary. On the contrary, a compressive wave reflects as a tensile wave after hitting a free boundary while a tensile wave reflects as a compressive wave after hitting a free boundary [14,15].

In impact events, the impacted end of a rod or a bar undergoes compression while the non-impacted end is free. Hence, a compressive wave will occur at the impacted end and propagates toward the free end. The compressive wave reflects from the free end with a tensile wave and propagates back to the impacted end. When the rod or the bar separates from the impacted specimen, the impacted end will become a free end. If this separation occurs before the tensile wave reaches the end, the tensile wave will be reflected to be a compressive one. The wave will then travel between the ends back and forth in compression and tension alternatively.

### 5.1 Technique Based on Assuming an Initial Wave

When an impact-induced wave propagates inside a rod or a bar, a reflected wave from part of the initial wave may interfere with the remaining part of the initial wave around the boundaries. The shape of the superimposed wave usually becomes very complex and does not bear the shape of the initial wave. For

impact events lasting a longer contact time or involving a softer specimen, the interference of the waves results in fine zigzags along the impact curves. For impact events lasting a shorter duration, the interference distorts the impact signals seriously.

The measured wave signals are results from superimposing the initial wave and the reflected waves. In order to recover the initial impact wave signals, an unwrapping technique is required. As a demonstration, an artificial initial wave is assumed. The wave is allowed to bounce between two ends. The initial wave and the reflected waves are superimposed to form a complex resultant wave. By comparing the artificially superimposed curve with the measured curve at the gage position, the assumed initial wave is then modified and the superposition procedures are performed again. The iterative modification and superposition are continued until the superimposed curve matches well with the measured wave. The assumed wave is then considered as the initial wave.

In the simulation of wave superposition, the commercial computer program MATLAB was used to formulate the required computational scheme for simulations. Figure 3.13 shows two examples; each contains an assumed initial wave, a superimposed wave, and the associated measured wave. The superimposed waves seem to agree with the measured waves up to some extent. The assumed initial wave seems to be reasonable, and the numerical method for identifying the superimposed wave seems to be feasible.

There is an apparent limit on the numerical method presented above. The method is only meant for elastic wave propagation. Any plastic deformation and

associated plastic wave will have to be handled with a more advanced method involving plastic wave propagation. Besides, if a boundary is not completely free, partial transmission and partial reflection may take place. The ratio of reflection to transmission is dependent on the interfacial condition of impact and the properties of the involved materials, and can further complicate the numerical method.

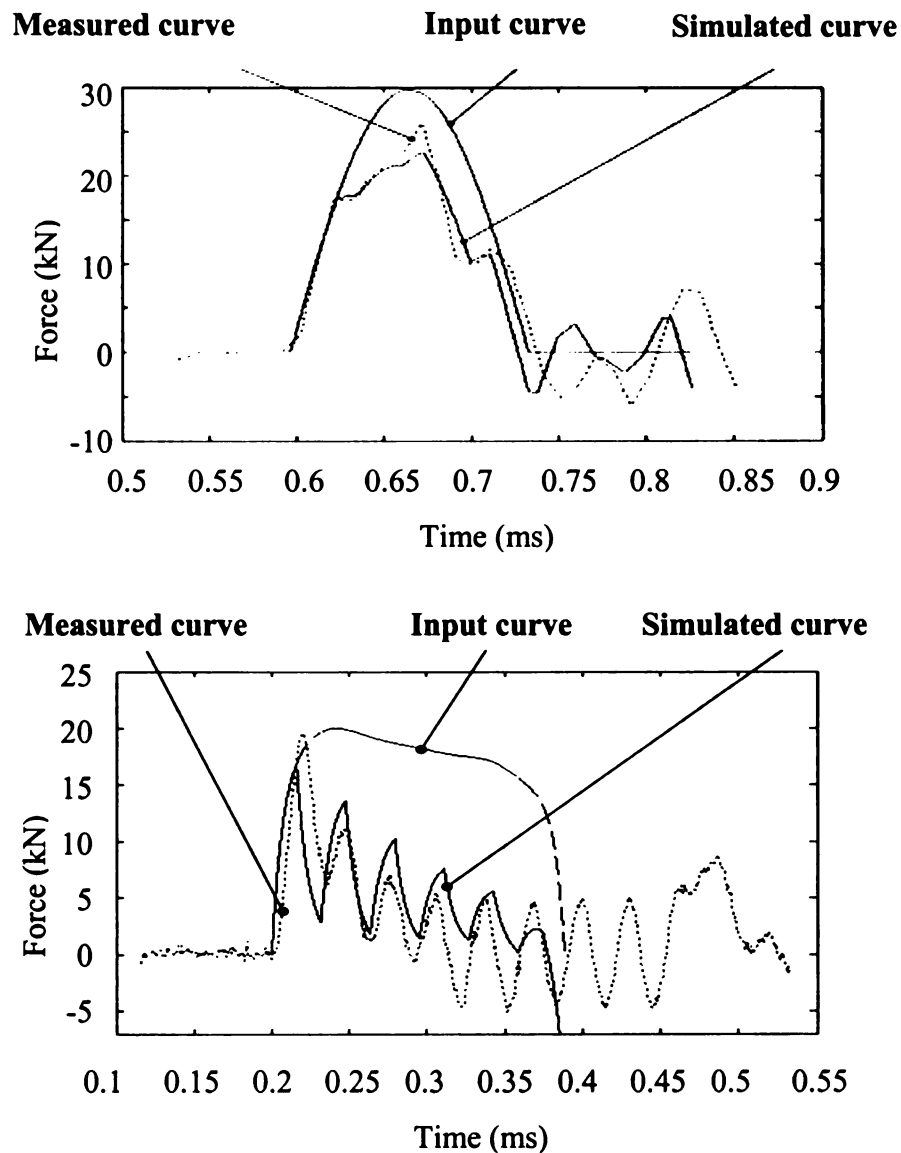


Figure 3.13 The assumed initial wave, superimposed wave and measured wave.

## 5.2 Two-Position Technique

Suppose that two pairs of strain gages are mounted on two different positions (position one and position two) along the axial direction of a rod. When the rod impacts onto a specimen, a compressive wave will be generated and propagate to gages on position one first and then gages on position two. The signal measured at position one will be measured at position two after a certain time interval. When the compressive wave reaches the free end of the rod, it will reflect as a tensile wave and propagates back to gages at position two first and then gages at position one. The reflected signals measured at the two positions will also have the same time interval. If the impacted end is still in contact with the specimen when the tensile wave reaches it, the tensile wave will be reflected with a fractional compressive wave, depending on the materials of the rod and the specimen, and propagates back to the strain gages. Otherwise, the tensile wave will be reflected completely as a compressive wave. The reflected wave will be measured at position one and then at position two.

For gages at position one, the first signal the gages detect should be the impact signal. In the second time, they should detect a signal combining the impact signal and the reflected signal from the free end. In the third time, the gages should detect a combined signal superimposing the impact signal, the first reflected signal from the free end, and the first reflected signal from the impacted end. Gages at position two should have similar detections but at different time instants due to their different location from position one.

Based on the wave propagation and wave superposition at position one and position two, a technique for identifying the initial impact signal can be established. To start with, assume a signal  $X$  is measured at position one at time  $T_0$ . After a time period  $T_1$ , it is measured at position two. If a reflected signal  $Y$  also reaches position two at time  $T_0+T_1$ , then position two will measure  $(X+Y)$ . Since the two positions will measure the same ongoing signal with a time interval  $T_1$ , the reflected signal can be calculated by  $(X+Y)-X=Y$ . The reflected signal  $Y$  will also reach position one after another  $T_1$  since the wave speed in the rod is a fixed value. So, at time  $T_0+2T_1$ , position one will measure  $X'+Y$ . Eliminating  $Y$  from the  $(X'+Y)$ , the ongoing wave  $X'$  at the time  $T_0+2T_1$  can be identified. Increasing  $T_0$  for other sampling data points and repeating the procedures, one can find the complete initial impact signal from the impact end that is not interfered by any reflected one. As a summary, the signal at position one can be used to identify the signal at position two which in turn can be used to identify the signal at position one with its reflected wave portion. A computer program based on this method was written with the use of LabVIEW.

In order to demonstrate this method, a rod made of stainless steel 347 with a diameter of 19 mm and a length of 203 mm was prepared. Two pairs of strain gages similar to the ones used earlier were installed at locations 19 mm and 95 mm from the impact end. All the gages were mounted along the axial direction. Each pair of gages consisted of two gages and was mounted on opposite surfaces of the rod. They were then connected to the opposite arms of a Wheatstone bridge circuit in order to eliminate any bending effect.



An 840 mm-long rod made of the same stainless steel and having the same diameter was used as an impacting target. It was also mounted with the same type of strain gages. Figure 3.14 shows the experimental setup. Three differential amplifiers with a bandwidth of 10 MHz and an input impedance of  $1\text{M}\Omega$  were used while the gain was set to 50. Two double-channel digital oscilloscopes with a bandwidth of 100 MHz and a sampling rate of 100 MS/s (Samples per second) were used for data acquisition. The longer rod was expected to receive impact-induced signals with less distortion than the shorter one [17-28].

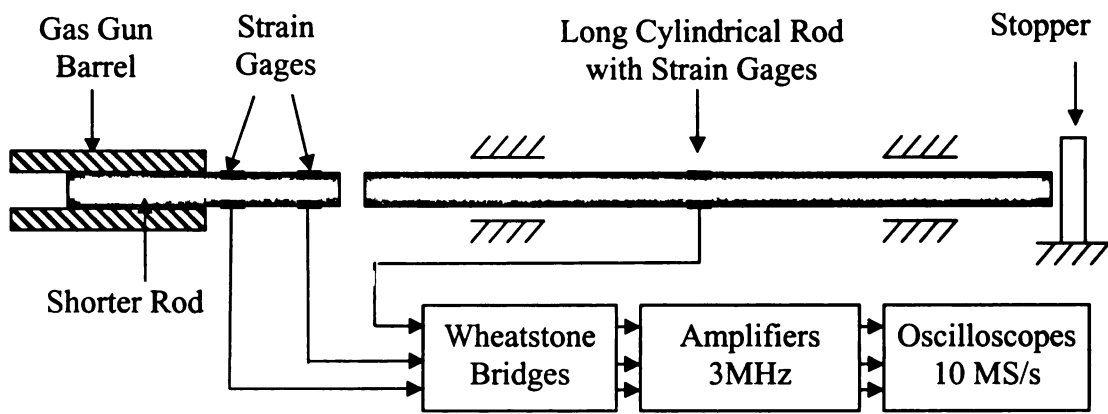


Figure 3.14 Experimental setup of the two-position technique.

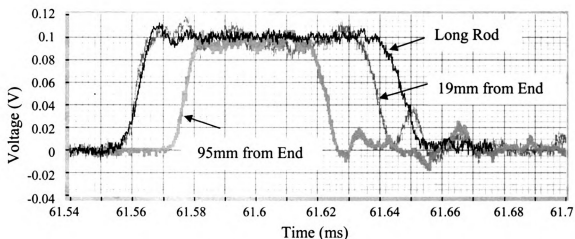


Figure 3.15(a) Experimental curves from two-position of a shorter rod and from a long rod.

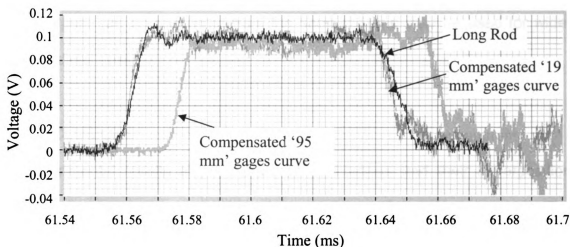


Figure 3.15(b) Results based on the two-position technique.

One set of experimental results can be seen in Figure 3.15(a). The enhanced dark curve represents signals obtained from the long rod. The other two curves are from gages located at position one and position two of the short rod. Results from both rods had identical sampling time and sampling rate since they were simultaneously sampled from three channels of the two oscilloscopes. The curve from the long rod was shifted along the time axis to match with the other two

curves. The three curves are quite different in period. The curve from the long rod has the longest period, it records the real impact signal [17-28]. The curves from the short rod have shorter periods which decrease as the gages located further away from the impact end.

Figure 3.15(b) shows the curves processed by the LabVIEW-based program with the use of signals from the two positions of the short rod. The curve from the long rod is also presented for comparison. Figure 3.15(b) shows that the processed signals of the short rod are almost the same as the initial impact signal measured from the long rod. With this two-position method, the initial impact signal can be recovered from the short rod and may be used for wide-band load cell design.

## 6. CONCLUSIONS

Experimental results showed that reflected waves and their superposition with the initial impact wave can complicate the impact force measurements. The complication increases as the impact duration becomes shorter. Based on a mechanical technique to redirect the reflected waves, a wave reduction method was proposed and verified. The initial wave associated with the impact force could be identified.

Besides the mechanical technique, two numerical techniques, the so-called Initial Wave Assumption technique and the Two-Point technique, were also proposed and verified to be able to recover the initial impact force wave.

The success of the wave reduction techniques to recover the initial impact force wave shed light on designing an instrumented projectile with a short rod.

## REFERENCES

- [1] Guoqi Zhu, Werner Goldsmith and C. K. H. Dharan, "Penetration of Laminated Kevlar by Projectiles—I. Experimental Investigation", *Int. J. Solids Structures*, Vol. 29, No 4, pp.399-420, 1992
- [2] Werner Goldsmith, Eric Tam, David Tomer, "Yawing Impact on Thin Plates by Blunt Projectiles", *Int. J. Impact Engng*, Vol. 16, No. 3, pp.479-498, 1995
- [3] Eirik Svinsas, Cathy O'Carroll, Cyril M. Wentzel, and Anders Carlberg, "Benchmark Trial Designed to Provide Validation Data for Modelling"
- [4] Michael A. Christopher, Tim S. Edwards, "Instrumented Projectile", NDIA 48<sup>th</sup> Annual Fuze Conference, NSWC / Dahlgren Division
- [5] Jun Lu, Subra Suresh, Guruswami Ravichandran, "Dynamic indentation for determining the strain rate sensitivity of metals", *Journal of the Mechanics and Physics of Solids*, 51(2003), pp.1923 – 1938
- [6] Jun Lu, "Mechanical Behavior of a Bulk Metallic Glass and its Composite over a Wide Range of Strain Rates and Temperatures", Thesis for the Degree of Doctor of Philosophy, California Institute of Technology, California, March, 2002
- [7] S. J. Bless, D. R. Hartman, "Ballistic Penetration of S-2 Glass Laminates", 21<sup>st</sup> International SAMPE Technical Conference, Sept. 25-28, 1989
- [8] Stephan J. Bless, Moshe Benyami, David Hartman, "Penetration Through Glass-Reinforced Phenolic", 22<sup>nd</sup> International SAMPE Technical Conference, Nov. 6-8, 1990. pp.293-303
- [9] J.H. Choi, C. H. Lee, S.N. Chang and S.K. Moon, "Long-Rod Impact Phenomena: Role of Wave Interaction on Crack Propagation", *Int. J. Impact Engng*. Vol. 17, pp.195-204, 1995
- [10] S. Venzi, A. H. Priest, and M. J. May, "Influence of Inertial Load in Instrumented Impact Tests", *Impact Testing of Metals*, ASTM STP 466, American Society for Testing and Materials, 1970, pp.165-180
- [11] Guojing Li, "Construction, Calibration and Application of a Split Hopkinson Pressure Bar", a thesis for the Master of Science, Department of Mechanical Engineering, Michigan State University, 2002
- [12] Karl F. Graff, "Wave Motion in Elastic Solids", Ohio State University, pp.75-

134, 1975.

- [13] C. Bacon, "Numerical prediction of the propagation of elastic waves in longitudinally impacted rods: application to Hopkinson testing", *International Journal of Impact Engineering*, 13 (4), pp.527-539, 1993.
- [14] James F. Doyle, "Wave Propagation in Structures, An FFT-Based Spectral Analysis Methodology", Springer-Verlag New York, Inc. 1989
- [15] James F. Doyle, "Waves Propagation in Structures, Spectral Analysis Using Fast Discrete Fourier Transforms", Second Edition, Mechanical Engineering Series, 1997
- [16] Ralph Burton, office of naval research, London, "Vibration and Impact", Dover Publications, Inc. New York 10014, 1968
- [17] Michael Adam Kaiser, "Advancements in the split Hopkinson bar test", Master's thesis, Blacksburg, Virginia, 1998.
- [18] D. J. Frew, M. J. Forrestal and W. Chen. "Pulse shaping techniques for testing brittle materials with a split Hopkinson pressure bar", *Experimental Mechanics*, 42 (1), pp.93-106, 2002.
- [19] D. J. Frew, M. J. Forrestal and W. Chen, "A split Hopkinson pressure bar technique to determine compressive stress-strain data for rock materials", *Experimental Mechanics*, 41 (1), pp.44-46, 2001.
- [20] W. Chen and F. Lu, "Dynamic compression testing of soft materials", *ASME Journal of Applied Mechanics*, 69, pp.214-223, 2002.
- [21] H. M. Hsiao, I. M. Daniel and R. D. Cordes, "Dynamic compressive behavior of thick composite materials", *Experimental Mechanics*, 38, pp.172-180, 1998.
- [22] O. Sawas, N. S. Brar and R. A. Brockman, "Dynamic characterization of compliant materials using an All-polymeric split Hopkinson bar", *Experimental Mechanics*, 38, pp.204-210, 1998.
- [23] Frank E. Hauser, "Techniques for measuring stress-strain relations at high strain rates", *Experimental Mechanics*, pp.395-402, 1966.
- [24] J. F. Bell, "An experimental diffraction grating study of the quasi-static hypothesis of the split Hopkinson bar experiment", *J. Mech. Phys. Solids*, 14, pp.309-327, 1966.
- [25] Robert L. Sierakowski and Shive K. Chaturvedi, "Dynamic loading and

characterization of fiber-reinforced composites”, John Wiley & Sons, Inc. New York, pp.41-77, 1997.

- [26] Jonas A. Zukas, Theodore Nicholas and Hallock. F. Swift, “Impact Dynamics”, John Wiley & Sons Inc. pp.287-308, 1982.
- [27] David E. Lambert and C. Allen Ross, “Strain rate effects on dynamic fracture and strength”, International Journal of Impact Engineering, 24, pp.985-998, 2000.
- [28] Weinong Chen, “Dynamic Failure Behavior of Ceramics under Multiaxial Compression”, Thesis for the Degree of Doctor of Philosophy, California Institute of Technology, 1995

## **CHAPTER FOUR**

### **DESIGN AND CALIBRATION OF AN INSTRUMENTED PROJECTILE**

#### **ABSTRACT**

Almost all free projectile impacts are of non-instrumented tests. They are simply based on the difference of kinetic energies of free projectiles before and after impacts. Accordingly, valuable information leading to the understanding of impact mechanism may be lost. Issues concerning wired and wireless projectiles are discussed. A preliminary design is also presented. Based on a mechanical wave reduction technique, this study presents the detailed construction of a wireless instrumented projectile, including the selection of the geometry, the manufacturing procedures, the circuit design of the microprocessor, and the assembly of the projectile. Calibrations on projectile body and electronic components were carefully performed. Testing results seemed to validate the feasibility of using the instrumented wireless projectile which has a bandwidth of 170 kHz for impact events with velocities up to 20m/s. Both the maximum impact velocity and the bandwidth are much higher than those commonly used in the instrumented drop-weight impactor.



## 1. INTRODUCTION

Dynamic loadings such as impact, crash and blast loadings are commonly found in the real world. Many dynamic testing techniques have been developed for laboratory uses ranging from material characterizations to testing simulations. Examples are the split Hopkinson's pressure bar (SHPB) for characterizing dynamic stress-strain relations, Taylor's impact test for finding dynamic yielding stress, instrumented drop-weight impact test for finding material response under low-velocity impacts, and gas gun for simulating ballistic impacts. Among the four techniques mentioned, SHPB and drop-weight impact test are instrumented tests while Taylor's impact and gas gun tests are non-instrumented.

Non-instrumented tests are much simpler than instrumented tests in terms of construction. They are usually built in the laboratory for simulating the loading conditions occurring in the real world. Instrumented tests, however, are equipped with sensors to detect physical quantities and require sophisticated data acquisition and signal processing systems for understanding the parameters involved in the loadings. Since dynamic loadings usually last a very short time period and involve many physical parameters during the events, instrumented tests are preferred over non-instrumented tests in studying dynamic loading events. This thesis research is aimed at developing an instrumented free projectile for simulating low-velocity ballistic impact tests. Detecting the wave propagation in the small projectile and converting the signal into loading history are the primary studies of this research.

Both numerical and mechanical methods have been proposed for elastic wave reductions in a previous study [chapter 3]. A numerical technique, the so-called two-position technique, requires acquiring a significant amount of data points during a short time interval while the wave travels between two positions of a short projectile. To meet this demand, a data acquisition unit must have a very high sampling rate, which usually comes with a large memory. Hence, the size of the data acquisition unit is also likely to be large. Such a data acquisition unit, however, cannot be attached to the small projectile economically. On the contrary, if the data points are to be transferred to a data acquisition unit located outside the projectile during operations, the lead wires will have to join the projectile and the data acquisition unit correctly. Otherwise, entanglement or even damage to the lead wires can take place during high-speed operations [chapter 3].

The mechanical method for wave reduction is essentially based on geometrical effects and does not require a high-performance data acquisition and signal processing unit for wave reduction as the numerical method. The data acquisition and signal processing unit can be relatively simple and possibly integrated with the body of the projectile. With no lead wires, such as a wireless design, the projectile can then be operated freely. Hence, the mechanical method should bear more advantages over the numerical method and is suitable for designing an instrumented free projectile for use in impact events. The objective of this study is focused on the feasibility of building such an instrumented free projectile.

## 2. SIGNAL TRANSFER

For the demonstration on instrumented rods mentioned earlier, only the rear sections of the rods were inserted into the gas gun barrel. The front sections with strain gages were left outside the gun barrel so the lead wires for the strain gages could be easily connected to the Wheatstone bridge circuits without being interfered by the gun barrel. In order to achieve higher impact velocities, the rods should be accelerated with either a higher gas pressure and/or with a longer acceleration time. This section is aimed at the techniques of signal transfer for designing an instrumented projectile for higher impacting velocities.

### 2.1 Wired Method

Signal transfer with lead wires was a primary concern in constructing instrumented projectiles [1,2]. As a first approach, the lead wire was wound around a projectile before it was inserted into a gun barrel. In the circuit design, one end of the lead wire should be connected to strain gages on the projectile, while the other to a Wheatstone bridge circuit located outside the gun barrel. As the projectile was accelerated, it would carry the lead wire with it along the gun barrel.

The design leaving lead wire inside the gun barrel seemed to be straightforward. However, it failed quite often. There were two major failure modes. One was related to the breakage of the lead wire. The other was related to the entanglement of the lead wire inside the gun barrel, resulting in unsuccessful launch of the projectile. Some studies were performed to identify

the cause of the failures and to explore the solutions. It was confirmed that the over-stretch of the lead wire around the joining point with the projectile could take place right after the sudden rise of the high-pressure gas, resulting in the breakage of the joining of the lead wire. The high-pressure gas rebounded from the projectile end could entangle the wound lead wire.

The high-pressure gas pushed the projectile forward which in turn pulled the lead wire with it. In order to overcome the failures of the lead wire, the lead wire should be enclosed inside a tube to avoid its direct contact with the high-pressure gas. The tube was made of copper and had an outside diameter of 9.5 mm. Its length is 980 mm, roughly two-fifths of the total length of the gun barrel. In assembly, the lead wire was inserted into the copper tube which was then inserted into the 13 mm diameter gun barrel and fixed to the gun barrel at one end, a closed end. One end of the lead wire was connected to the projectile through the other end, an open end of the copper tube while the other was pulled out of a hole at the closed end of the tube and then the gun barrel.

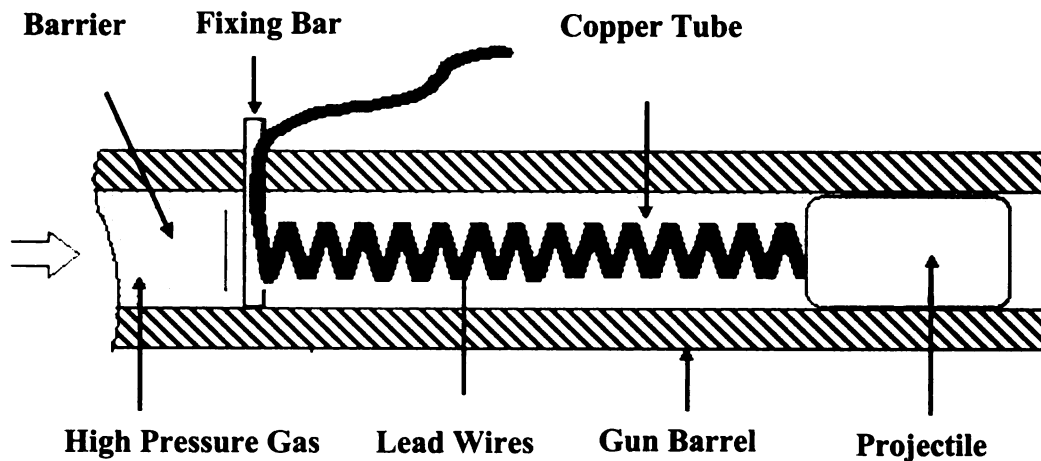


Figure 4.1 Assembly of the wired projectile.

The wound lead wire should be finer and stronger and have at least four conducting lines for connecting the two strain gages to a Wheatstone bridge circuit. A telephone cord was used for this purpose. This wired technique worked well for signal transfer. The telephone cord was used more than ten times without any damage. Figure 4.2 shows an experimental result of an instrumented stainless steel 347 rod with diameter 12.5 mm and length 38 mm impacting on a fixed 100 mm x 100 mm x 25 mm aluminum plate. The signal measured by the strain gages on the rod was transferred with the protected wound lead wires. The impact velocity was 51 m/s. The rod was accelerated a distance of 1 m inside the gun barrel before impacting on the specimen, so the lead wires were stretched and extended to the same distance too. Figure 4.2 does not show large oscillation in the section of the curve before the impact signal section. This indicates that the cord wire did not introduce any significant resistance change during the operations.

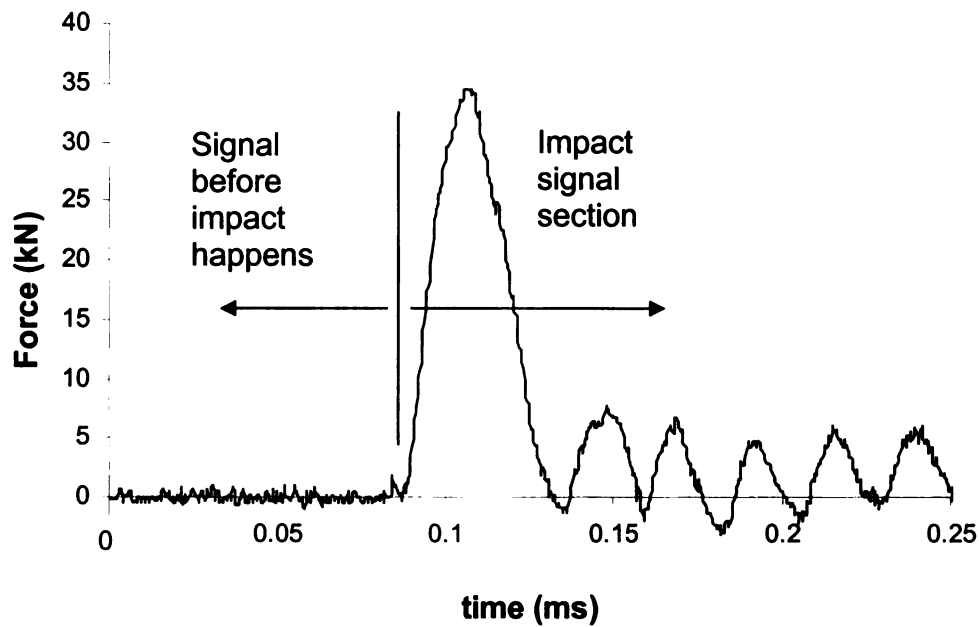


Figure 4.2 Result measured by an instrumented rod with the protected wound-lead wire

## 2.2 Wireless Technique

A wireless technique is perhaps the ultimate solution to solve the problems related to the lead wire failures. However, some potential difficulty should not be underestimated.

### A. Conductive Technique

An instrumented projectile can be made in close contact with the gun barrel [3,4]. Hence, the gas gun barrel, the projectile, and a conductive specimen can be integrated to form a closed circuit for signal transfer. This technique, however, limits the sensor to be piezoelectric or similar types and requires the specimens to be conductive.

## **B. Radio Signal Transfer Technique**

A radio signal transmitter can be built up with the projectile to transfer the measured signals with a certain frequency. A corresponding signal receiver can be used to accept the measured signals within a certain distance. Such a technique requires a high data transfer rate for the transmitter and receiver. Since the transmitter will need to be built together with the projectile, it should be battery powered and small enough, especially in diameter to fit inside the gun barrel. A built-in differential amplifier may also be needed. However, it was difficult to find a signal transmitter with a suitable size and a high signal transfer rate for the instrumented projectile.

## **C. Wireless Technique**

The measured signals can be saved to a built-in memory chip attached to the projectile. The fundamental idea is to amplify the signals detected by strain gages or other sensors attached to the projectile with a small amplifier chip and then sample and save them to a memory chip. All the chips and the associated battery should be integrated with the projectile body together. After each impact test, the instrumental projectile will then be unsealed to remove the chips for further data processing.

## **3. DESIGN OF AN INSTRUMENTED PROJECTILE**

In order to launch the instrumented free projectile from a circular gun barrel, the projectile must be of a cylindrical shape. Since the data acquisition and signal processing unit is to be attached to the cylindrical body and subjected to harsh impact environments, it should be enclosed inside the projectile to avoid being damaged by the high-pressure gas and the large impact force involved in the impact events. As discussed in a previous study [chapter 3], a parabolic surface at the end of a rod can help in reducing wave reflections in the rod. A demonstration based on a flat bar, however, was presented in the previous study. The use of the two-dimensional bar, instead of a three-dimensional rod, was because the former was much easier to machine than the latter. However, it should be noted that only the three-dimensional rod can accommodate the data acquisition and signal processing unit and be launched by the gas gun.

In the previous study, a two-dimensional double parabolic-line end was machined for a flat bar such that one half of the wave fronts generated from impacts was redirected to one focal point, while the other half of the wave fronts was redirected to the other focal point. In the present study, two three-dimensional curved surfaces were prepared for the circular end of the projectile body because of the difficulty in machining two three-dimensional parabolic surfaces. Figure 4.3 shows the schematic of the three-dimensional cylindrical projectile. The two curved lines in the middle section of the cylindrical body are actually two axially symmetric curved surfaces. Each of the two focal points (actually a focal ring) is located at the root of a tail that is able to redirect each set of the wave fronts reaching the focal point to the tip end of the tail. This



eventually reduces the intensity of the wave fronts to an insignificant level. To machine the two three-dimensional parabolic surfaces, a special cutting tool was required. Since no such a cutting tool was available to the author during the period of this research, two three-dimensional curved surfaces closely resembling the two parabolic surfaces were used as a substitute.

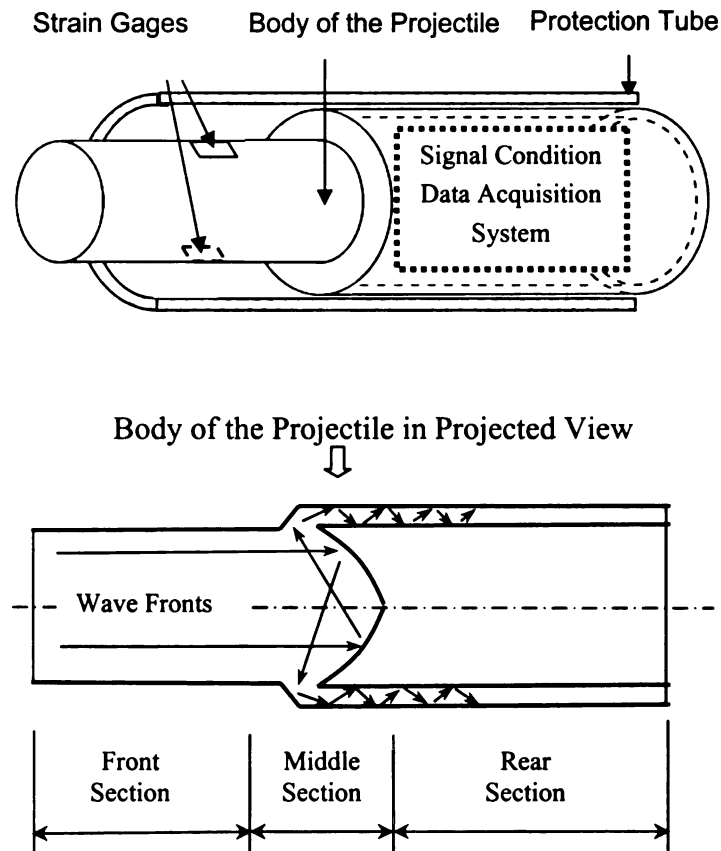


Figure 4.3 Layout of the instrumented projectile.

### 3.1 Cutting Tools

A  $\Phi 16$  mm cylindrical rounding endmill with a radius of 6.35 mm cutting arc was selected for machining the major portion of the wave-reduction geometry, i.e. the double three-dimensional curved surfaces of the projectile body. There were two reasons for choosing this cutting tool. One reason was due to its capability of machining an arc with a radius of 6.35 mm that was very similar to the ideal parabolic surface for redirecting the wave fronts to a small zone. Another reason was because the diameter of the endmill was close to the size of a desired data acquisition and signal processing unit [Appendix A] that had a width of 15 mm and played the primary role in the determination of the inner diameter of the projectile body. Beyond the double curved section, a tail section was required to further reduce the wave intensity. A round-corner cutting tool with a radius of 2.38 mm cutting edge was used.

Figure 4.4 shows the images of the cutting tools.

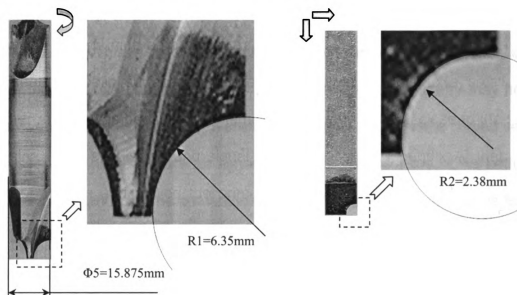


Figure 4.4 Images of endmill (left) and round-corner cutting tool (right).

### 3.2 Projectile Body

Shown in Figure 4.3, the body of the projectile can be divided into three sections. The front section is a cylinder for impact, the middle section has a curved shape for wave redirection, while the rear section is a hollow cylinder for wave divergence. Figure 4.5(a) shows the drawing of the overall geometry of the body of the projectile. The length of the front section is selected based on the theory of one-dimensional wave propagation [5-11] and the convenience for installation of strain gages. The shape of the middle section is determined by the availability of cutting tools, instead of an optimal shape for wave transfer. The length of the rear section is based on the need for wave divergence and the volume of the rear section for holding the data acquisition and signal processing unit, i.e. the SP&DAQ board, the battery, and shock absorption cushions.

### 3.3 Wave Transfer Section

The key to achieve wave reduction was to eliminate wave reflection at the end of the projectile body as much as possible. A special geometry may help to achieve such a goal. Figure 4.5(b) shows the details of the middle curved section and associated nomenclature for dimensions. The dash-dot line at the bottom of Figure 4.5(b) stands for the centerline of the body. The lower right arc is formed with a center at point B and a radius  $R1$ . The parallel lines on the left-hand side between LINE 1 (outer radius  $R3$ ) and LINE 2 (inner radius  $R4$ ) represent one-dimensional wave fronts traveling along the projectile body after impact.

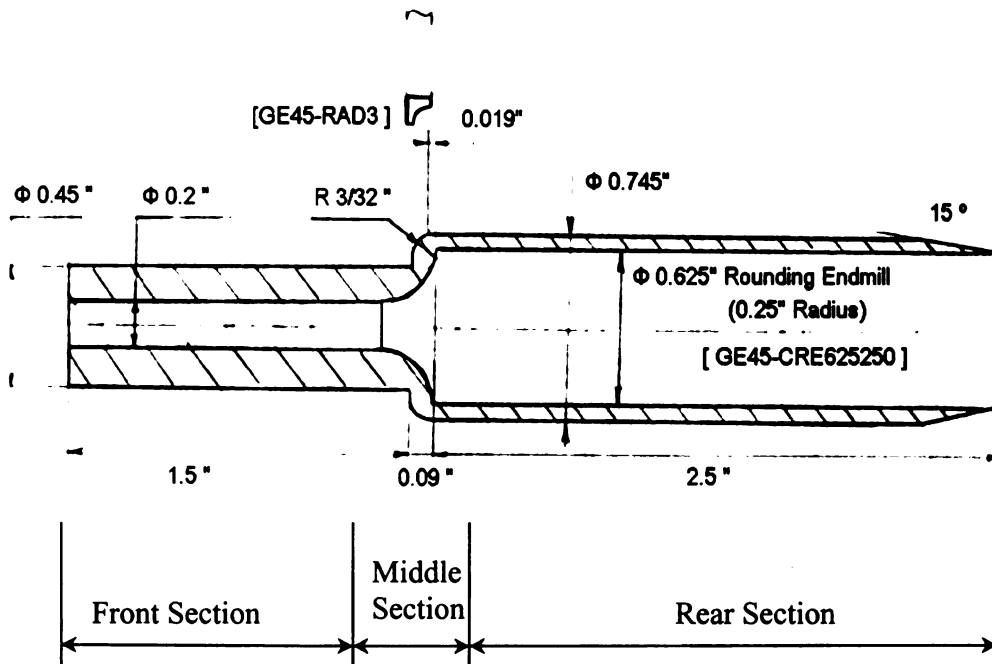


Figure 4.5(a) Overall geometry and dimensions of the projectile body.

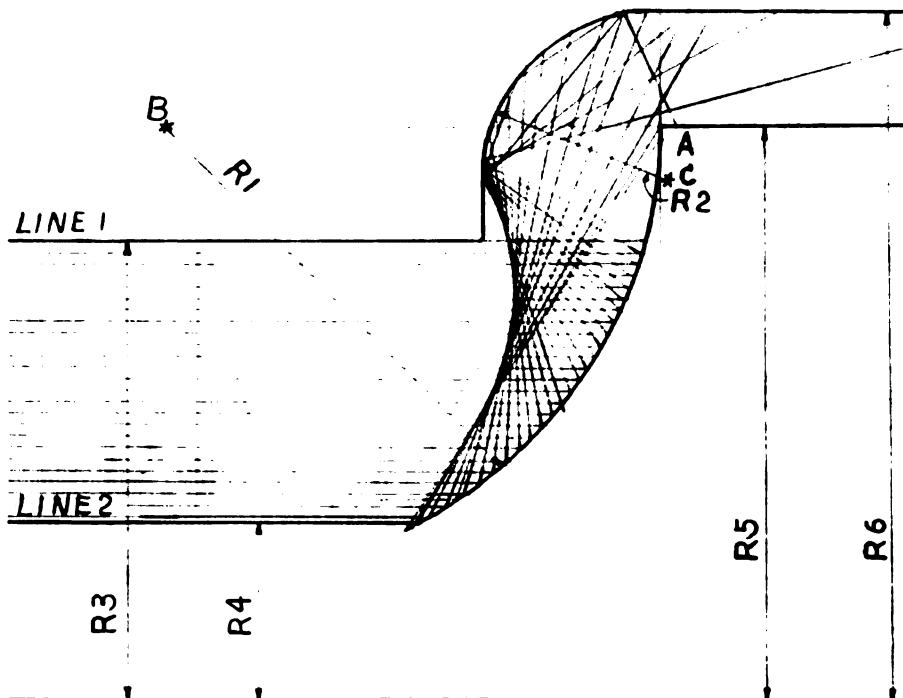


Figure 4.5(b) Schematic of the wave transfer mechanism.

When the wave fronts reach the lower right arc, they are redirected to a small zone on the upper left arc governed by the law of wave reflection in solids [12-19]. For wave reduction purpose, the wave fronts need to be further transferred into a rear section, i.e. the tail section, for wave divergence. The arc formed by the center C and the radius R2 in Figure 4.5(b) can help to achieve this goal. The rear section is essentially a hollow section with R5 as the inner radius and R6 as the outer radius. The upper left arc could be machined by a round-corner cutting tool. However, the lower right arc was the most difficult part to machine. For convenience of machining, the front section of the projectile body was made hollow with an inner radius R4. Hence, there was no end surface like the one given in Figure 4.3.

### 3.4 Instrumentation and Assembly

Two strain gages were installed on the surface of the front section of the projectile body. They were oriented along the axial direction and opposite to each other. They were then connected to the two opposite arms of a Wheatstone bridge circuit. The output strain signal from the Wheatstone bridge was amplified by an amplifier circuit and then sampled and stored in a microprocessor. The amplifier circuit, the microprocessor, and the resistors in the Wheatstone bridge circuit were built together in a data acquisition and signal processing (SP&DAQ) board [Appendix A].

For protecting the strain gages during the operation of the projectile, a protection gear was necessary. Besides, the lead wires connecting the gages

and the data acquisition and signal processing unit also required protection. An aluminum tube with a length of 100 mm, an inner diameter of 19 mm, and an outer diameter of 21 mm was chosen as a protection jacket.

In assembly, the projectile body was inserted into the aluminum tube. Two circular rings and one conic ring were used to hold the projectile body tightly to the aluminum tube. Weld glue was also applied between the rear section of the projectile body and the aluminum tube. An aluminum lid was installed in the rear end of the tube after the battery and the SP&DAQ board were installed inside the rear section of the projectile body. Figure 4.6(a) shows a schematic of the overall assembly of the instrumented projectile while Figure 4.6(b) and 4.6(c) are the photographs of all individual parts of the instrumented projectile and the assembled instrumented projectile. For a signal triggering purpose, an infrared phototransistor was installed in the front end of the aluminum tube.

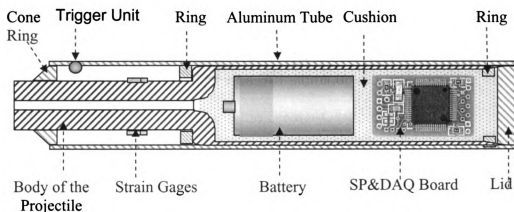


Figure 4.6 (a) Schematic layout of the instrumented projectile

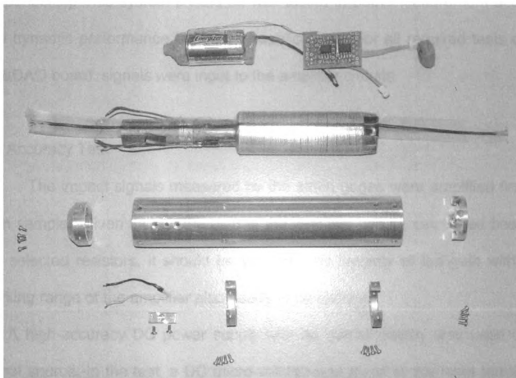


Figure 4.6(b) Parts of the instrumented projectile.



Figure 4.6(c) Assembled instrumented projectile.

#### 4. TESTING SIGNAL MEASUREMENTS

The penny-thin SP&DAQ board was used in the instrumented projectile rather than a high-performance amplifier and oscilloscope. It was designed compact enough so that it can be integrated with the instrumented projectile body

[Appendix A]. This system should be well tested in both measurement accuracy and dynamic performance before any applications. For all required tests on the SP&DAQ board, signals were input to the amplifier circuits.

#### 4.1 Accuracy Test

The impact signals measured by the strain gages were amplified first and then sampled. Even though the gain of the amplifier can be calculated based on the selected resistors, it should be verified. The linearity of the gain within the working range of the amplifier also needs to be checked.

A high-accuracy DC power supply with an output display was used as the signal source. In the test, a DC micro-voltage was given to the input terminal of the amplifier circuit. The board was then triggered for data sampling and storing. The stored data was then transferred to a computer. During the data processing, the measured data points were expressed in voltage and presented against the corresponding input voltage. Figure 4.7 shows the results of seven tests for the SP&DAQ board. The measured gain for this board is 155, a little smaller than 156, which is the theoretical gain calculated from the nominal resistance of the resistors.



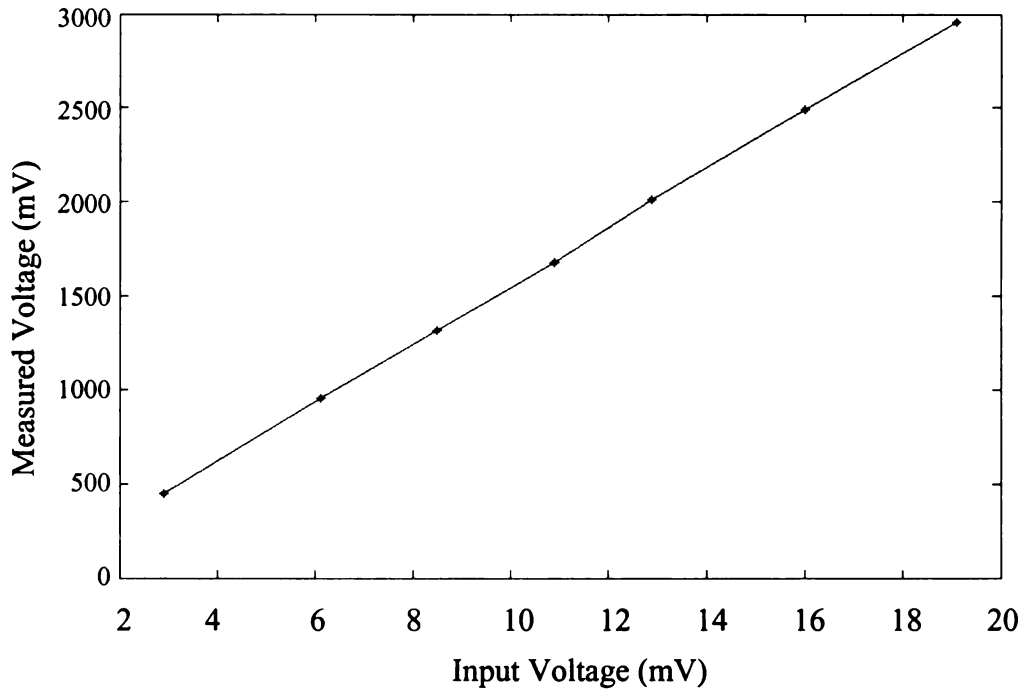


Figure 4.7 Input and output of a constant voltage test.

#### 4.2 Dynamic Signal Test

The SP&DAQ board was designed to measure dynamic signals. For later applications, it is necessary to identify the dynamic performance of the board, e.g. the sampling rate and the bandwidth of the whole system. The identification process was based on a dynamical signal test.

A signal generator was used as a signal source for the required dynamic test. Since the amplifier circuit required two inputs, one was always greater than the other, otherwise the output of the amplifier circuit would be zero [Appendix A, 20, 21, 22]. A continuous square wave with a micro-voltage and a proper positive offset was generated and forwarded to the 'always larger' input terminal of the amplifier circuit, while the other input terminal was connected to the ground. The

board was triggered by providing a required voltage to the trigger terminal, and then a part of the square wave series was amplified and sampled. Figure 4.8 shows the sampled result of an input square wave of 1075 Hz and 15 mV with an offset of 7.5 mV. In order to ensure the accuracy of the input square wave signal, the frequency was double checked by an oscilloscope. Based on the results shown in Figure 4.8, the sampling rate of the microprocessor was calculated by counting the sampled data points within a unit time. Using only the interior oscillator of the microprocessor and setting it to work at its highest frequency, the board was able to acquire 115 k samples per second (S/s). With the help of an extra 8 MHz oscillator for the microprocessor in the board, the microprocessor achieved 171 kS/s. The op-amps used in the SP&DAQ board have a bandwidth of 50 MHz, but the available microprocessors during this thesis research can only achieve roughly 200 kS/s. Due to the low sampling rate, the bandwidth of the whole SP&DAQ system is about 170 kHz.

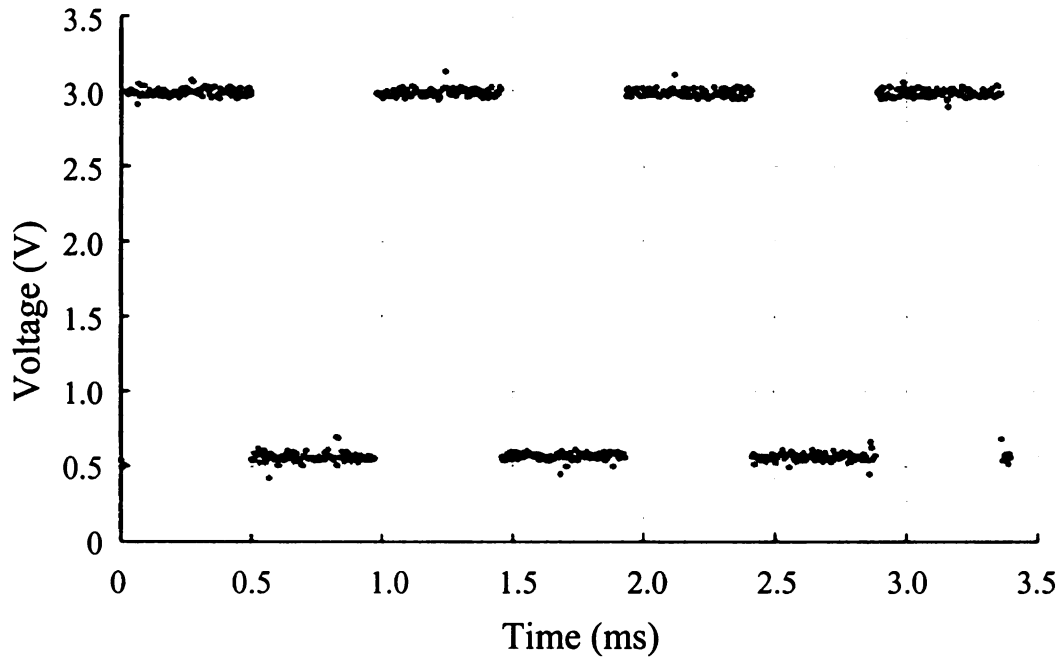


Figure 4.8 Square wave testing result.

## 5. TESTING WAVE REDUCTION

The wave reduction capability of the projectile needed to be identified before being used for any application. To begin with, the projectile body was half inserted into a gas gun barrel, leaving the front section outside the gun barrel, and was then launched onto a long instrumented rod aligned coaxially with the instrumented projectile. The long rod was made of stainless steel 347 and had a diameter of 12.7 mm and a length of 730 mm. A pair of strain gages was installed on the opposite surfaces about 334 mm from the impact end. Signals from both the projectile and the long rod were recorded simultaneously. Because the front section of the projectile body (where the strain gages were installed) was left outside of the gas gun barrel, there was no lead wire damage during testing. Therefore, the high-performance differential amplifier and the oscilloscope can be used for signal amplification and data acquisition. Identical Wheatstone bridge

circuits, amplifiers, and computer based oscilloscopes were used for both the instrumented projectile and the long rod.

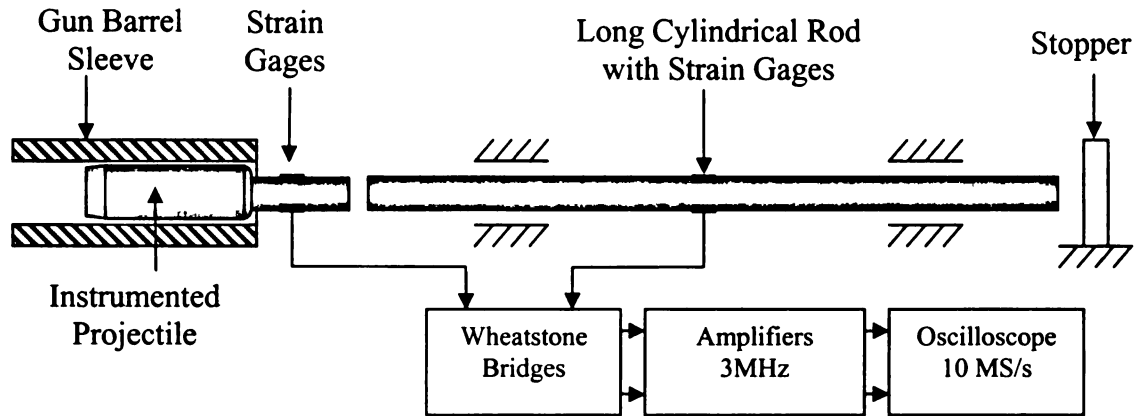


Figure 4.9 Setup of the wave reduction test experiment.

The impact-induced signal was amplified by a differential amplifier with a bandwidth of 3 MHz and acquired by a computer based oscilloscope with a sampling rate of 5 MS/s. Based on the setup of using a gun barrel sleeve, as shown in Figure 4.9, without manufacturing a new gun barrel, the wave reduction capability of the projectile body could be assessed for impact speeds up to 20 m/s. To avoid wave superposition in the location where strain gages were mounted, the impact duration should be equal or less than twice the time the wave travels from the gages to the nearest end of the rod [5-11]. When a long rod impacts with a short one, the impact duration is very much decided by the short one. So it is often required to have impact durations shorter than the time the wave travels between the two ends of the long rod. However, for the long rod to be completely exempted from wave superposition, the gage position is

essentially important. If the gage is located in the middle of the long rod, the chance for the wave to reflect from both ends and be superimposed at the gage position will be equal. If the gage is close to one end, even though the duration of a wave is shorter than the time the wave travels between the two ends, wave superposition at the gage position may still happen.

Both the wave propagations in the long rod and the short projectile were assumed to be one-dimensional. If the cross-section of the front section of the projectile body was identical to that of the long rod and they collided with each other coaxially, one-dimensional wave theory should satisfactorily predict the same impact force from both of them. Due to the limited selection of the cutting tools available as mentioned earlier, the front section of the projectile body was made hollow with an inner diameter of 5 mm and an outer diameter of 11.4 mm, which was not the same as the solid long rod with a diameter of 12.7 mm. The difference in cross-section might cause the imperfect use of one-dimensional wave propagation theory. Hence, similar but not identical results from both of them were expected.

Figure 4.10 shows the impact results from both the short projectile and the long rod. As expected, the two curves are not identical though they resemble each other up to some extent, implying the feasibility of using the short projectile. The result from the long rod shows that the initial waves and the reflected wave do not superimpose with each other. The result from the short projectile also does not show any obvious reflected waves except a little oscillation right after the impact wave, likely due to imperfection from the machining of the projectile

body. It then is concluded that the short projectile works well against wave reflection and superposition.

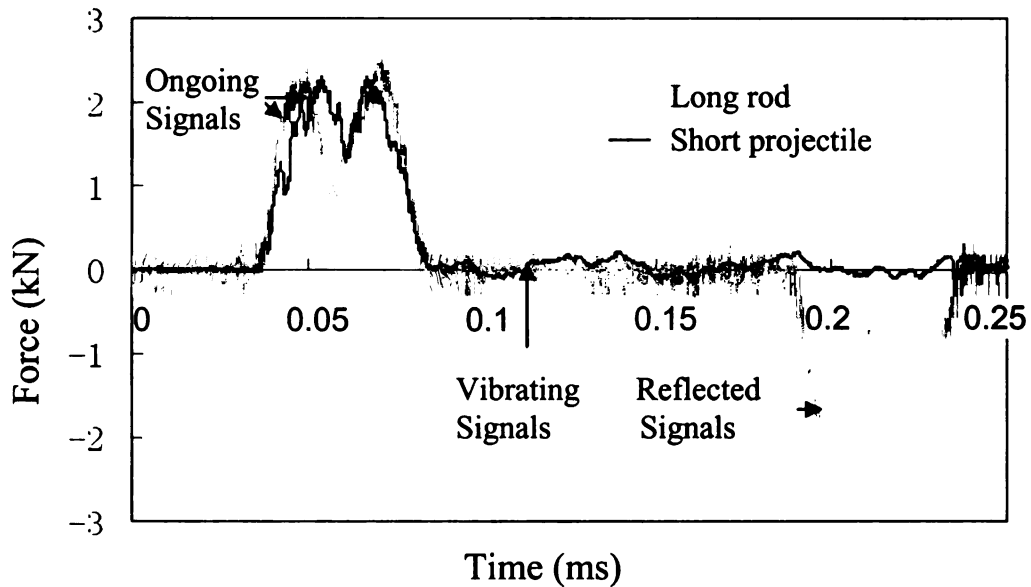


Figure 4.10 Comparison between the results from the long bar and the projectile body.

## 6. CALIBRATION OF THE INSTRUMENTED PROJECTILE

The instrumented projectile needs to be calibrated before being used for impact testing. The setup for calibration was similar to future real applications except that the testing specimen was substituted by a long instrumented rod. The velocity of the instrumented projectile was measured by a speed measurement device [Appendix A], and the infrared emitting diodes on it were used to trigger the data acquisition for the instrumented projectile. Once a test was completed, the projectile was unsealed and the recorded data on the SP&DAQ board was downloaded onto a computer for analysis.

As mentioned above, the only difference between the calibration and a real application is the target for impact. In the calibration, a long instrumented rod was used as the target instead of a real specimen. The long instrumented rod was very similar to the rod used for dynamic testing used earlier except the rod length and the positions of the strain gages. The rod used for calibration had a length of 1790 mm and the gages were installed at a location 430 mm from the impact end. The reason for using this longer rod than the one used before (730 mm) was aimed at increasing the impact duration between the instrumented projectile and the longer instrumented rod.

Figure 4.11 shows the setup of the calibration for the instrumented projectile. A calibration test based on a projectile speed of 15 m/s was performed. Figure 4.12 shows the result measured by the instrumented projectile, while Figure 4.13 shows the same result in force domain from the longer instrumented rod.

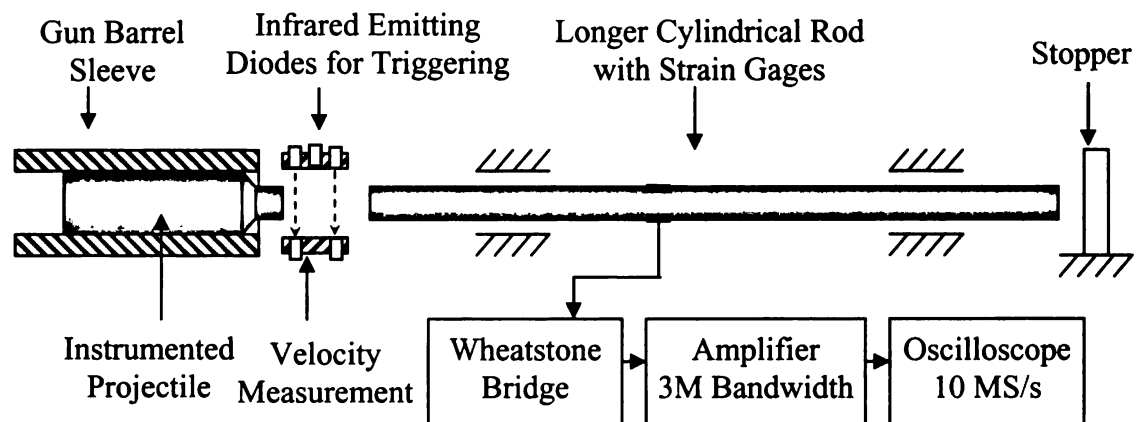


Figure 4.11 Setup for the calibration of the instrumented projectile.

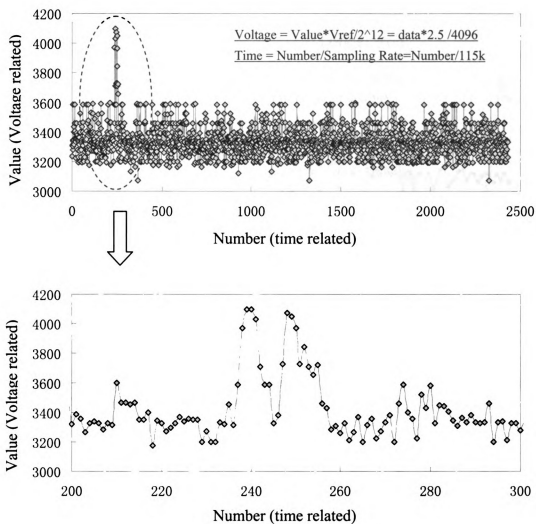


Figure 4.12 Impact result measured by the instrumented projectile.



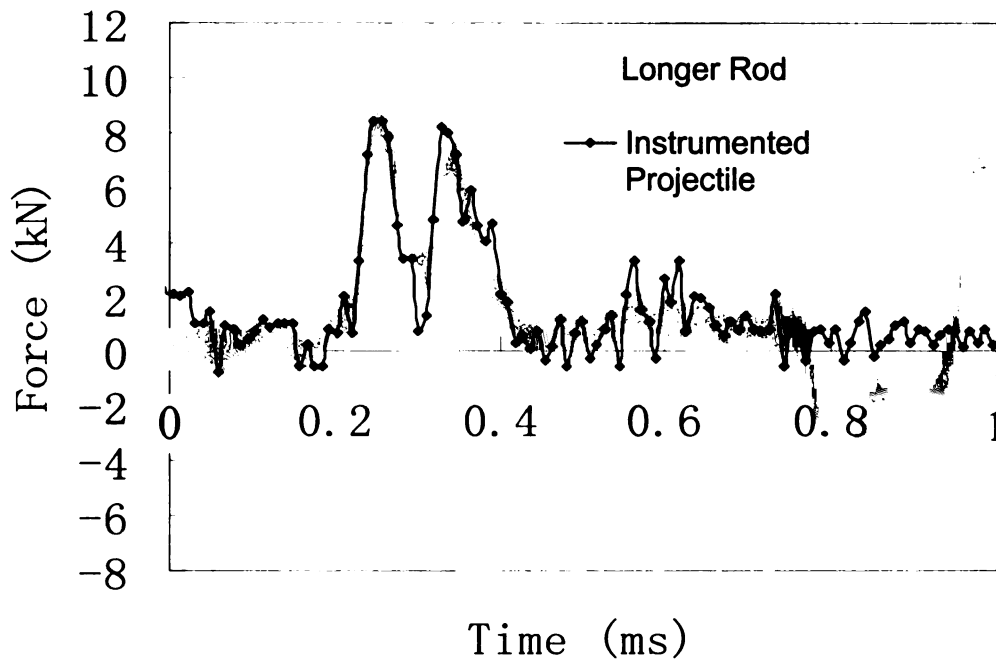


Figure 4.13 Comparison between the result from the longer rod and that from the instrumented projectile when they impact with each other.

## 7. CASE STUDY OF THE INSTRUMENTED PROJECTILE

Figure 4.14(a) shows a setup for the application of the instrumented projectile and Figure 4.14(b) shows the impact force history measured by the instrumented projectile impacting onto a 114 mm x 76 mm x 25.4 mm aluminum plate having fixed edges. The impact speed of the instrumented projectile was 14 m/s. A ring-shaped indentation was found on the aluminum plate with a depth of about 0.1 mm. The ring-shape indentation was caused by the hollow cylindrical head of the instrumented projectile.

Figure 4.14(c) shows the impact force history measured by a load cell in a low-velocity drop-weight impact tester for the same type of aluminum plate mentioned above. The plate had a fixed boundary condition around four edges,

as well. The impact speed was 4 m/s. A semi-sphere indentation with roughly 5 mm in diameter and 0.5 mm in depth was found on the aluminum plate. The semi-spherical indentation was caused by the solid semi-spherical head of the low-velocity impact tester.

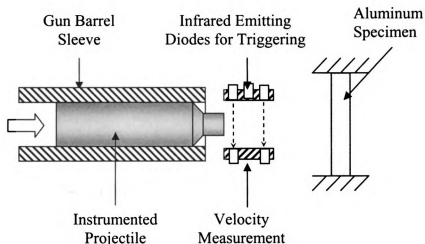


Figure 4.14(a) Setup for impact test based on instrumented projectile.

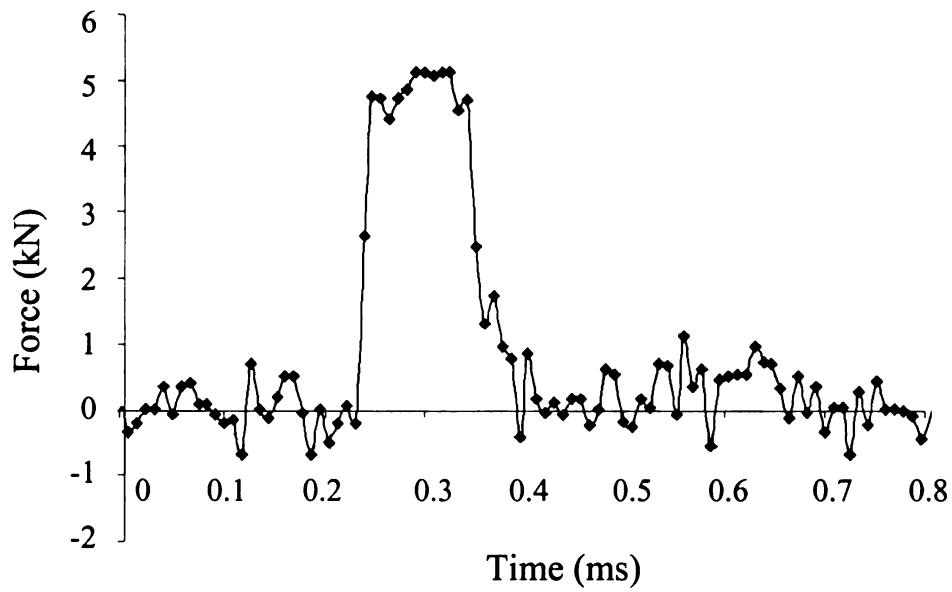


Figure 4.14(b) Force history measured by instrumented projectile.

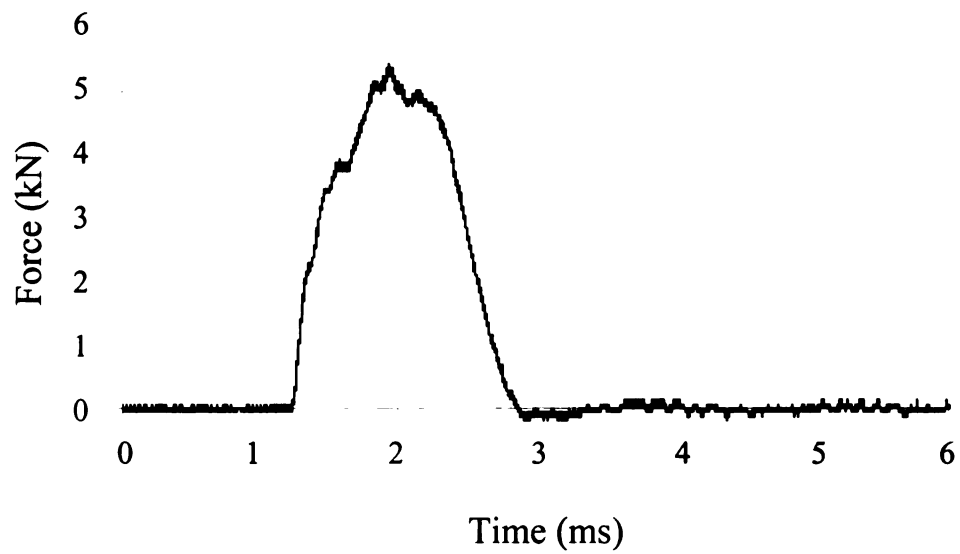


Figure 4.14(c) Force history measured by a low-velocity drop-weight impact tester.

## 8. DISCUSSIONS

The calibration test shows that the prototype instrumented projectile meets the requirements for a wireless high-bandwidth force transducer. The following issues may be addressed for future improvements.

### 8.1 Longer Gun Barrel

The current setup allows the instrumented projectile be accelerated up to 20m/s. It provides enough power for the instrumented projectile to reach a high impact force when impacting on a 'hard specimen', such as a stainless steel rod. However, it is not powerful enough for real applications such as ballistic impact. A longer gun barrel is needed for high-speed ballistic impacts.

### 8.2 Wave Transfer Section

The current wave reduction mechanism was achieved by using the cutting tools available. The cutting tools unfortunately do not have the ideal geometry to machine double parabolic surfaces for focusing wave fronts onto a ring for wave transfer and eventually divergence. In order to machine the double curved surfaces of the middle transfer section, the inner portion of the front section of the projectile body needed to be removed, resulting in a hollow tube instead of a desired solid circular rod.

### 8.3 The Sampling Rate

For the microprocessor used in the SP&DAQ board, the maximum sampling rate was 200 kS/s (Samplings per second). With its own oscillator and the battery used, the sampling rate is 115 kS/s; with the help of an extra 8 MHz oscillator, the sampling rate is 171 kS/s. To increase the sampling rate to the maximum of the microprocessor, 200 kS/s, an extra oscillator with a higher frequency should be used, and the power voltage of the microprocessor should also be increased.

#### 8.4 Triggering Mechanism

A 940nm infrared phototransistor was used for the measurement of projectile speed as well as the triggering of the data acquisition system. The trigger terminal of the microprocessor was connected to the positive terminal (+3 VDC) of the power supply through a 1 k $\Omega$  resistor that was also connected to the ground of the system through the infrared phototransistor. The voltage at the trigger terminal would be kept with a high voltage by this setup, and the control program used a low voltage (0 - 0.4 VDC) as a trigger signal. When the phototransistor received an infrared light from the emitting diode, it lowered the voltage of the trigger terminal to trigger the data acquisition system. This action required an infrared light with a high intensity and long duration. When the speed of the projectile increases, more infrared emitting diodes along the path of the projectile would be required to ensure the phototransistor has more time to receive the infrared light.

#### 8.5 The Connectors

Some connectors were used for the power and data transferring interfaces of the SP&DAQ board. Due to the limited space, relatively smaller connectors were used. Some unsuccessful tests during the course of the study were traced down to the failure of the connectors. Small and reliable connectors are needed for future improvement.

## 8.6 Assembly Issues

Two rings were attached to the inside of the aluminum tube to hold the rear section of the projectile body and weld glue was also applied between the tube and the rear section of the projectile body. However, these were still not sufficient for impacts involving large forces. A new assembling technique is highly necessary.

## 9. CONCLUSIONS

An instrumented projectile was designed and constructed. The wave reduction section of the instrumented projectile was not optimal due to the limitation of the available cutting tools. Based on a series of calibration tests on the instrumented projectile itself, as well as its components, the ability of the instrumented projectile to be used as a low-velocity (up to 20 m/s) and a high-bandwidth (170 kHz) dynamic force transducer was validated.

## REFERENCES

- [1] Jurg Dual, "Application of a Transducer Embedded in a Projectile for Penetration Force Measurement", Thesis for Master Degree, University of California, Berkeley, July 10, 1984
- [2] S. P. Virostek, J. Dual and W. Goldsmith, "Direct Force Measurement in Normal and Oblique Impact of Plates by Projectiles", *Int. J. Impact Engng* Vol. 6, No. 4, pp.247-269, 1987
- [3] Joshua Liss, Werner Goldsmith, "Plate Perforation Phenomena due to Normal Impact by Blunt Cylinders", *Int. J. Impact Engng*, Vol. 2, No. 1, pp.37-64, 1984
- [4] S. Venzi, A. H. Priest, and M. J. May, "Influence of Inertial Load in Instrumented Impact Tests", *Impact Testing of Metals*, ASTM STP 466, American Society for Testing and Materials, 1970, pp.165-180
- [5] James F. Doyle, "Waves Propagation in Structures, Spectral Analysis Using Fast Discrete Fourier Transforms", Second Edition, Mechanical Engineering Series, 1997
- [6] C. Bacon, "Numerical prediction of the propagation of elastic waves in longitudinally impacted rods: application to Hopkinson testing", *International Journal of Impact Engineering*, 13 (4), 527-539, 1993.
- [7] Jonas A. Zukas, Theodore Nicholas and Hallock. F. Swift, *Impact Dynamics*, John Wiley & sons Inc. 287-308, 1982.
- [8] D. J. Frew, M. J. Forrestal and W. Chen. "Pulse shaping techniques for testing brittle materials with a split Hopkinson pressure bar", *Experimental Mechanics*, 42 (1), 93-106, 2002.
- [9] Michael Adam Kaiser, *Advancements in the split Hopkinson bar test*, Master's thesis, Blacksburg, Virginia, 1998.
- [10] Frank E. Hauser, "Techniques for measuring stress-strain relations at high strain rates", *Experimental Mechanics*, 395-402, 1966.
- [11] J. F. Bell, "An experimental diffraction grating study of the quasi-static hypothesis of the split Hopkinson bar experiment", *J. Mech. Phys. Solids*, 14, 309-327, 1966.
- [12] Gerald L. Jones and Edmund G. Henneke, II, "Reflection of Stress Waves at

a Free Boundary in Quartz Single Crystals", IEEE Transactions on Sonics and Ultrasonics, Vol, Su-20, No. 3, July 1973

- [13] Kasaburo Harumi, Tetsuo Saito, "Educational Films for Ultrasonic Engineers", IEEE Ultrasonics Symposium, 1982, pp. 1074-1078
- [14] M. D. Sharma, "3-D wave propagation in a general anisotropic poroelastic medium: reflection and refraction at an interface with fluid", Geophys. J. Int. (2004) 157, pp. 947-958
- [15] Baljeet Singh, "Reflection of P and SV waves from free surface of an elastic solid with generalized thermodiffusion", Earth Syst. Sci. 114, No. 2, April 2005, pp. 159-168
- [16] Baljeet, Singh, "Reflection of homogeneous elastic waves from free surface of nematic elastomer half-space", J. Phys. D: Appl. Phys. 40 (2007), pp. 584-592
- [17] Zhi-Jun Dai, Zhen-Bang Kuang, She-Xu Zhao, "Reflection and transmission of elastic waves at the interface between an elastic solid and a double porosity medium", International Journal of Rock Mechanics and Mining Sciences 43 (2006) pp. 961-971
- [18] Kunyu Wu, Qiang Xue, and Laszlo Adler, "Reflection and transmission of elastic waves from a fluid-saturated porous solid boundary", J. Acoust. Soc. Am. 87(6), June 1990
- [19] Jose M. Carcione, "Reflection and transmission of qP-qS plane waves at a plane boundary between viscoelastic transversely isotropic media", Geophys. J. Int. (1997) 129, pp. 669-680
- [20] Texas Instruments, "2.2V, 50MHz, Low-Noise, Single-Supply Rail-to-Rail Operational Amplifiers", SBOS365B, June, 2006, Revised Sep. 2006
- [21] Bonnie Baker, "Single-Supply, Low-Power Measurements of Bridge Networks", Burr-Brown Application Bulletin, April, 1993
- [22] James Karki, "Signal Conditioning Wheatstone Resistive Bridge Sensors", Application Report, Texas Instruments, SLOA034, Sept., 1999



## **CHAPTER FIVE**

### **CONCLUSIONS AND RECOMMENDATIONS**

#### **1. CONCLUSIONS**

The vertical impact systems are simpler and less costly than the horizontal impact systems. However, the latter are free of gravitational effect and can achieve higher impact velocity. In measuring the contact-impact forces, strain-gage based sensors are not sensitive to oscillation as much as accelerometers. This is because the former are based on deformation while the latter, the motion. This is especially true in vertical impact tests. Among the strain-gage based sensors, the load cell seems to be more effective for relatively soft specimens, while the striker is more suitable for recording hard impact if the wave superposition effects can be eliminated. Accordingly, a horizontal impact system using a strain-gage-based force transducer seems to be an ideal system for contact-impact testing.

Experimental results showed that reflected waves and their superposition with the initial impact wave can complicate the impact force measurements. The complication increases as the impact duration becomes shorter. Based on a mechanical technique to redirect the reflected waves, a wave reduction method was proposed and verified. The initial wave associated with the impact force could be identified.

Besides the mechanical technique, two numerical techniques, the so-called Initial Wave Assumption technique and the Two-Point technique, were also proposed and verified to be able to recover the initial impact force wave.

The success of the wave reduction techniques to recover the initial impact force wave shed light on designing an instrumented projectile with a short rod. Preliminary studies for both wired and wireless instrumented projectiles were explored.

An instrumented projectile was designed and constructed. The wave reduction section of the instrumented projectile was not optimal due to the limitation of the available cutting tools. Based on a series of calibration tests on the instrumented projectile itself, as well as its components, the ability of the instrumented projectile to be used as a low-velocity (up to 20 m/s) and a high-bandwidth (170 kHz) dynamic force transducer was validated.

## 2. RECOMMENDATIONS

The calibration test shows that the prototype instrumented projectile meets the requirements for a wireless high-bandwidth force transducer. The following issues may be addressed for future improvements.

The current setup allows the instrumented projectile to be accelerated up to 20m/s. It provides enough power for the instrumented projectile to reach a high impact force when impacting on a 'hard specimen', such as a stainless steel rod. However, it is not powerful enough for real applications such as ballistic impact. A longer gun barrel is needed for high-speed ballistic impacts.

The current wave reduction mechanism was achieved by using the cutting tools available. The cutting tools unfortunately do not have the ideal geometry to machine double parabolic surfaces for focusing wave fronts onto a ring for wave transfer and eventually divergence. In order to machine the double curved surfaces of the middle transfer section, the inner portion of the front section of the projectile body needed to be removed, resulting in a hollow tube instead of a desired solid circular rod.

For the microprocessor used in the SP&DAQ board, the maximum sampling rate was 200 kS/s (kilo-Samples per second). With its own oscillator and the battery used, the sampling rate is 115 kS/s; with the help of an extra 8 MHz oscillator, the sampling rate is 171 kS/s. To increase the sampling rate to the maximum of the microprocessor, 200 kS/s, an extra oscillator with a higher frequency should be used, and the power voltage of the microprocessor should also be increased.

A 940nm infrared phototransistor was used for the measurement of projectile speed, as well as the triggering of the data acquisition system. The trigger terminal of the microprocessor was connected to the positive terminal (+3 VDC) of the power supply through a 1 k $\Omega$  resistor that was also connected to the ground of the system through the infrared phototransistor. The voltage at the trigger terminal would be kept with a high voltage by this setup, and the control program used a low voltage (0 - 0.4 VDC) as a trigger signal. When the phototransistor received an infrared light from the emitting diode, it lowered the voltage of the trigger terminal to trigger the data acquisition system. This action

required an infrared light with a high intensity and long duration. When the speed of the projectile increases, more infrared emitting diodes along the path of the projectile would be required to ensure the phototransistor has more time to receive the infrared light.

Some connectors were used for the power and data transferring interfaces of the SP&DAQ board. Due to the limited space, relatively smaller connectors were used. Some unsuccessful tests during the course of the study were traced down to the failure of the connectors. Small and reliable connectors are needed for future improvement.

Two rings were attached to the inside of the aluminum tube to hold the rear section of the projectile body and weld glue was also applied between the tube and the rear section of the projectile body. However, these were still not sufficient for impacts involving large forces. A new assembling technique is highly necessary.

## **APPENDIX A**

### **DESIGN A PENNY-SIZE SIGNAL PROCESSING AND DATA ACQUISITION (SP&DAQ) SYSTEM**

#### **1. INTRODUCTION**

The instrumented projectiles are designed to measure the dynamic force history during impacts; they will be shot out from the gas gun powered by high pressure Nitrogen gas or air. The signal measurement unit and its battery should be put into the instrumented projectile and move with it during impact tests. The impact information measured will be saved by the measurement unit during impacts. The saved data is then transferred out for further data processing.

Besides the instrumented projectile unit, the whole system also includes a gas gun unit, a speed measurement unit, a trigger unit, and a calibration unit. The instrumented projectile, the trigger, and the speed measurement units will be discussed in this section.

#### **2. DESIGN OVERVIEW**

When the instrumented projectile impacts the specimen, the impact force history is measured by two strain gages installed on the projectile. The gages are connected to the opposite arms of a Wheatstone bridge circuit, which is followed by a signal amplifier. The data acquisition system digitizes the amplified signals

and saves them during impact tests. After the test, the saved digitized signals will be transferred out.

The whole electrical measurement system includes: a Wheatstone bridge circuit section; a signal amplifier section; a data acquisition section and a data saving section. Because the instrumented projectile is used for dynamic force measurement, a trigger section is also needed. After the test, a data transferring section will be used to transfer the saved data out.

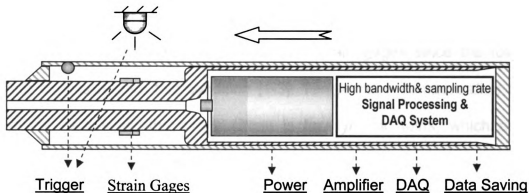


Figure A1 Schematic layout of the measurement system of the instrumented projectile

Because the whole system is powered by a battery, the energy consumption should always be kept in mind. For example, using strain gages with larger resistance, choosing low energy consuming chips, and programming the system to low energy consuming status when waiting for trigger, etc. Since the instrumented projectiles are designed for impact tests, the amplifiers should have high bandwidth and the data acquisition part should have a high sampling rate. The data saving speed should keep the same rate with the data sampling.

## 2.1 Strain Gages and Wheatstone Bridge

Strain gages are used to sense the impact force. At a cross-section of the cylindrical projectile body, two strain gages are installed oppositely across the diameter. They are then connected to the opposite arms of a Wheatstone bridge circuit in order to measure the compression & tension waves and eliminate the bending effects of the projectile. The Wheatstone bridge is chosen here because of its differential output -- the useful signals could be amplified without any kind of filtering. Another two arms of the Wheatstone bridge are resistors; their resistances should be a little larger than the strain gages since the followed amplifier circuits require this condition [1-3]. Temperature compensation is not considered here since the whole circuit is for dynamic tests, which usually happen in a fraction of second.

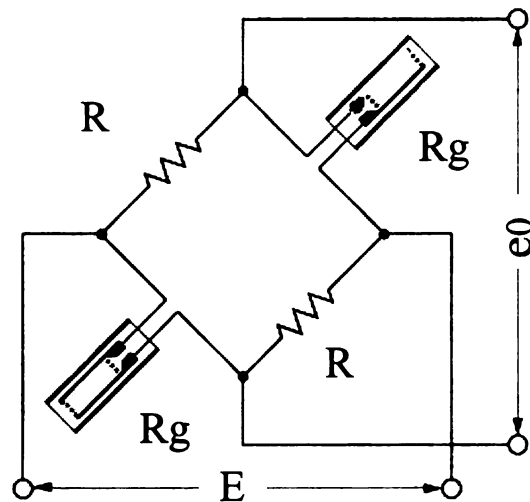


Figure A2 Schematic of the Wheatstone bridge

The whole instrumented projectile measurement unit is powered by a battery, and the Wheatstone bridge circuits are the major energy consuming parts in the whole system. 1000 ohm strain gages are used because they consume less

energy than the common 350 ohm and 120 ohm strain gages. The gage length should be less than 3 mm for the elastic wave measurement [4,5].

## 2.2 Amplifier

It is designed that the materials of the projectiles only deformed in their elastic stage. Therefore, the strain signals from the instrumented projectiles are relatively small, this requires the signals to be amplified for the subsequence data acquisition and saving.

Differential amplifiers are ideal for the signals from the Wheatstone bridge circuits. The differential amplifier circuit containing three operational amplifiers (op-amp) is usually used, one for amplifying, and another two for improving the input impedance [6]. The op-amps in the differential amplifier circuit require the dual polarity power supply. However, the single battery cannot provide these without the help of some special circuits.

There is an amplifying circuit which has high input impedance and contains only two op-amps. It requires one input to be always larger than the other; if it is equal or less than another one, the output would be zero [1-3]. In this circuit, the op-amps could be powered with normal DC power sources. For the impact tests, the first pulse is the focus, and it always contains compression signals. The signals after the first pulse should be constant or just have minimal vibration due to the special geometry of the projectiles. In order to save space and reduce the energy consumption, the amplifying circuit with two op-amps is used. To make



sure one output is always larger than another one, two extra resistors with small resistance are added to the dummy arms of the Wheatstone bridge circuit.

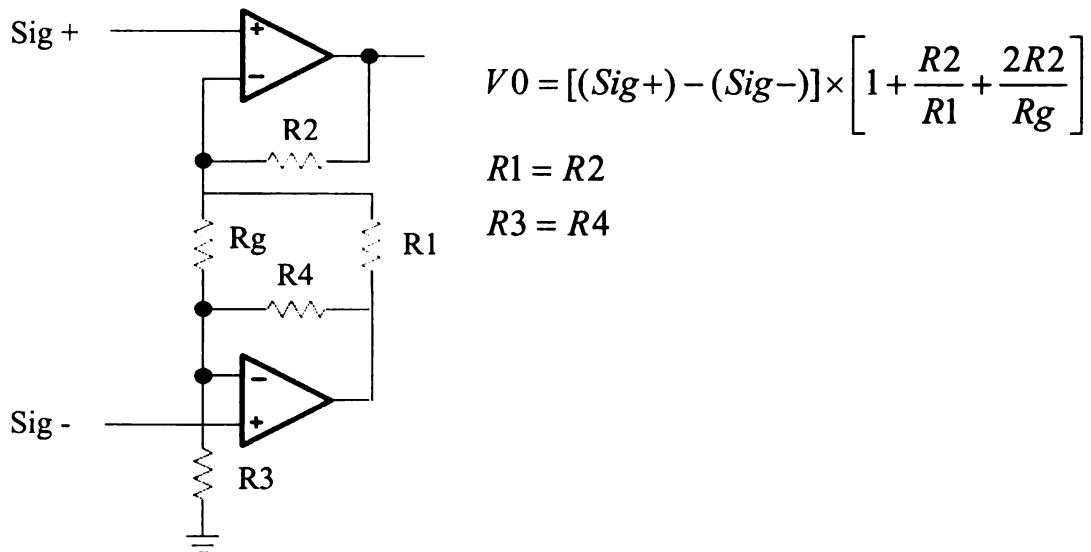


Figure A3 Schematic of the amplifier circuit.

## 2.3 Data Acquisition and Saving

The amplified impact signals are to be digitized and saved for later data processing. Since the instrumented projectiles are designed for measuring impact force histories with very short durations, the sampling rate of the data acquisition should be as high as possible. For most microprocessors during this thesis research, the maximum sampling rate is about 200 k samples per second.

The sampled data should be saved immediately. Therefore, the data saving rate must be the same with the data sampling rate. RAM is the suitable media for the data saving, rather than flash memory, hard disc, etc. because the high data saving rate can be achieved easily. RAM requires continuous electrical power to maintain the data.

An impact usually lasts only a few milliseconds. The high sampling rate with limited memory cannot acquire the desired impact signals in such a short duration without proper triggering. There are two common sampling modes with triggering. One is, the processor keeps sampling and saving, the new data will overwrite the old one inside the memory; when the trigger comes, it will keep sampling and saving for a certain time, then stop; The other is, the whole data acquisition and saving system waits for the trigger, when the trigger event happens, they wake up and begin to sample. Because the electrical system of the instrumented projectile is powered by a battery, the energy consumption becomes a major concern. Therefore, the second operation mode is used for the controlling program of the microprocessor.

## 2.4 Trigger

With the limited memory and extra high sampling rate, an efficient trigger is a key factor for a successful measurement.

An infrared phototransistor and several infrared emitting diodes are used together to trigger the data acquisition and saving. The infrared phototransistor is installed in the instrumented projectile, while the infrared emitting diodes are installed on the outlet of the gas gun barrel. When the projectile passes by the infrared emitting diodes, the phototransistor in the projectile will sense the infrared radiation and cause the voltage variation on it, which can be used for triggering.

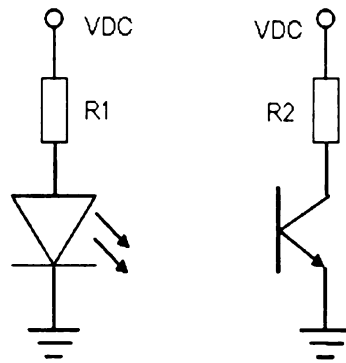


Figure A4 The schematic triggering circuits with the infrared emitting diode and infrared phototransistor.

### 3. DESIGN AND MANUFACTURING

#### 3.1 Strain Gages

1.524 mm gauge length strain gages with 1000 ohm resistance from the Vishay Company are used in the instrumented projectiles. Small length gages are chosen because they are more suitable for sensing strain waves [7]. Larger resistance gages are chosen since they will consume less electrical energy.

#### 3.2 Trigger

Peak wavelength 940 nm with 19 mm diameter infrared phototransistors and infrared emitting diodes are selected for the triggering. One infrared phototransistor is installed in the projectile while 28 infrared emitting diodes are installed on a sleeve, which is coaxially installed at the outlet of the gun barrel. The infrared emitting diodes are in 4 x 7 array, four of them are installed in the same cross section of the sleeve, roughly 20 degrees between the neighbored ones, and there are 7 layers altogether along the axial direction. Installing 28

infrared emitting diodes instead of one is to avoid mis-triggering during tests. The infrared emitting diodes are always on during tests. When the projectile passes by, the infrared phototransistor can sense the infrared emission and trigger the data acquisition and saving system. Since the visible light's wavelengths are from 400 nm to 700 nm, choosing a phototransistor with 940 nm peak wavelength can reduce the influences of the visible lights. Choosing small size parts is due to the limited space for the parts in the projectile.

### 3.3 Signal Processing, Data Acquiring and Saving Unit (SP&DAQ unit)

The dummy resistors of the Wheatstone bridge circuits, the op-amps and the resistors of the amplifying circuits, the microprocessors for data acquisition and saving, and the accessory parts for the circuit are all designed to be in the same unit. The drawing of the circuit is showed in Figure A5.



129

### 3.4 Microprocessor

An MSP430f1611 microcontroller from TI was chosen to be the microprocessor for the data acquisition and saving [8-12]. Its features include: an ultra low power consumption processor with low supply voltage range, 1.8 – 3.6 V; five power-saving modes, wake-up time from standby mode is less than 6  $\mu$ s; dual 12 bit A/D converters with synchronization; 48 kB flash memory, in which the control program can be saved; 10 kB RAM, which can be used to save the measured data.

This microprocessor can be controlled by the programs written in C language or in the assembly language. C language is easier for programming, but the program in C language can only control half of the total 10 kB RAM. Finally, the assembly language is used to write the control program of the microprocessor.

The program is based on the Interrupt mode. It includes a main program and several subroutines. The main program sets up and initializes all the interrupt vectors and the RAM; a data acquisition and saving subroutine is programmed for digitalizing the signals and saving them; a trigger interrupt subroutine is used to start the data acquisition and saving subroutine; a data transferring interrupt subroutine is designed to transfer the measured data out and reset the vectors for next test. The data acquisition and saving subroutine used the highest frequency clock (up to 8 MHz) for the highest sampling rate. The standby and the data transfer subroutine used the lowest frequency clock (33 KHz) for power saving purpose.

In the main program, there are several alternative variables which include a variable to set the input channel numbers: single or dual channels; a variable to decide the data acquisition reference voltage: 3 V or 2.5 V; a variable to decide the data accuracy: 8 bit or 12 bit; a variable to increase the trigger delay time. These variables can be combined, thus making it easier to obtain a suitable program to download to the microcontrollers for different tasks.

An LED indicator is used to show the running status of the program [13]. It is ON when the electrical power is added to the microprocessor and it is OFF after the data acquisition and data saving. When the data is transferred out, the LED indicator is turned on again to indicate that the system is ready for the next test.

The microcontroller is of 64-Pin Quad Flat Pack. The total dimension is 11.8 mm x 11.8 mm x 1.45 mm. It makes the total width of the electrical board not less than 12 mm; it also makes the diameter of the projectile larger than the expected size – half inch.

### 3.5 Amplifiers

An operational amplifier OPA2365 from the TI Company is used for the amplifier circuit [2]. It can be powered by a range from +2.2 VDC to +5.5 VDC, and has 50 MHz bandwidth and relatively low noise. There are two op-amps in one SO-8 package. Therefore, it is easier to achieve the desired differential amplifier circuit with one amplifier chip.

In the design, there are two amplifying circuits corresponding to the possible two input channels. There are two amplifier chips installed on the electrical print board.

### 3.6 Resistors for the Wheatstone Bridge

The strain gages installed on the instrumented projectile have  $1000 \pm 0.3\%$  ohm resistance. Accordingly, originally  $1000 \pm 0.1\%$  ohm resistors are selected for the dummy arms of the Wheatstone bridges. Even though it is not necessary to make the bridge circuit balance for dynamic measurements, an almost zero output at unloading status would be preferred since it makes the followed signal amplifying and data acquisition easier.

As mentioned before, the amplifying circuit needs one input to be always larger than the other. Therefore, an extra  $6 \pm 5\%$  ohm resistor is put into each resistor's arm in series (shown in Figure A5, the right-upper corner). Since the projectile is desired to work in the elastic stage, the strain signals from the strain gages have a fixed range. The extra resistors will make the outputs of the Wheatstone bridge to meet the requirement of the chosen amplifying circuit – one output is always larger than the other.

### 3.7 Print Board and Soldering

After the breadboard verifications, the print board is designed and some pieces are manufactured. The print board is designed as small as possible, and all of the electrical parts are chosen in their relatively small packages.



The 'ExpressPCB' company provides convenient service for manufacturing customer designed print board. The drawings of the board are made with the software provided by this company. The board is penny-sized and double-sided, with length 26 mm and width 15 mm.

The 64 pins small chips are soldered with a normal soldering gun. The surface mounted chips are very sensitive to moisture, they had to be kept in a dry cabinet and their moisture rate must be monitored [14].

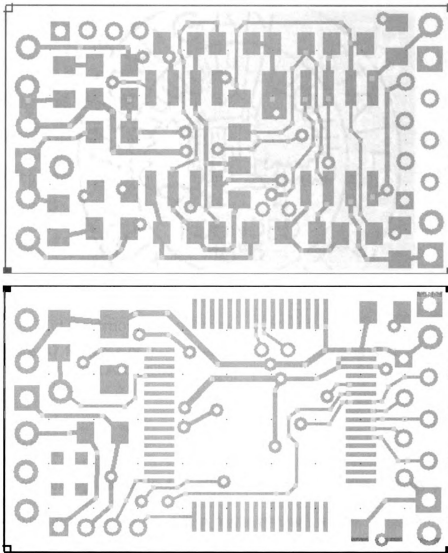


Figure A6 Both sides of the print board

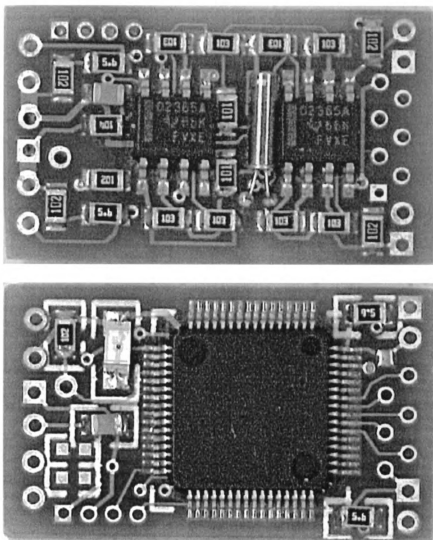


Figure A7 Pictures of the soldered Signal Processing and Data Acquisition Unit.

### 3.1 Battery

Even though all selected chips are so called low energy consuming ones, their working currents are still in micro ampere levels. Table A1 shows the power

consumption of each components and their summation when tested under 3.3 VDC voltages.

Table A1 Electrical current consumption of each component

Voltage = 3.3V	Microcontroller	Signal Amplifier	Bridge	Sum
Current (mA)	1.15	6.24*2	8.3*2	30.23

The total currents are beyond the ability of the normal button batteries. A Lithium battery—EL1CR2 from the Energizer company is selected, its feature includes: 3.0 V nominal voltage with 800 mAh capacity; 11 grams in weight. It has 15.1 mm in diameter and 27 mm in length. One battery can power all of these electrical parts, and its volume, especially the diameter, meets the requirement.

### 3.9 Wiring

The strain gages are installed on the surface of the front part of the projectile. The battery and the signal processing, data acquisition and saving unit are at the rear part, inside of the projectile. Wires have to be used to connect them. Because the body of the projectile has strict geometrical limitations, there is no possibility for the connecting wires to go through directly. The wires have to be installed between the main projectile body and the protection tube. Since there is only tiny space left between this two, the small square cross-section enamel insulated wire, 134-AWP, from the Vishay Company is selected and glued inside

of the gap between the projectile body and the protection tube. Because the projectile and the protection tube are also glued together permanently, 50% extra wires are installed in case of wires broken during impacts.

### 3.10 Connectors

There are two sets of connectors used. One is between the battery and the SP&DAQ unit, and another is for the data transferring port of the SP&DAQ unit. The battery cannot be connected permanently, and it will be replaced after several tests, so a connector is very necessary here. The connector for data transferring will be used after each test, because the impact information will be read out through it.

Since the battery and the SP&DAQ unit occupies almost all the space inside of the projectile, the connectors have to be tiny. Because the power must remain on for the microprocessor, especially its RAM memory, the connectors must be very reliable. The 1 mm micro socket and header with 2 conductors and 4 conductors are chosen and carefully soldered for the connections.

### 3.11 Battery and SP&DAQ unit protection

The battery and the SP&DAQ unit are installed into the instrumented projectile and run with it. They will sustain the impact force during tests. The survivability of the battery and the SP&DAQ unit during tests is worthy of discussion.

The board needs electrical power during the impact tests, and the power should be kept on until the data is transferred out. If the power supply is disconnected, the system will be shut down; all of the measured data will be lost.

The possible power disconnection could happen at the terminals of the battery. The battery cannot be soldered due to safety and performance reasons. How to connect the wires with the terminals of the battery becomes a problem. There is a hole at the anode terminal of the battery, which can be used to tie the wire. For the cathode terminal, a small spring is used to keep the connection.

Two rubber pads are tightly attached to both ends of the battery; they are tied with thin fish line. The rubber pads will work like cushions to reduce the possible battery damage during impacts. There are two rubber pads attached to the electrical print board, as well. The board is also wrapped with electrical tape to ease the lateral acceleration of the chips during impacts.

## 4. SUPPORTING SYSTEMS

### 4.1 The Control Programs

The control program is written in assembly language. It is written, debugged with specific software, and then downloaded into the microprocessor. The software is called IAR Embedded Workbench, the program developing environment for TI's MSP 430 family microprocessors. Another MSP430f1611 developing kit from the SoftBaugh company is also used. It includes a testing board with the microprocessor and some accessories; a USBP MSP430 Flash Programming Adapter for implanting the program into the

microprocessors; and an installation program for modifying the IAR environment and for installing the driver of the USBP Programming Adapter.

The IAR software is installed first, and then the installation program from SoftBaugh modifies the IAR for its hardware. The program for the microprocessor is written, debugged in the modified IAR environment, and then downloaded to the microprocessor in the testing board for verification until the program is finally successful for the task. For any new manufactured SP&DAQ unit, the control program is opened in the IAR software first, and then downloaded to the microprocessor of the unit through the USBP MSP430 Programming Adapter.

#### 4.2 Data Transferring Circuit and Software

The data saved in the RAM of the microcontroller is in binary format. They should be transferred into a computer as hexadecimal numbers or decimal numbers for further processing. An interface box is designed and manufactured, and a free interface program is downloaded for this purpose.

The microcontroller has many pins for input/output, two of them are chosen for the data transferring. In the data transfer subroutine of the program, one of these pins is appointed to be the data transfer controller and another to be data port. At anytime during running the program, if the microcontroller gets data from the data transfer controller pin with specific format and value, the program will go to the data transferring interrupt subroutine and send all the data in the RAM out through the data port.

The COM port of a desktop computer is used to communicate with the microcontroller under the RS232 interface protocol. Because the microcontroller has a different communication protocol, a data transfer interface box is designed and manufactured.

The data transfer interface box bases on the chip – MAX3223, which is for the RS232 protocol communication. The drawing is shown below. From the drawing, one can see that the board and computer will share common ground. When the computer gives commands through its COM port—DB9, the MAX3223 will translate the command to the format the board can understand and then send it. When the board sends the data out, the MAX3223 will receive first, then transfer the data to the computer.

The power of the MAX3223 is given by a power supply unit. The MAX3223 chip can be powered from 3 V to 5.5 V, 3.3 V is chosen as its power supply for the safety of the board. Since the board is powered with a 3 V battery, the same level power supplies can reduce the risks for both sides in case of malfunction.

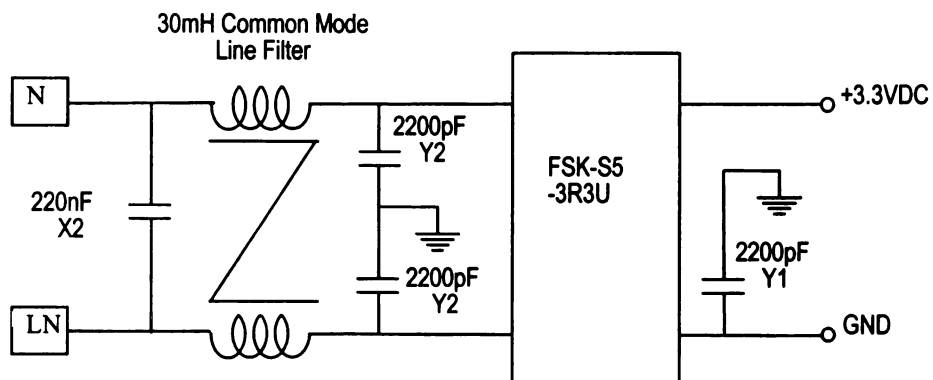
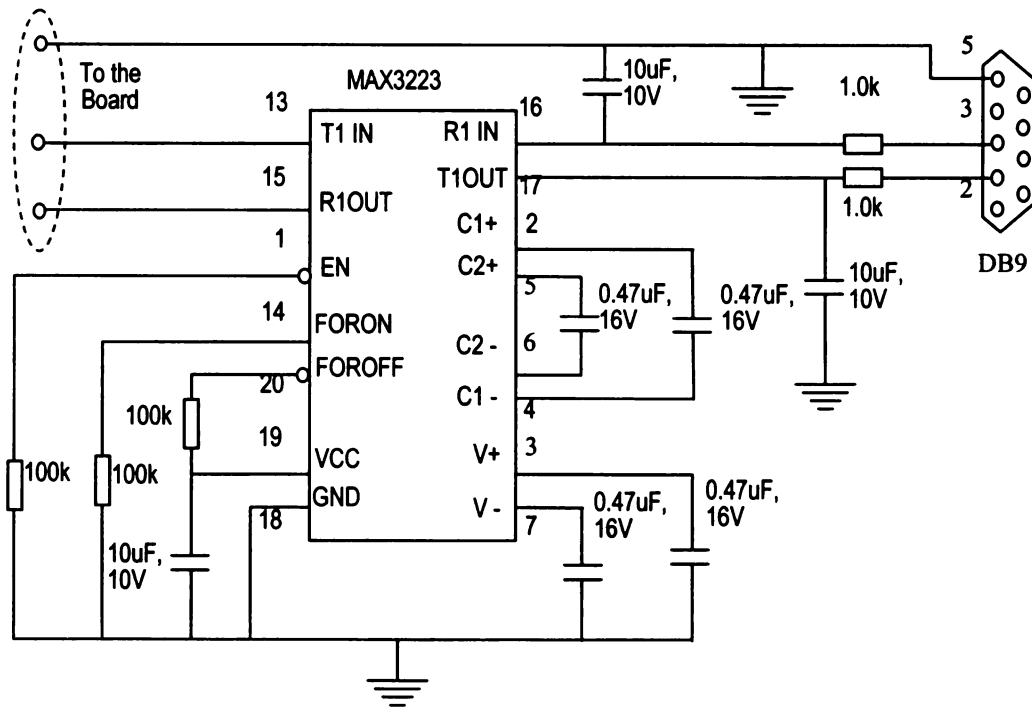


Figure A8 Circuit drawings of the data transferring (upper) and its power supply (down)



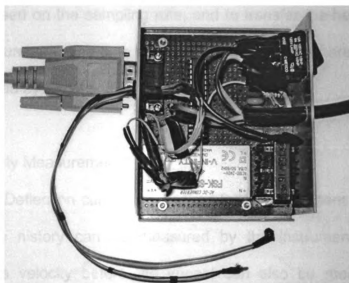


Figure A9 Picture of the data transferring box

Software is also needed to control the COM port to communicate with the microprocessor through the COM port and the RS232 interface box. A free COM port control software ComMaster is downloaded and used for this purpose.

The ComMaster is free software for COM port(s) monitoring, testing, debugging, and filtering. Its basic functions are used here to send the 'getting data' command to the electrical board and receive the data and show them in hexadecimal format. The data can then be saved for further data processing.

#### 4.1 Program for Data Processing

The data transferred from the COM port is in hexadecimal format. They are converted into decimal number for the followed data processing, and the matched time series is also needed to be added to the data file.

A Matlab program is made for this purpose, it is used to calculate the time series based on the sampling rate, and to transfer the hexadecimal numbers to decimal numbers. The time series and the date series are in column style. They can be read by Excel software.

#### 4.4 Velocity Measurements

Force-Deflection curves are desired for the specimens under impact loading. The force history can be measured by the instrumented projectiles. If the projectile's velocity before the impact can also be measured, the deflection history can then be calculated.

As mentioned before, an infrared phototransistor can be used as an electrical switch when working with a matched infrared emitting diode. When the infrared phototransistor is installed into a serial circuit, the voltage between its two terminals will change if its faced infrared is blocked. The velocity measurement system is base on this fact. Actually, two sets of the infrared emitting diodes and infrared phototransistors are working together. They are installed at two axial positions of a sleeve, which is installed at the outlet end of the gas gun barrel coaxially. At each cross-section, the infrared phototransistor and the infrared emitting diode are installed oppositely into the sleeve's wall. The emitting diodes are always on during tests, so the phototransistor can get the infrared normally. When the projectile is shot out, it will pass by the sleeve and blocks the infrared. Therefore, the voltage on the phototransistor will change. The projectile passes the two positions one by one. The time interval can be monitored through an

oscilloscope by monitoring the voltages of the two phototransistors. With a well measured distance between the two cross-sections, the velocity of the projectile can be calculated out.

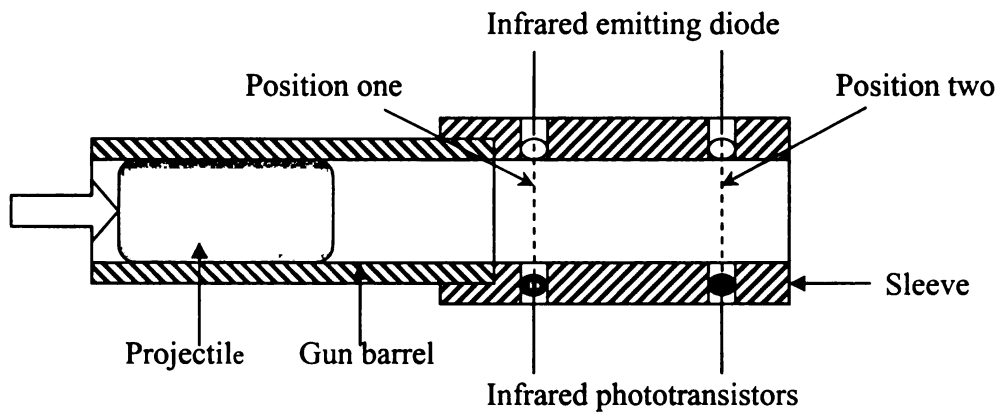


Figure A10 Schematic of the velocity measurement

## REFERENCES

- [1] Bonnie Baker, "Single-Supply, Low-Power Measurements of Bridge Networks", Burr-Brown Application Bulletin, April, 1993
- [2] Texas Instruments, "2.2V, 50MHz, Low-Noise, Single-Supply Rail-to-Rail Operational Amplifiers", SBOS365B, June, 2006, Revised Sep. 2006
- [3] James Karki, "Signal Conditioning Wheatstone Resistive Bridge Sensors", Application Report, Texas Instruments, SLOA034, Sept., 1999
- [4] James F. Doyle, "Waves Propagation in Structures, Spectral Analysis Using Fast Discrete Fourier Transforms", Second Edition, Mechanical Engineering Series, 1997
- [5] Ralph Burton, office of naval research, London, "Vibration and Impact", Dover Publications, Inc. New York 10014, 1968
- [6] Dennis L. Feucht, "Handbook of Analog Circuit Design", Academic Press, Inc., San Diego, California, 1990
- [7] Jonas A. Zukas, Theodore Nicholas and Hallock. F. Swift, "Impact Dynamics", John Wiley & sons Inc. 287-308, 1982.
- [8] Texas Instruments, "Mixed signal microcontroller (Rev. E) (msp430f1611.pdf)", SLAS368E, Texas, October 2002, Revised August 2006
- [9] Texas Instruments, "MSP430F15x/16x/161x" SLAZ018B, Texas, 7/23/2007
- [10] Texas Instruments, "MSP430x1xx Family User's Guide", Texas, SLAU049F, 2006
- [11] SoftBaugh, "Using the USBP with a Third-Party IDE", Suwanee, Georgia, Feb, 2006
- [12] Murugavel Raju, "Digital FIR Filter Design Using the MSP430F16x", Application Report, Texas Instruments, SLAA228, Nov., 2004
- [13] J. Honsi, "Porting of RF Blinking LED Software Example to CC2420-MSP430", Application Note, Chipcon Products from Texas Instruments, ANO033, 2004
- [14] Stephen W. Hinch, "Handbook of Surface Mount Technology", Longman Group UK limited, England, 1988

## APPENDIX B

### THE MICROPROCESSOR'S CONTROL PROGRAM FOR DATA SAMPLING AND SAVING – IN ASSEMBLY LANGUAGE

```
#include "msp430x16x.h"          ; #define controlled include file
#define PointerTX R9
#define PointerRX R10

A0result EQU 1100h              ; Channel A0 results
A1result EQU 2500H              ; Channel A1 results
endmem EQU 3800H                ; end of memory

Channel_num EQU 1               ; AD Channel number:0 for only A0, 1: A0 & A1
Delay_time1 EQU 2h              ; Delay time1 from trigger to start ADC12
Delay_time2 EQU 2h              ; Delay time2 from trigger to start ADC12
Adc_bit EQU 00h                 ; ADC bits: 00h for 12bits(word),02h for 8bit(byte)
sample_num EQU 2800h            ; Sampling Number saved in the ram
Voltage_ref EQU 2               ; Voltage reference: 3 for VAcc, 2 for 2.5

;
NAME main                       ; module name

PUBLIC main                     ; make the main label visible
                                ; outside this module

;-----
;      Interrupt Vectors (15) RESET
;-----
ORG 0FFFEh
DC16 init                      ; set reset vector to 'init' label

;-----
;      Interrupt Vectors (14) NMI interrupt
;-----
ORG 0FFFCh
DW NMIPROC                    ; NMI interrupt process

;-----
;      Interrupt Vectors (13)
;-----
ORG 0FFFAh
DW int_no_13                  ; Timer_B7 interrupt process

;-----
;      Interrupt Vectors (12)
;-----
ORG 0FFF8h
DW int_no_12                  ; Timer_B7 interrupt process
```

```

;-----
;      Interrupt Vectors (11)
;-----
      ORG  0FFF6h
      DW  int_no_11          ; interrupt process
;-----
;      Interrupt Vectors (10)
;-----
      ORG  0FFF4h
      DW  int_no_10          ; interrupt process
;-----
;      Interrupt Vectors (9) for UART0 receive
;-----
      ORG  0FFF2h            ;
      DW  USART0RX_ISR      ; USART0 receive
;-----
;      Interrupt Vectors (8) for UART0 transmit
;-----
      ORG  0FFF0h            ;
      DW  USART0TX_ISR      ; USART0 transmit
;-----
;      Interrupt Vectors (7) for ADC12
;-----
      ORG  0FEEh             ; ADC12 Interrupt Vector
      DW  ADC12ISR          ;
;-----
;      Interrupt Vectors (6)
;-----
      ORG  0FEECh
      DW  int_no_6           ; interrupt process
;-----
;      Interrupt Vectors (5)
;-----
      ORG  0FEEAh
      DW  int_no_5           ; interrupt process
;-----
;      Interrupt Vectors (4)
;-----
      ORG  0FEE8h
      DW  int_no_4           ; interrupt process
;-----
;      Interrupt Vectors (3)
;-----
      ORG  0FEE6h
      DW  int_no_3           ; interrupt process
;-----
;      Interrupt Vectors (2)
;-----
      ORG  0FEE4h
      DW  int_no_2           ; interrupt process
;-----
;      Interrupt Vectors (1) for I/O Port P2
;-----
      ORG  0FEE2H            ;I/O Port P2
      DW  IOP2
;-----

```

```

;      Interrupt Vectors (0)
;-----
      ORG  0FFE0h
      DW  int_no_0          ; interrupt process
;-----
      RSEG  CSTACK          ; pre-declaration of segment
      RSEG  CODE            ; place program in 'CODE' segment
init:  MOV  #SFE(CSTACK), SP      ; set up stack
main:  NOP                  ; main program
      MOV.W #WDTPW+WDTHOLD,&WDTCTL ; Stop watchdog timer
;+++++++ Set high DCO frequency CLK ++++++++
      BIS.B #RSEL2+RSEL1+RSEL0, &BCSCTL1
      BIS.B #DCO2+DCO1+DCO0, &DCOCTL
;+++++++ Clear RAM ++++++++
      mov.w #2700h,R5          ;clear ram: 1100h--3800h
clrram: mov.w #0000h,A0result(R5)
      decd  R5
      jnz  clrram
      mov.w #0000h,R12        ;counter for trigger number
;+++++++UART0 initialization+++++++
SetupP3  bis.b #030h,&P3SEL      ; P3.4,5 = USART0 TXD/RXD
SetupUART0 bis.b #UTXE0+URXE0,&ME1 ; Enable USART0 TXD/RXD
      bis.b #CHAR,&UCTL0        ; 8-bit characters
      mov.b #SSEL0,&UTCTL0      ; UCLK = ACLK
      mov.b #003h,&UBR00        ; 32k/9600 - 3.41
      mov.b #000h,&UBR10        ;
      mov.b #04Ah,&UMCTL0       ; Modulation 4A
      bic.b #SWRST,&UCTL0       ; **Initialize USART state machine**
      bis.b #URXIE0+UTXIE0,&IE1 ; Enable USART0 RX/TX interrupt
      bic.b #UTXIFG0,&IFG1      ; Clear initial flag on POR
      bic.b #OFIFG,&IFG1
      clr.w PointerRX          ;
;+++++++Port1 Port2 initialization+++++++
      bis.b #01h,&P1DIR          ;set P1.0 to output direction
      bis.b #20h,&P1DIR          ;set P1.5 to output direction
      bis.b #40h,&P1DIR          ;set P1.6 to output direction
      mov.b #00h,&P1IFG
      mov.b #00,&P1IE
      mov.b #0feh, &P2DIR        ;set P2 to output direction
      mov.b #0h,&P2IFG           ;CLEAR interrupt flag register
      mov.b #01h, &P2IES         ;set P2.0 interrupt edge is high-to-low
      mov.b #01h, &P2IE         ;P2.0 interrupt is enabled
;+++++++ADC12 initialization+++++++
      bis.b #BIT0+BIT1,&P6SEL    ; Enable A/D inputs  +BIT2+BIT3
      mov.b #Channel_num,R6      ;get AD sampling mode
      add.b #Adc_bit,R6          ;R6=00h : A0 12bits
                                   ;R6=01h : A0 A1 12bits
                                   ;R6=02h : A0 8bits
                                   ;R6=03h : A0 A1 8bits
      bis.b #01h,&P1OUT          ;turn on the LED
      bic.b #20h,&P1OUT
SetupADC12 mov  #Voltage_ref, R5
      cmp  #02h,R5
      jnz  REF_VCC
      mov  #REFON+REF2_5V+SHT0_0+MSC+ADC12ON,&ADC12CTL0;Internal 2.5v reference
                                   ; Turn on ADC12, use int. osc.

```

```

; extend sampling time so won't
; get overflow
; Set MSC so conversions triggered
; automatically
jmp goon
REF_VCC mov #SHT0_0+MSC+ADC12ON,&ADC12CTL0;external VAcc reference
goon mov.b #Channel_num, R4
cmp.b #1,R4
jnz Ch1
mov #SHP+CONSEQ_3,&ADC12CTL1 ;Two channel A0 and A1
; Use sampling timer, set mode
mov #BIT1,&ADC12IE ; Enable ADC12IFG.1 for ADC12MEM1
mov.b #INCH_0,ADC12MCTL0 ; A0 goes to MEM0
mov.b #EOS+INCH_1,ADC12MCTL1 ; A1 goes to MEM1, end of sequence
jmp Ch_end
Ch1: mov.b #INCH_0+EOS,ADC12MCTL0 ;one channel A0
mov #SHP+CONSEQ_2,&ADC12CTL1 ;SAMPCON: sampling timer,repeat-
;single-channel;+ADC12DIV_0
mov #BIT0,&ADC12IE ; Enable ADC12IFG.0 for ADC12MEM1
Ch_end clr R5 ; Clear pointer
Mainloop mov.w #0ffff,R4
mov.b #0h,&P2IFG ;CLEAR interrupt flag register
bic.b #01h,&P2IFG
bic.b #01h,&P2IFG
bic.b #01h,&P2IFG
bic.b #01h,&P2IFG
bic.b #01h,&P2IFG
mov.b #0h,&P2IFG
bis #GIE,SR ; Hold in LPM0, Enable interrupts CPUOFF+
MMainloop nop ; Need only for debug
jmp MMainloop ;
;-----
delay5ms: mov.w #Delay_time2,R14 ; Delay time to R15
delay5ms1: nop
dec.w R14
jnz delay5ms1
ret
;-----
ADC12ISR ; Interrupt Service Routine for ADC12
;-----
cmp.b #00h,R6 ;how many bits to save
jnz adcmodel
mov &ADC12MEM0,A0result(R5) ;A0 only,12bits. Move results to RAM
cmp.w #2700h,R5
jlo incword
jmp endconv
adcmodel: cmp.b #01h,R6
jnz adcmode2
mov &ADC12MEM0,A0result(R5) ;A0 & A1,12bits. Move results to RAM
mov &ADC12MEM1,A1result(R5)
cmp.w #1300h,R5
jlo incword
jmp endconv
adcmode2: cmp.b #02h,R6
jnz adcmode3
mov &ADC12MEM0,R8 ;A0 only, 8bits
rra.w R8
rra.w R8

```



```

        rra.w R8
        rra.w R8
        mov.b R8,A0result(R5)      ;save byte to RAM
        cmp.w #2600h,R5
        jlo incbyte
        jmp endconv
adcmode3: cmp.b #03h,R6
        jnz endconv
        mov &ADC12MEM0,R8
        rra.w R8
        rra.w R8
        rra.w R8
        rra.w R8
        mov.b R8,A0result(R5)
        mov &ADC12MEM1,R8
        rra.w R8
        rra.w R8
        rra.w R8
        rra.w R8
        mov.b R8,A1result(R5)
        cmp.w #1300h,R5
        jlo incbyte
        jmp endconv
incbyte: inc R5
        jmp ADC12_ISR_1
incword: incd R5
        jmp ADC12_ISR_1
endconv: bic #ENC,&ADC12CTL0      ; ADC12 Conversion disabled
        bis.b #20h,&P1OUT          ;turn off led
        mov.b #0h,&P2IFG          ;CLEAR P2 interrupt flag register
        clr R5                    ;Clear point
        mov #0,&ADC12IFG          ;Clear ADC12 interrupt flag register
        jmp ADC12_ISR_1
ADC12_ISR_1 reti
;-----
; Interrupt Service Routine for ADC12
;-----
IOP2:   mov.b #0h,&P2IFG          ;CLEAR interrupt flag register
        xor.b #001h,&P1OUT        ; Toggle P1.0
        mov.b #0h,&P2IFG          ;CLEAR interrupt flag register
;       bic.b #01h, &P2IE
        cmp #0ffffh,R4
        jnz IOP3
        mov.w #Delay_time1,R15    ; Delay time to R15
Delay1: call #delayp5ms           ; Delay time to R15
        dec.w R15                 ; Decrement R15
        jnz Delay1               ; Delay over?
        bis #ENC,&ADC12CTL0       ; Enable conversions
        bis #ADC12SC,&ADC12CTL0  ; Start conversions
        inc R12
        mov.w #0000h,R4
IOP3:   reti
;-----
USART0TX_ISR;
;-----
        cmp.w #endmem,PointerTX  ; Complete string TX'ed?

```

```

        jeq    Done0                ;
        mov.b  @PointerTX+,&TXBUF0  ;
        jmp    Done
Done0    bic.b  #20h,&P1OUT          ;turn on led
        bic.b  #01h,&P1OUT          ;turn on led*****
        mov.b  #00h,&P2IFG
        mov.w  #0ffff,R4
        clr.w  PointerRX
;        mov.b  #01h, &P2IE          ;enable P2.0 interrupt
Done    reti                        ;
;-----
USART0RX_ISR;
;-----
        mov.b  &RXBUF0,A0result(PointerRX) ; Store RX data
        inc.w  PointerRX            ;
        cmp.b  #4,PointerRX        ;
        jne    USART_Done          ;
        dec    PointerRX
        mov.b  A0result(PointerRX),R11 ;
        dec    PointerRX
        add.b  A0result(PointerRX),R11
        dec    PointerRX
        add.b  A0result(PointerRX),R11
        dec    PointerRX
        add.b  A0result(PointerRX),R11
        cmp.w  #00aah,R11
        jnz    USART_a
        mov.w  R12,A0result
        mov.b  #Channel_num,&A0result+2
        mov.b  #Adc_bit,&A0result+3
        mov.w  #A0result,PointerTX ;
        mov.b  @PointerTX+,&TXBUF0  ;
USART_a  clr.w  PointerRX
USART_Done  reti                    ;
;-----
NMIPROC;
;-----
        reti
;-----
int_no_13;
;-----
        reti
;-----
int_no_12;
;-----
        reti
;-----
int_no_11;
;-----
        reti
;-----
int_no_10;
;-----
        reti
;-----
int_no_6;

```

```
;-----  
    reti  
;-----  
int_no_5;  
;-----  
    reti  
;-----  
int_no_4;  
;-----  
    reti  
;-----  
int_no_3;  
;-----  
    reti  
;-----  
int_no_2;  
;-----  
    reti  
;-----  
int_no_0;  
;-----  
    reti  
    END
```

## THE MATLAB PROGRAM FOR CHANGING DATA FORMAT FROM HEXADECIMAL TO DECIMAL

152

```

        break;
    end
end
elseif P(3) == 1 & P(4) == 0 %two channel 12 bit
    for i=1:2430
        data = fscanf(fid,'%x',2);
        data1(i) = data(2)*256+data(1);
    end
    fseek(fid,3*5120,-1);
    for i=1:2430
        data = fscanf(fid,'%x',2);
        data2(i) = data(2)*256+data(1);
    end
    fprintf(fid1,'two channel 12 bit ADC\n');
    fprintf(fid1,'Sampling Time(ms)\t\tCh-1 Force(N) \t Ch-2 Force(N)\n');
    for i=1:2430
        fprintf(fid1,'\t %s \t\t\t %s \t\t\t %s\n',num2str(i*str2double(s_time), '%.4f'),num2str(data1(i)*str2double(para1), '%.4f'),num2str(data2(i)*str2double(para2), '%.4f'));
    end
elseif P(3) == 1 & P(4) == 1 %two channel 8 bit
    for i=1:4860
        data = fscanf(fid,'%x',1);
        data1(i) = data;
    end
    fseek(fid,3*5120,-1);
    for i=1:4860
        data = fscanf(fid,'%x',1);
        data2(i) = data;
    end
    fprintf(fid1,'two channel 8 bit ADC\n');
    fprintf(fid1,'Sampling Time(ms)\t\tCh-1 Force(N) \t Ch-2 Force(N)\n');
    for i=1:4860
        fprintf(fid1,'\t %s \t\t\t %s \t\t\t %s\n',num2str(i*str2double(s_time), '%.4f'),num2str(data1(i)*str2double(para1), '%.4f'),num2str(data2(i)*str2double(para2), '%.4f'));
    end
end
end
fclose(fid);
fclose(fid1)

```

## APPENDIX D

### MATLAB PROGRAM FOR THE NUMERICAL METHOD

#### – INITIAL WAVE ASSUMPTION

##### A. MAIN PROGRAM

```
%Wave propagation simulation. Long impact period, short bar, wave reflect
%and reinter the bar several times before the impact finish.
de=7560;          %density
E=192000000000;   %Young's Modulus
dam=0.003;        %damping
%Area=(0.75*0.0254/2)^2*3.14159265; %area of the bar intersection
le=3*0.0254;      %length of the bar
ws=sqrt(E/de);    %wave speed in the bar

%fr=2*3.14159265/(2*le/ws); %frequency
fr=2*pi*800; %anglar frequency of input force
k1=sqrt(((fr^2)*de-i*fr*dam)/E) % coefficient in the wave equation
%k1=fr/ws
%k1=sqrt(((fre^2)*de)/E);
forceperiod=pi;   %period of the impact force

po0=0;            %impact end
po1=1.5*0.0254;   %first gages position
%po2=3.0*0.0254; %second gages position
%po3=4.5*0.0254; %third gages position

lr=1;             %wave lose at the rear end--free end
lf=0.8;           %wave lose at the front end--impact end

tb=2*((le-po1)/ws); %the time constance that wave needs to travel back to the gages again
ta=2*(po1/ws);      %the time constance that wave from reflect wave to input wave again

tf=3.14159265;     %force period

fc=17500; %constant for time stages to match the wave number in experimental curve

dt=1050; %drawing constant to match the time of the experimental data
da=30; %drawing constant to match the magnitude of the experimental data
ds=0.2; %drawing constant to shift the time value to match the experimental data

t0=0:tb/100:tb;    %time stage before the wave go back to the gages, no vibration
[p0]=forcein(fc*0,fc*(tb)); %use the subprogram (function'forcein'), which is in the same directory

t1=tb:(ta)/100:(tb+ta); %time stage that the reflect wave overlaps with input wave
t1a=0:(ta)/100:(ta); %time for reflect wave

[p1]=forcein(fc*tb,fc*(tb+ta));
[p1a]=forcein(0,fc*ta);
```

```

t2=(tb+ta):tb/100:(tb+ta+tb); %time state that the wave pass gage again from input direction
t2a=ta:tb/100:(tb+ta);
t2b=0:tb/100:tb;          %time for input wave
[p2]=forcein(fc*(tb+ta),fc*(tb+ta+tb));
[p2a]=forcein(fc*(ta),fc*(tb+ta));
[p2b]=forcein(0,fc*(tb));

```

```

t3=(tb+ta+tb):ta/100:(tb+ta+tb+ta);
t3a=(tb+ta):ta/100:(tb+ta+ta);
t3b=tb:ta/100:(ta+tb);
t3c=0:ta/100:ta;
[p3]=forcein(fc*(tb+ta+tb),fc*(tb+ta+tb+ta));
[p3a]=forcein(fc*(tb+ta),fc*(ta+tb+ta));
[p3b]=forcein(fc*(tb),fc*(tb+ta));
[p3c]=forcein(fc*(0),fc*(ta));

```

```

t4=(tb+ta+tb+ta):tb/100:(tb+ta+tb+ta+tb);
t4a=(tb+ta+ta):tb/100:(tb+ta+ta+tb);
t4b=(ta+tb):tb/100:(ta+tb+tb);
t4c=ta:tb/100:(tb+ta);
t4d=0:tb/100:tb;
[p4]=forcein(fc*(tb+ta+tb+ta),fc*(tb+ta+tb+ta+tb));
[p4a]=forcein(fc*(tb+ta+ta),fc*(tb+ta+tb+ta));
[p4b]=forcein(fc*(tb+ta),fc*(tb+ta+tb));
[p4c]=forcein(fc*(ta),fc*(tb+ta));
[p4d]=forcein(fc*(0),fc*(tb));

```

```

t5=(tb+ta+tb+ta+tb):ta/100:(tb+ta+tb+ta+tb+ta);
t5a=(tb+ta+ta+tb):ta/100:(tb+ta+ta+tb+ta);
t5b=(ta+tb+tb):ta/100:(ta+tb+tb+ta);
t5c=(ta+tb):ta/100:(tb+ta+ta);
t5d=tb:ta/100:(tb+ta);
t5e=0:ta/100:ta;
[p5]=forcein(fc*(tb+ta+tb+ta+tb),fc*(tb+ta+tb+ta+tb+ta));
[p5a]=forcein(fc*(tb+ta+tb+ta),fc*(tb+ta+tb+ta+ta));
[p5b]=forcein(fc*(tb+ta+tb),fc*(tb+ta+tb+ta));
[p5c]=forcein(fc*(tb+ta),fc*(tb+ta+ta));
[p5d]=forcein(fc*(tb),fc*(tb+ta));
[p5e]=forcein(fc*(0),fc*(ta));

```

```

t6=(tb+ta+tb+ta+tb+ta):tb/100:(tb+ta+tb+ta+tb+ta+tb);
t6a=(tb+ta+ta+tb+ta):tb/100:(tb+ta+ta+tb+ta+tb);
t6b=(ta+tb+tb+ta):tb/100:(ta+tb+tb+ta+tb);
t6c=(ta+tb+ta):tb/100:(tb+ta+ta+tb);
t6d=(tb+ta):tb/100:(tb+ta+tb);
t6e=ta:tb/100:(ta+tb);
t6f=0:tb/100:tb;
[p6]=forcein(fc*(tb+ta+tb+ta+tb+ta),fc*(tb+ta+tb+ta+tb+ta+tb));
[p6a]=forcein(fc*(tb+ta+tb+ta+ta),fc*(tb+ta+tb+ta+tb+ta));
[p6b]=forcein(fc*(tb+ta+tb+ta),fc*(tb+ta+tb+ta+tb));

```

[p6c]=forcein(fc\*(ta+tb+ta),fc\*(tb+ta+tb+ta));  
[p6d]=forcein(fc\*(tb+ta),fc\*(tb+ta+tb));  
[p6e]=forcein(fc\*(ta),fc\*(ta+tb));  
[p6f]=forcein(fc\*(0),fc\*(tb));

t7=(tb+ta+tb+ta+tb+ta+tb):ta/100:(tb+ta+tb+ta+tb+ta+tb+ta);  
t7a=(tb+ta+ta+tb+ta+tb):ta/100:(tb+ta+ta+tb+ta+tb+ta);  
t7b=(ta+tb+tb+ta+tb):ta/100:(ta+tb+tb+ta+tb+ta);  
t7c=(ta+tb+ta+tb):ta/100:(tb+ta+ta+tb+ta);  
t7d=(tb+ta+tb):ta/100:(tb+ta+tb+ta);  
t7e=(ta+tb):ta/100:(ta+tb+ta);  
t7f=tb:ta/100:(tb+ta);  
t7g=0:ta/100:ta;  
[p7]=forcein(fc\*(tb+ta+tb+ta+tb+ta+tb),fc\*(tb+ta+tb+ta+tb+ta+tb+ta));  
[p7a]=forcein(fc\*(tb+ta+ta+tb+ta+tb),fc\*(tb+ta+ta+tb+ta+tb+ta));  
[p7b]=forcein(fc\*(ta+tb+tb+ta+tb),fc\*(ta+tb+tb+ta+tb+ta));  
[p7c]=forcein(fc\*(ta+tb+ta+tb),fc\*(tb+ta+ta+tb+ta));  
[p7d]=forcein(fc\*(tb+ta+tb),fc\*(tb+ta+tb+ta));  
[p7e]=forcein(fc\*(ta+tb),fc\*(ta+tb+ta));  
[p7f]=forcein(fc\*(tb),fc\*(tb+ta));  
[p7g]=forcein(fc\*(0),fc\*(ta));

t8=(tb+ta+tb+ta+tb+ta+tb+ta):tb/100:(tb+ta+tb+ta+tb+ta+tb+ta+tb);  
t8a=(tb+ta+ta+tb+ta+tb+ta):tb/100:(tb+ta+ta+tb+ta+tb+ta+tb);  
t8b=(ta+tb+tb+ta+tb+ta):tb/100:(ta+tb+tb+ta+tb+ta+tb);  
t8c=(ta+tb+ta+tb+ta):tb/100:(tb+ta+ta+tb+ta+tb);  
t8d=(tb+ta+tb+ta):tb/100:(tb+ta+tb+ta+tb);  
t8e=(ta+tb+ta):tb/100:(ta+tb+ta+tb);  
t8f=(tb+ta):tb/100:(tb+ta+tb);  
t8g=ta:tb/100:(ta+tb);  
t8h=0:tb/100:tb;  
[p8]=forcein(fc\*(tb+ta+tb+ta+tb+ta+tb+ta),fc\*(tb+ta+tb+ta+tb+ta+tb+ta+tb));  
[p8a]=forcein(fc\*(tb+ta+ta+tb+ta+tb+ta),fc\*(tb+ta+ta+tb+ta+tb+ta+tb));  
[p8b]=forcein(fc\*(ta+tb+tb+ta+tb+ta),fc\*(ta+tb+tb+ta+tb+ta+tb));  
[p8c]=forcein(fc\*(ta+tb+ta+tb+ta),fc\*(tb+ta+ta+tb+ta+tb));  
[p8d]=forcein(fc\*(tb+ta+tb+ta),fc\*(tb+ta+tb+ta+tb));  
[p8e]=forcein(fc\*(ta+tb+ta),fc\*(ta+tb+ta+tb));  
[p8f]=forcein(fc\*(tb+ta),fc\*(tb+ta+tb));  
[p8g]=forcein(fc\*(ta),fc\*(ta+tb));  
[p8h]=forcein(fc\*(0),fc\*(tb));

t9=(tb+ta+tb+ta+tb+ta+tb+ta+tb):ta/100:(tb+ta+tb+ta+tb+ta+tb+ta+tb+ta);  
t9a=(tb+ta+ta+tb+ta+tb+ta+tb):ta/100:(tb+ta+ta+tb+ta+tb+ta+tb+ta);  
t9b=(ta+tb+tb+ta+tb+ta+tb):ta/100:(ta+tb+tb+ta+tb+ta+tb+ta);  
t9c=(ta+tb+ta+tb+ta+tb):ta/100:(tb+ta+ta+tb+ta+tb+ta);  
t9d=(tb+ta+tb+ta+tb):ta/100:(tb+ta+tb+ta+tb+ta);  
t9e=(ta+tb+ta+tb):ta/100:(ta+tb+ta+tb+ta);  
t9f=(tb+ta+tb):ta/100:(tb+ta+tb+ta);  
t9g=(ta+tb):ta/100:(ta+tb+ta);  
t9h=tb:ta/100:(tb+ta);  
t9i=0:ta/100:ta;

[p9]=forcein(fc\*(tb+ta+tb+ta+tb+ta+tb+ta+tb),fc\*(tb+ta+tb+ta+tb+ta+tb+ta+tb+ta));  
[p9a]=forcein(fc\*(tb+ta+ta+tb+ta+tb+ta+tb),fc\*(tb+ta+ta+tb+ta+tb+ta+tb+ta));



[p9b]=forcein(fc\*(ta+tb+tb+ta+tb+ta+tb),fc\*(ta+tb+tb+ta+tb+ta+tb+ta));  
 [p9c]=forcein(fc\*(ta+tb+ta+tb+ta+tb),fc\*(tb+ta+ta+tb+ta+tb+ta));  
 [p9d]=forcein(fc\*(tb+ta+tb+ta+tb),fc\*(tb+ta+tb+ta+tb+ta));  
 [p9e]=forcein(fc\*(ta+tb+ta+tb),fc\*(ta+tb+ta+tb+ta));  
 [p9f]=forcein(fc\*(tb+ta+tb),fc\*(tb+ta+tb+ta));  
 [p9g]=forcein(fc\*(ta+tb),fc\*(ta+tb+ta));  
 [p9h]=forcein(fc\*(tb),fc\*(tb+ta));  
 [p9i]=forcein(fc\*(0),fc\*(ta));

t10=(tb+ta+tb+ta+tb+ta+tb+ta+tb+ta):tb/100:(tb+ta+tb+ta+tb+ta+tb+ta+tb+ta+tb);  
 t10a=(tb+ta+ta+tb+ta+tb+ta+tb+ta):tb/100:(tb+ta+ta+tb+ta+tb+ta+tb+ta+tb);  
 t10b=(ta+tb+tb+ta+tb+ta+tb+ta):tb/100:(ta+tb+tb+ta+tb+ta+tb+ta+tb);  
 t10c=(ta+tb+ta+tb+ta+tb+ta):tb/100:(tb+ta+ta+tb+ta+tb+ta+tb);  
 t10d=(tb+ta+tb+ta+tb+ta):tb/100:(tb+ta+tb+ta+tb+ta+tb);  
 t10e=(ta+tb+ta+tb+ta):tb/100:(ta+tb+ta+tb+ta+tb);  
 t10f=(tb+ta+tb+ta):tb/100:(tb+ta+tb+ta+tb);  
 t10g=(ta+tb+ta):tb/100:(ta+tb+ta+tb);  
 t10h=(tb+ta):tb/100:(tb+ta+tb);  
 t10i=ta:tb/100:(ta+tb);  
 t10j=0:tb/100:tb

[p10]=forcein(fc\*(tb+ta+tb+ta+tb+ta+tb+ta+tb+ta),fc\*(tb+ta+tb+ta+tb+ta+tb+ta+tb+ta+tb));  
 [p10a]=forcein(fc\*(tb+ta+ta+tb+ta+tb+ta+tb+ta),fc\*(tb+ta+ta+tb+ta+tb+ta+tb+ta+tb));  
 [p10b]=forcein(fc\*(ta+tb+tb+ta+tb+ta+tb+ta),fc\*(ta+tb+tb+ta+tb+ta+tb+ta+tb));  
 [p10c]=forcein(fc\*(ta+tb+ta+tb+ta+tb+ta),fc\*(tb+ta+ta+tb+ta+tb+ta+tb));  
 [p10d]=forcein(fc\*(tb+ta+tb+ta+tb+ta),fc\*(tb+ta+tb+ta+tb+ta+tb));  
 [p10e]=forcein(fc\*(ta+tb+ta+tb+ta),fc\*(ta+tb+ta+tb+ta+tb));  
 [p10f]=forcein(fc\*(tb+ta+tb+ta),fc\*(tb+ta+tb+ta+tb));  
 [p10g]=forcein(fc\*(ta+tb+ta),fc\*(ta+tb+ta+tb));  
 [p10h]=forcein(fc\*(tb+ta),fc\*(tb+ta+tb));  
 [p10i]=forcein(fc\*(ta),fc\*(ta+tb));  
 [p10j]=forcein(fc\*(0),fc\*(tb));

t11=(tb+ta+tb+ta+tb+ta+tb+ta+tb+ta+tb):ta/100:(tb+ta+tb+ta+tb+ta+tb+ta+tb+ta+tb+ta);  
 t11a=(tb+ta+ta+tb+ta+tb+ta+tb+ta+tb):ta/100:(tb+ta+ta+tb+ta+tb+ta+tb+ta+tb+ta);  
 t11b=(ta+tb+tb+ta+tb+ta+tb+ta+tb):ta/100:(ta+tb+tb+ta+tb+ta+tb+ta+tb+ta);  
 t11c=(ta+tb+ta+tb+ta+tb+ta+tb):ta/100:(tb+ta+ta+tb+ta+tb+ta+tb+ta);  
 t11d=(tb+ta+tb+ta+tb+ta+tb):ta/100:(tb+ta+tb+ta+tb+ta+tb+ta);  
 t11e=(ta+tb+ta+tb+ta+tb):ta/100:(ta+tb+ta+tb+ta+tb+ta);  
 t11f=(tb+ta+tb+ta+tb):ta/100:(tb+ta+tb+ta+tb+ta);  
 t11g=(ta+tb+ta+tb):ta/100:(ta+tb+ta+tb+ta);  
 t11h=(tb+ta+tb):ta/100:(tb+ta+tb+ta);  
 t11i=(ta+tb):ta/100:(ta+tb+ta);  
 t11j=tb:ta/100:(tb+ta);  
 t11k=0:ta/100:ta;

[p11]=forcein(fc\*(tb+ta+tb+ta+tb+ta+tb+ta+tb+ta+tb),fc\*(tb+ta+tb+ta+tb+ta+tb+ta+tb+ta+tb+ta));  
 [p11a]=forcein(fc\*(tb+ta+ta+tb+ta+tb+ta+tb+ta+tb),fc\*(tb+ta+ta+tb+ta+tb+ta+tb+ta+tb+ta));  
 [p11b]=forcein(fc\*(ta+tb+tb+ta+tb+ta+tb+ta+tb),fc\*(ta+tb+tb+ta+tb+ta+tb+ta+tb+ta));  
 [p11c]=forcein(fc\*(ta+tb+ta+tb+ta+tb+ta+tb),fc\*(tb+ta+ta+tb+ta+tb+ta+tb+ta));  
 [p11d]=forcein(fc\*(tb+ta+tb+ta+tb+ta+tb),fc\*(tb+ta+tb+ta+tb+ta+tb+ta));  
 [p11e]=forcein(fc\*(ta+tb+ta+tb+ta+tb),fc\*(ta+tb+ta+tb+ta+tb+ta));  
 [p11f]=forcein(fc\*(tb+ta+tb+ta+tb),fc\*(tb+ta+tb+ta+tb+ta));  
 [p11g]=forcein(fc\*(ta+tb+ta+tb),fc\*(ta+tb+ta+tb+ta));  
 [p11h]=forcein(fc\*(tb+ta+tb),fc\*(tb+ta+tb+ta));  
 [p11i]=forcein(fc\*(ta+tb),fc\*(ta+tb+ta));

```
[p1 l j]=forcein(fc*(tb),fc*(tb+ta));
[p1 l k]=forcein(fc*(0),fc*(ta));
```

```
f0=p0.*exp(-i*k1*pol); % force history that no vibration
f1=p1.*exp(-i*k1*pol)-lr*p1a.*exp(-i*k1*(2*le-pol));
f2=p2.*exp(-i*k1*pol)-lr*p2a.*exp(-i*k1*(2*le-pol))+lr*lf*p2b.*exp(-i*k1*(2*le+pol));
f3=p3.*exp(-i*k1*pol)-lr*p3a.*exp(-i*k1*(2*le-pol))+lr*lf*p3b.*exp(-i*k1*(2*le+pol))-
lr^2*lf*p3c.*exp(-i*k1*(4*le-pol));
f4=p4.*exp(-i*k1*pol)-lr*p4a.*exp(-i*k1*(2*le-pol))+lr*lf*p4b.*exp(-i*k1*(2*le+pol))-
lr^2*lf*p4c.*exp(-i*k1*(4*le-pol))+lr^2*lf^2*p4d.*exp(-i*k1*(4*le+pol));
f5=p5.*exp(-i*k1*pol)-lr*p5a.*exp(-i*k1*(2*le-pol))+lr*lf*p5b.*exp(-i*k1*(2*le+pol))-
lr^2*lf*p5c.*exp(-i*k1*(4*le-pol))+lr^2*lf^2*p5d.*exp(-i*k1*(4*le+pol))-lr^3*lf^2*p5e.*exp(-
i*k1*(6*le-pol));
f6=p6.*exp(-i*k1*pol)-lr*p6a.*exp(-i*k1*(2*le-pol))+lr*lf*p6b.*exp(-i*k1*(2*le+pol))-
lr^2*lf*p6c.*exp(-i*k1*(4*le-pol))+lr^2*lf^2*p6d.*exp(-i*k1*(4*le+pol))-lr^3*lf^2*p6e.*exp(-
i*k1*(6*le-pol))+lr^3*lf^3*p6f.*exp(-i*k1*(6*le+pol));
f7=p7.*exp(-i*k1*pol)-lr*p7a.*exp(-i*k1*(2*le-pol))+lr*lf*p7b.*exp(-i*k1*(2*le+pol))-
lr^2*lf*p7c.*exp(-i*k1*(4*le-pol))+lr^2*lf^2*p7d.*exp(-i*k1*(4*le+pol))-lr^3*lf^2*p7e.*exp(-
i*k1*(6*le-pol))+lr^3*lf^3*p7f.*exp(-i*k1*(6*le+pol))-lr^4*lf^3*p7g.*exp(-i*k1*(8*le-pol));
f8=p8.*exp(-i*k1*pol)-lr*p8a.*exp(-i*k1*(2*le-pol))+lr*lf*p8b.*exp(-i*k1*(2*le+pol))-
lr^2*lf*p8c.*exp(-i*k1*(4*le-pol))+lr^2*lf^2*p8d.*exp(-i*k1*(4*le+pol))-lr^3*lf^2*p8e.*exp(-
i*k1*(6*le-pol))+lr^3*lf^3*p8f.*exp(-i*k1*(6*le+pol))-lr^4*lf^3*p8g.*exp(-i*k1*(8*le-
pol))+lr^4*lf^4*p8h.*exp(-i*k1*(8*le+pol));
f9=p9.*exp(-i*k1*pol)-lr*p9a.*exp(-i*k1*(2*le-pol))+lr*lf*p9b.*exp(-i*k1*(2*le+pol))-
lr^2*lf*p9c.*exp(-i*k1*(4*le-pol))+lr^2*lf^2*p9d.*exp(-i*k1*(4*le+pol))-lr^3*lf^2*p9e.*exp(-
i*k1*(6*le-pol))+lr^3*lf^3*p9f.*exp(-i*k1*(6*le+pol))-lr^4*lf^3*p9g.*exp(-i*k1*(8*le-
pol))+lr^4*lf^4*p9h.*exp(-i*k1*(8*le+pol))-lr^5*lf^4*p9i.*exp(-i*k1*(10*le-pol));
f10=p10.*exp(-i*k1*pol)-lr*p10a.*exp(-i*k1*(2*le-pol))+lr*lf*p10b.*exp(-i*k1*(2*le+pol))-
lr^2*lf*p10c.*exp(-i*k1*(4*le-pol))+lr^2*lf^2*p10d.*exp(-i*k1*(4*le+pol))-lr^3*lf^2*p10e.*exp(-
i*k1*(6*le-pol))+lr^3*lf^3*p10f.*exp(-i*k1*(6*le+pol))-lr^4*lf^3*p10g.*exp(-i*k1*(8*le-
pol))+lr^4*lf^4*p10h.*exp(-i*k1*(8*le+pol))-lr^5*lf^4*p10i.*exp(-i*k1*(10*le-
pol))+lr^5*lf^5*p10j.*exp(-i*k1*(10*le+pol));
f11=p11.*exp(-i*k1*pol)-lr*p11a.*exp(-i*k1*(2*le-pol))+lr*lf*p11b.*exp(-i*k1*(2*le+pol))-
lr^2*lf*p11c.*exp(-i*k1*(4*le-pol))+lr^2*lf^2*p11d.*exp(-i*k1*(4*le+pol))-lr^3*lf^2*p11e.*exp(-
i*k1*(6*le-pol))+lr^3*lf^3*p11f.*exp(-i*k1*(6*le+pol))-lr^4*lf^3*p11g.*exp(-i*k1*(8*le-
pol))+lr^4*lf^4*p11h.*exp(-i*k1*(8*le+pol))-lr^5*lf^4*p11i.*exp(-i*k1*(10*le-
pol))+lr^5*lf^5*p11j.*exp(-i*k1*(10*le+pol))-lr^6*lf^5*p11k.*exp(-i*k1*(12*le-pol));
```

```
%f1=p1.*exp(-i*k1*pol)+p2.*exp(-i*k1*(2*le-pol));
```

```
%f1=p1.*exp(-i*k1*pol)-p2.*exp(-i*k1*(2*le-pol));
```

```
%plot(t/10,y0,t/10,y1,t/10,y2,t/10,y3,(t+5)/10,y1,(t+10)/10,y2,(t+15)/10,y3);
```

```
plot(ds+dt*t0,da*p0,'k--',ds+dt*t1,da*p1,'k--',ds+dt*t2,da*p2,'k--',ds+dt*t3,da*p3,'k--',ds+dt*t4,da*p4,'k--',
'ds+dt*t5,da*p5,'k--',ds+dt*t6,da*p6,'k--',ds+dt*t7,da*p7,'k--',ds+dt*t8,da*p8,'k--',ds+dt*t9,da*p9,'k--',
'ds+dt*t10,da*p10,'k--',ds+dt*t11,da*p11,'k--');
```

```
hold on;legend('input');hold on;
```

```
plot(ds+dt*t0,da*f0,'k-',ds+dt*t1,da*f1,'k-',ds+dt*t2,da*f2,'k-',ds+dt*t3,da*f3,'k-',ds+dt*t4,da*f4,'k-',
'ds+dt*t5,da*f5,'k-',ds+dt*t6,da*f6,'k-',ds+dt*t7,da*f7,'k-',ds+dt*t8,da*f8,'k-',ds+dt*t9,da*f9,'k-',
'ds+dt*t10,da*f10,'k-',ds+dt*t11,da*f11,'k-');
```

```
hold on;
```

```
legend('input','output');hold on;
```

```
AXIS ([0.1 0.55 -7 25]);
```

```
data13=xlsread('test3-gage1-3'); %load the experimental data from the Excel file 'test3-gage1'
```

```
cht13=data13(:,1); %give the first column to te, that is the time
```

```

ch1=data13(:,2);    %give the second column to ch1, that is the gage one
ch3=data13(:,3);

data2=xlsread('3inch150rev');
cht2=data2(:,1);
ch2=data2(:,2);

%plot(cht13,ch1,cht13,ch3); hold;
plot(cht2,ch2,':'); hold;
hold on;

xlabel('t (ms)');
ylabel('Force (unit)')
title('3inch150, impactinterfacelose=20%')
%legend('input','output')
%subplot
%plot(t+100000,y)
%for each Y, the reflect wave should be added in. that is: the inverse Y
%with x value as 2L-x; the t should be something like 2L-t but some how
%different, L/V=t0; if t is from 0 to pi/1000, then it travels almost 3 or
%4 times along the bar.
% be careful, at each stage, the force history is the sum of all the input
% and reflects

```

## B. SUBPROGRAM FOR THE INPUT CURVE

```

function [b]=forcein(x, y)
t=x:(y-x)/100:y;
s=0;
c1=1; k1=0.15;
%m1=0.00; m2=0.; m3=0.; m4=0.; m5=0.;
%d1=0.00; d2=0.00; d3=0.; d4=0; d5=0.;
data=xlsread('impactforcehistory'); %load the experimental data from the Excel file 'test3-gage1'
time=data(:,1);    %give the first column to te, that is the time
force=data(:,2);    %give the second column to ch1, that is the gage one

p=polyfit(time, force, 10)
%f=polyval(p,time)

for i=1:101,

    if(s>=0)

        %f(i)=sin(t(i))/0.9+sin(3*t(i))/3+sin(5*t(i))/5+sin(7*t(i))/7+sin(9*t(i))/9+sin(11*t(i))/11+sin(13*t(i))/13+sin(15*t(i))/15+sin(17*t(i))/17+sin(19*t(i))/19+sin(21*t(i))/21+sin(23*t(i))/23;
        f(i)=c1*(sin(t(i)));

        %f(i)=p(1)*t(i)^10+p(2)*t(i)^9+p(3)*t(i)^8+p(4)*t(i)^7+p(5)*t(i)^6+p(6)*t(i)^5+p(7)*t(i)^4+p(8)*t(i)^3+p(9)*t(i)^2+p(10)*t(i)^1+p(11);
        % f(i)=c1*sin(t(i))+k1*(cos(t(i))-
        1)+m1*sin(1.1*t(i))+m2*sin(1.3*t(i))+m3*sin(1.5*t(i))+m4*sin(1.7*t(i))+m5*sin(1.9*t(i))+d1*sin(t(i)/1.1)+d2*sin(t(i)/1.3)+d3*sin(t(i)/1.5)+d4*sin(t(i)/1.7)+d5*sin(t(i)/1.9);
        b(i)=f(i);
        if (t(i)>3.14159265)

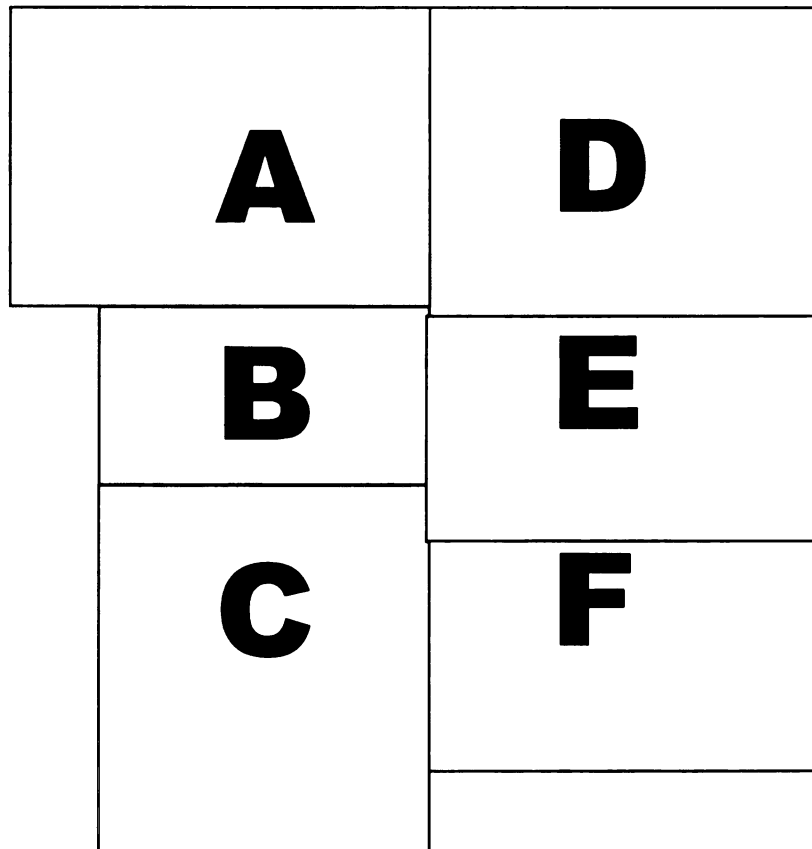
```

```
    b(i)=0;  
    if (b(i)<0)  
        b(i)=0;  
    end  
  
end  
end  
end
```

## APPENDIX E

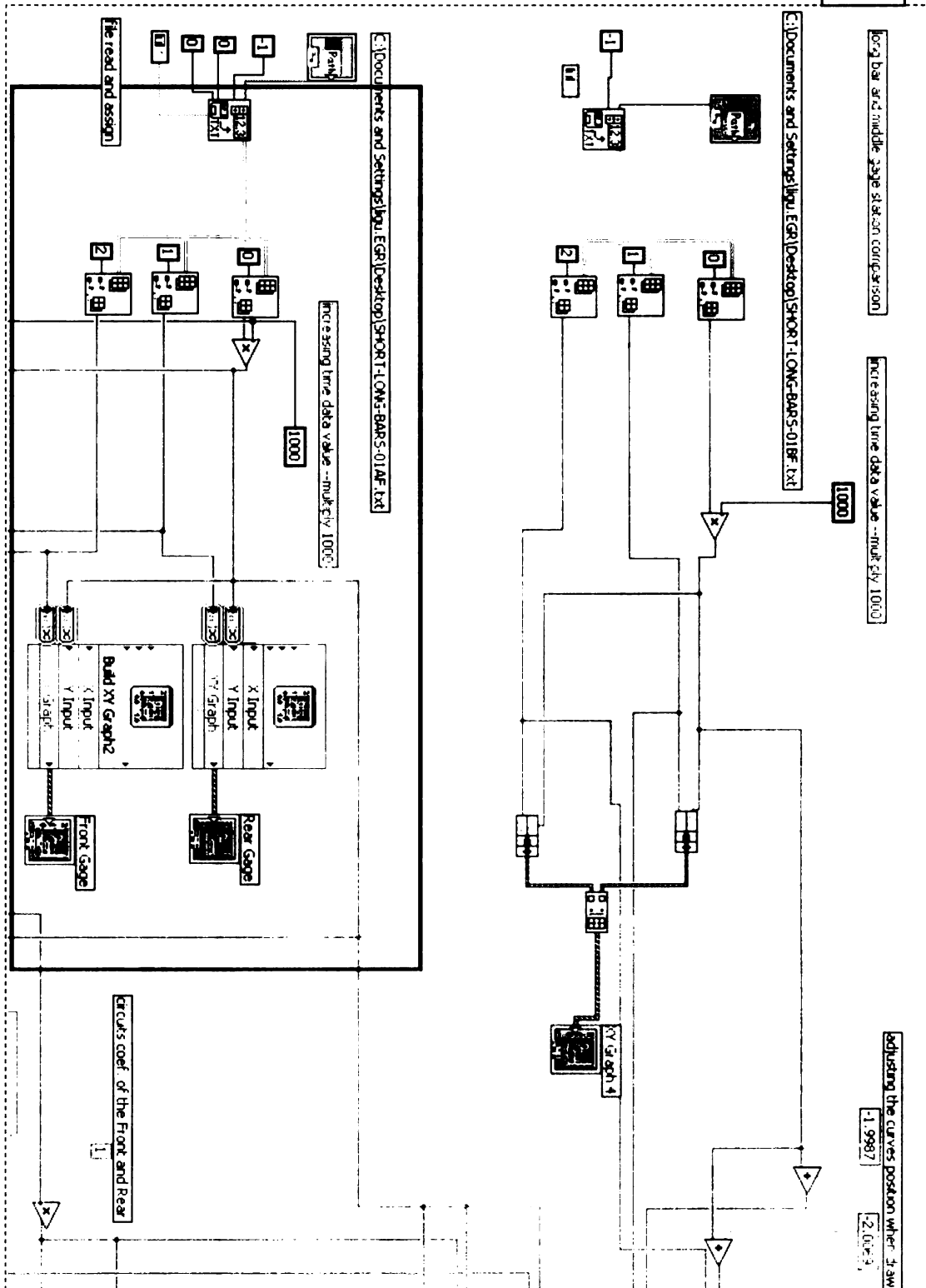
### LABVIEW PROGRAM FOR THE NUMERICAL METHOD

-- TWO-POSITION

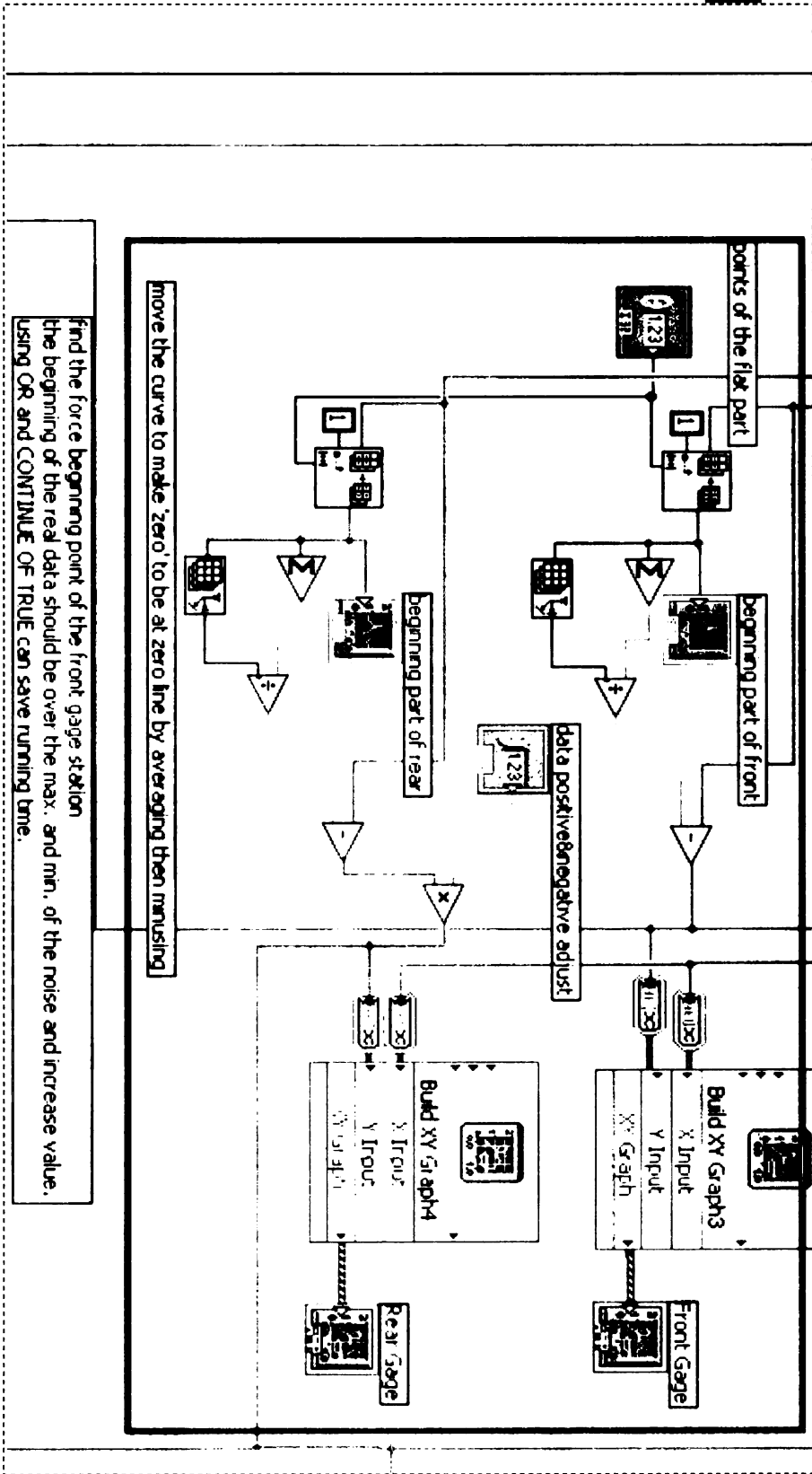


**A**

**PART A – Scale: 75%**



B

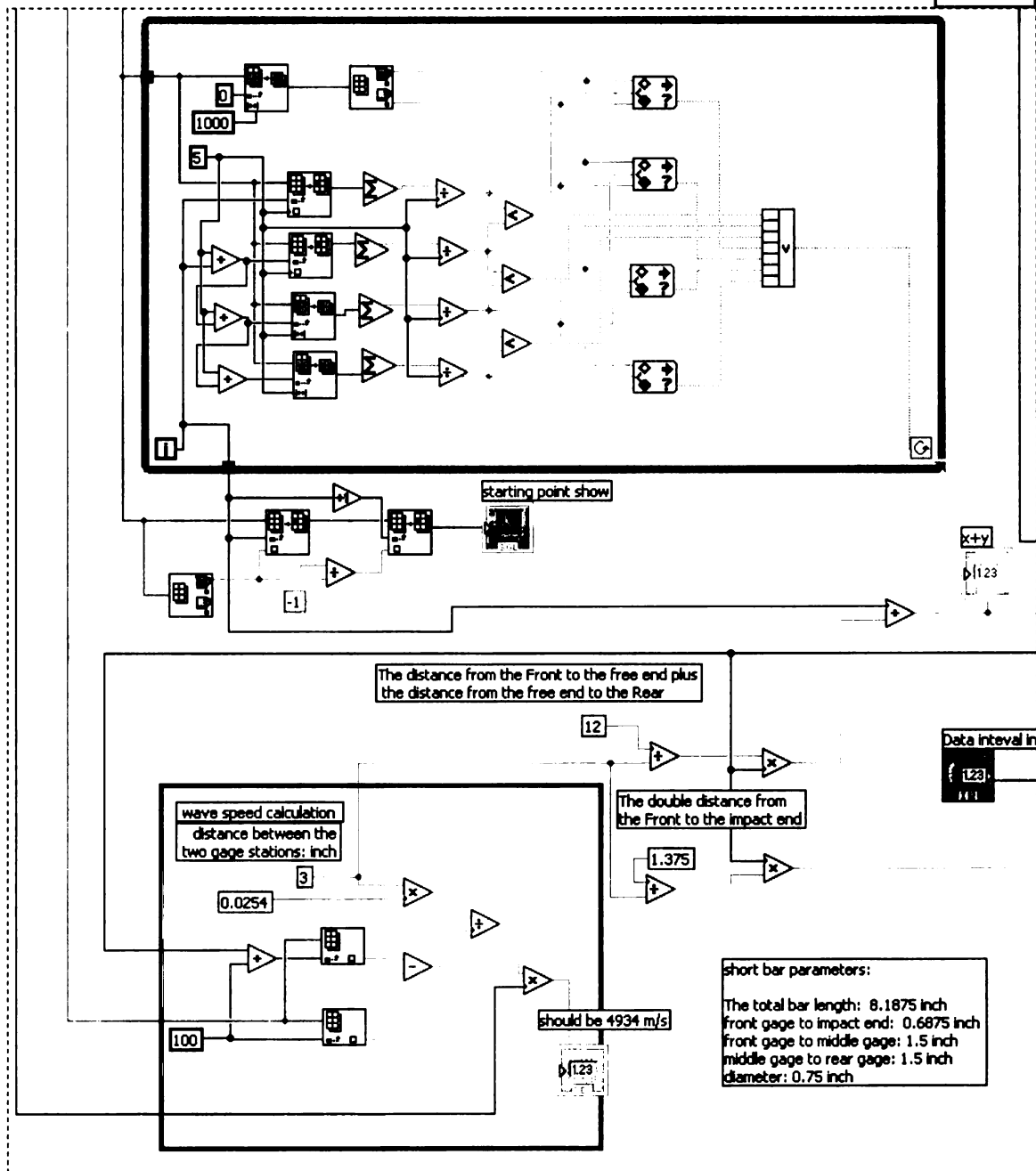


find the force beginning point of the front gage station  
the beginning of the read data should be over the max. and min. of the noise and increase value.  
using OR and CONTINUE OF TRUE can save running time.

move the curve to make zero to be at zero line by averaging then minus

PART C – Scale: 75%

C

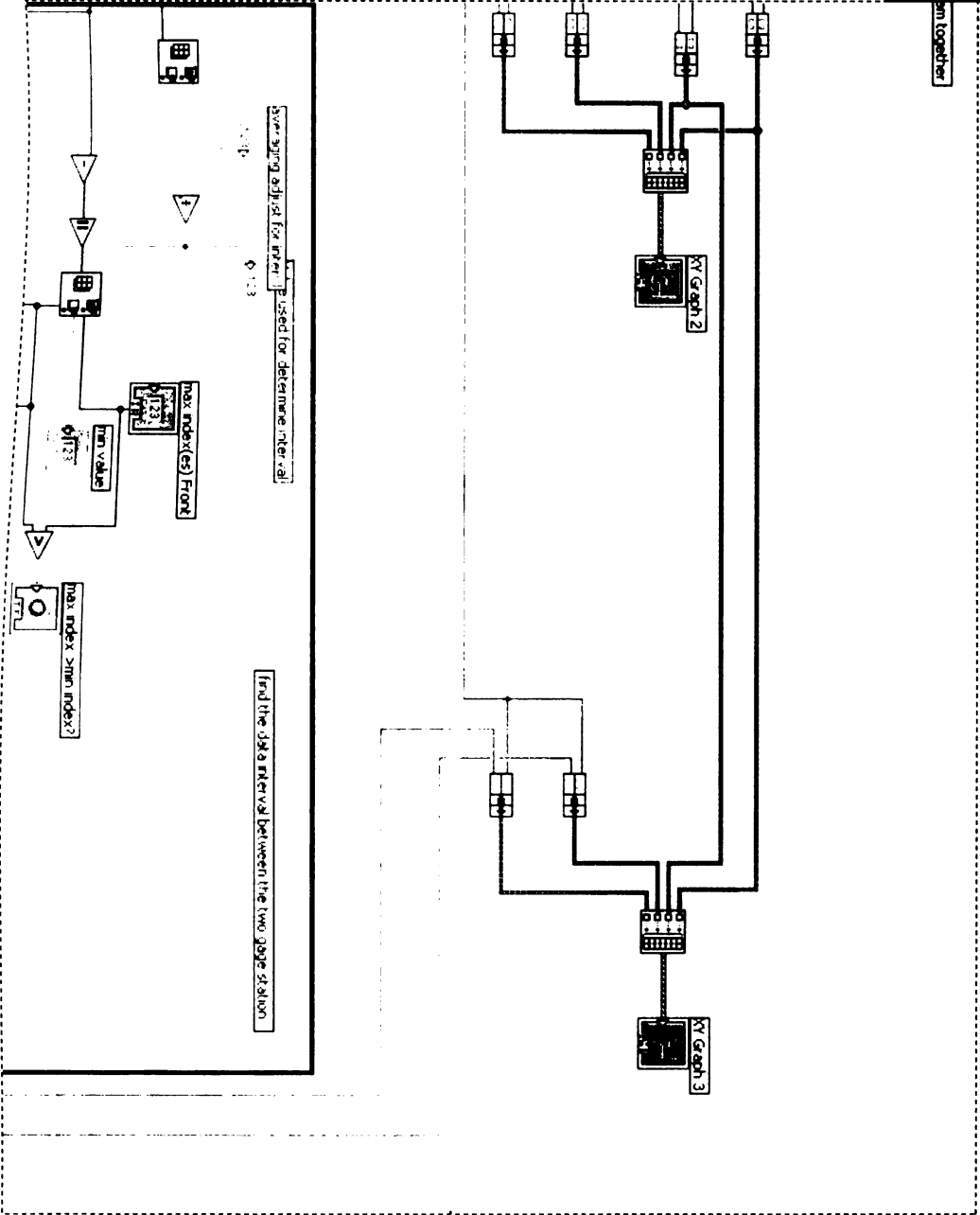




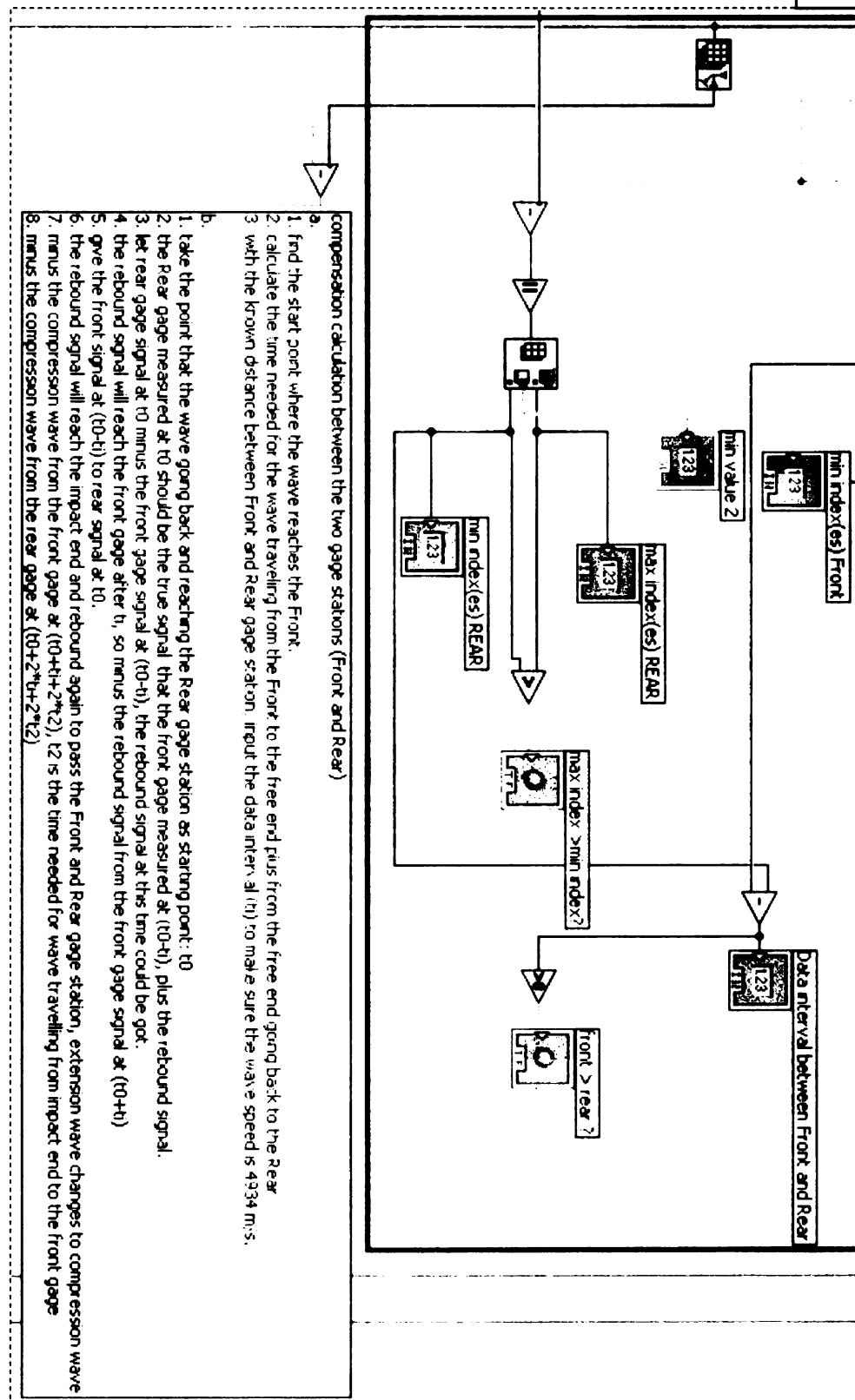
PART D- Scale: 75%

**D**

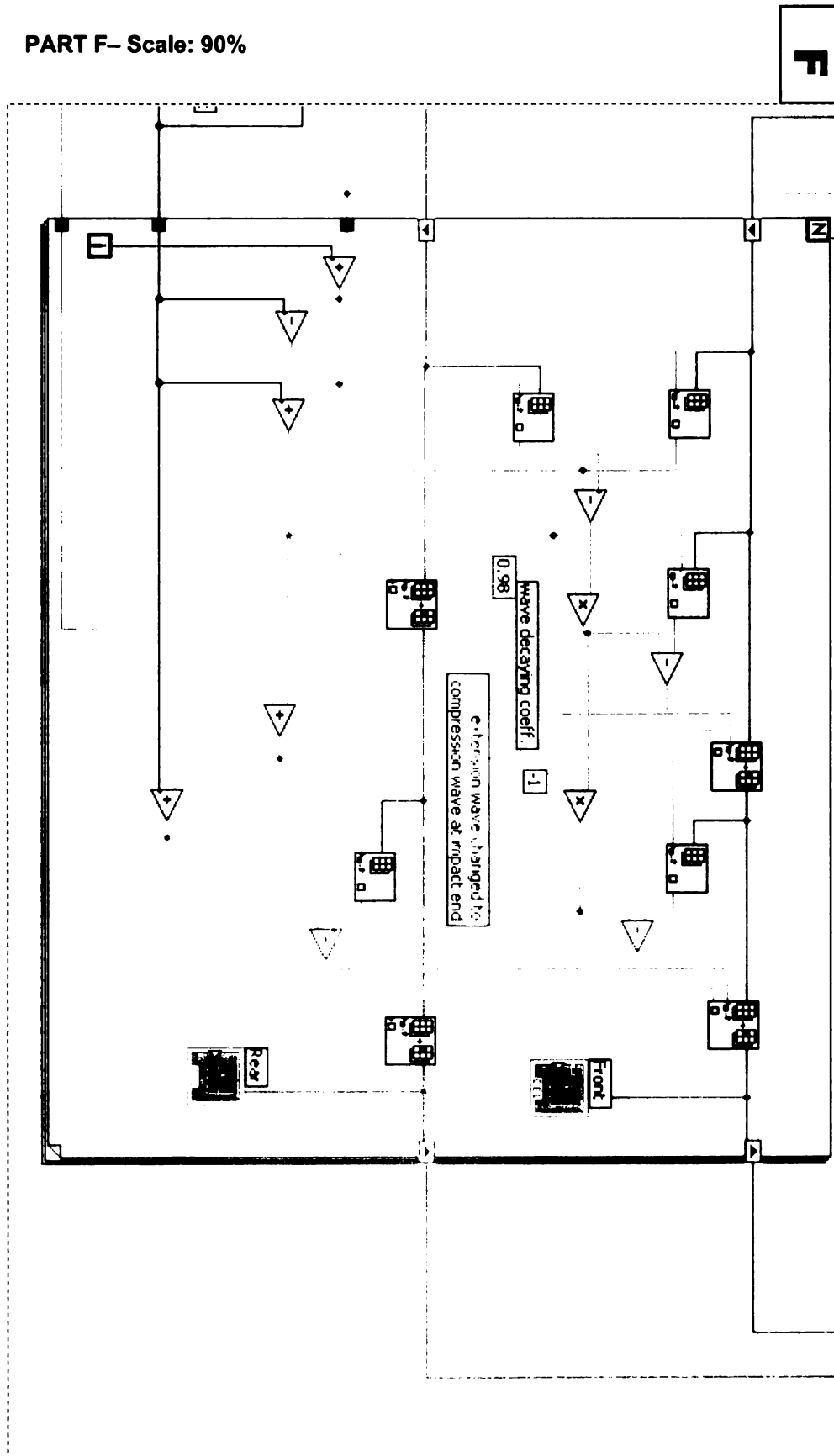
sim together



**PART E- Scale: 90%**



PART F- Scale: 90%



MICHIGAN STATE UNIVERSITY LIBRARIES



3 1293 02956 7983